UNIVERSIDADE ESTADUAL PAULISTA
"JÚLIO DE MESQUITA FILHO"

FACULDADE DE ENGENHARIA BAURU
unesp

SÃO PAULO STATE UNIVERSITY (UNESP)

GRADUATE PROGRAM IN MECHANICAL ENGINEERING
BAURU SCHOOL OF ENGINEERING

ANTHONY GASPAR TALON

GRINDING OF ADVANCED CERAMICS USING SUSTAINABLE MANUFACTURING TECHNIQUES

BAURU

2026

ANTHONY GASPAR TALON

GRINDING OF ADVANCED CERAMICS USING SUSTAINABLE MANUFACTURING TECHNIQUES

Thesis submitted to the Graduate Program in Mechanical Engineering at São Paulo State University (UNESP) in partial fulfillment of the requirements for the degree of Doctor in Mechanical Engineering.

Advisor: Prof. Dr. Eduardo Carlos Bianchi

Co-advisor: Prof. Dr. José Claudio Lopes

BAURU

2026

Talon, Anthony Gaspar
T152g GRINDING OF ADVANCED CERAMICS USING SUSTAINABLE MANUFACTURING TECHNIQUES / Anthony Gaspar Talon. -- Bauru, 2026
112 p.

Tese (Doutorado) - Universidade Estadual Paulista (Unesp), Faculdade de Engenharia, Bauru
Orientador: Eduardo Carlos Bianchi
Coorientador: José Claudio Lopes

1. Grinding. 2. Diamond wheel. 3. Advanced ceramic. 4. MQL. 5. Sustainability. I. Título.

UNIVERSIDADE ESTADUAL PAULISTA

Câmpus de Bauru

ATA DA DEFESA PÚBLICA DA TESE DE DOUTORADO DE ANTHONY GASPAR TALON, DISCENTE DO PROGRAMA DE PÓS-GRADUAÇÃO EM ENGENHARIA MECÂNICA, DA FACULDADE DE ENGENHARIA - CÂMPUS DE BAURU.

Aos 22 de setembro de 2026, às 9h, por meio de Videoconferência, realizou-se a defesa de TESE DE DOUTORADO de ANTHONY GASPAR TALON, intitulada "GRINDING OF ADVANCED CERAMICS USING SUSTAINABLE MANUFACTURING TECHNIQUES". A Comissão Examinadora foi constituída pelos seguintes membros: Prof. Dr. JOSÉ CLAUDIO LOPES (Participação Presencial) do(a) Departamento de Engenharia Mecânica / UNESP / Câmpus de Bauru - FEB, Prof. Dr. LUIZ EDUARDO DE ANGELO SANCHEZ (Participação Presencial) do(a) Departamento de Engenharia Mecânica / UNESP / Câmpus de Bauru - FEB, Prof. Dr. RAFAEL LIBERATTI IAVARONE (Participação Presencial) do(a) Departamento de Engenharia Mecânica / UNESP / Câmpus de Bauru - FEB, Prof. Dr. ROSEMAR BATISTA DA SILVA (Participação Virtual) do(a) Departamento de Engenharia Mecânica / Universidade Federal de Uberlândia, Prof. Dr. CARLOS EIJI HIRATA VENTURA (Participação Virtual) do(a) Departamento de Engenharia Mecânica / Universidade Federal de São Carlos, Após a exposição pelo doutorando e arguição pelos membros da Comissão Examinadora que participaram do ato, de forma presencial e/ou virtual, o discente recebeu o conceito final:_ **APROVADO** _ _ _ _ _ _ _ _ _ _ _ _ _ . Nada mais havendo, foi lavrada a presente ata, que após lida e aprovada, foi assinada pelo(a) Presidente(a) da Comissão Examinadora.

gov.br Documento assinado digitalmente
JOSE CLAUDIO LOPES
Data: 22/09/2026 17:05:06-0300
Verifique em https://validar.iti.gov.br

Prof. Dr. JOSÉ CLAUDIO LOPES

I dedicate this work to my wife, Maria, and to my parents, Airton and Agnes, for their constant encouragement, support, and patience throughout these years. I also dedicate it to the friends I made along this journey, whose companionship made it all the more meaningful.

ACKNOWLEDGMENTS

First and foremost, I thank God for the opportunity to undertake this journey and for granting me the strength to face and overcome the challenges encountered along the way.

To my wife, Maria Luiza, I express my deepest gratitude for her constant encouragement, companionship, and, above all, understanding and patience during the times when I needed to be away to pursue this dream.

To my parents, Airton and Agnes, I am grateful for always valuing my education, encouraging my studies, and teaching me that knowledge is one of the greatest achievements we can attain. I will be forever grateful for all the efforts and sacrifices they made to provide me with an education.

To my advisor, Full Professor Eduardo Carlos Bianchi, and my co-advisor, Professor José Claudio Lopes, I express my profound gratitude for the trust they have placed in me since my undergraduate studies, for the countless opportunities they have given me, and for their invaluable guidance throughout my academic journey. I am also grateful for their friendship, teachings, and professional and personal examples, which I will carry with me throughout my life.

I extend my sincere appreciation to the Graduate Program in Mechanical Engineering at the School of Engineering of São Paulo State University "Júlio de Mesquita Filho" (UNESP), Bauru campus, and to all the professors who contributed to my education. In particular, I thank Full Professor Luiz Eduardo de Angelo Sanchez for his support, friendship, and the valuable knowledge he shared with me over the years.

To my great friend and research colleague, Matheus de Souza Rodrigues, I express my heartfelt gratitude for his partnership, availability, and unwavering support throughout every stage of this journey. His contributions were invaluable during the most challenging moments of this work, and his assistance was essential to the completion of this research.

I am grateful to the Abrasive Machining Laboratory for the opportunities it provided for my academic, professional, and personal development, as well as for the friendships formed over the years. In particular, I thank my friend Rafael Liberatti Iavarone for his partnership, support, and the many moments we shared throughout this journey.

I gratefully acknowledge the São Paulo Research Foundation (FAPESP) for funding this research under Grant No. 2023/00741-2. Finally, I express my sincere gratitude to everyone who, directly or indirectly, contributed to this research and was part of this important stage of my life.

“If I have seen further, it is by standing on the shoulders of giants.”

(Isaac Newton)

RESUMO

Existe uma crescente demanda por materiais capazes de atuar em aplicações de alto desempenho, nas quais são exigidas elevada dureza, resistência ao desgaste, estabilidade térmica, resistência química e precisão dimensional. Nesse contexto, as cerâmicas avançadas, como a alumina, têm ganhado destaque em setores estratégicos, incluindo as indústrias mecânica, eletrônica, biomédica, aeroespacial e automotiva. Entretanto, devido à sua elevada dureza e fragilidade, esses materiais apresentam grande dificuldade de usinagem, tornando a retificação um processo essencial para garantir qualidade superficial, integridade da peça e precisão geométrica. Apesar de sua importância, a retificação de cerâmicas avançadas ainda apresenta desafios técnicos, econômicos e ambientais, principalmente relacionados ao desgaste do rebolo diamantado, à geração de defeitos superficiais e ao elevado consumo de fluido de corte no método convencional abundante. Dessa forma, este trabalho teve como objetivo avaliar diferentes estratégias de lubrirrefrigeração na retificação de alumina com rebolo diamantado, comparando o método convencional, a mínima quantidade de lubrificante (MQL), o MQL com fluido diluído e o MQL diluído associado ao sistema de jato de limpeza do rebolo, denominado wheel cleaning jet (WCJ). Foram analisadas variáveis relacionadas ao desempenho do processo, à integridade superficial, ao desgaste do rebolo e à sustentabilidade, incluindo força tangencial, energia específica, potência de retificação, razão G, desgaste diametral do rebolo, rugosidade, topografia da superfície, microscopia, custo e emissão de CO_2. Os resultados mostraram que a aplicação isolada do MQL diluído pode reduzir a demanda energética e os impactos ambientais, mas compromete o desempenho do rebolo e a qualidade da superfície retificada. Por outro lado, a associação do MQL diluído com o WCJ melhorou a remoção de debris, reduziu o empastamento do rebolo e favoreceu uma condição de corte mais estável. Assim, conclui-se que o uso do WCJ é fundamental para tornar o MQL diluído mais eficiente na retificação de alumina. Essa estratégia apresentou o melhor equilíbrio entre desempenho técnico, preservação do rebolo, integridade superficial, redução de custos e menor impacto ambiental, mostrando-se uma alternativa promissora ao método convencional abundante na retificação de cerâmicas avançadas com rebolo diamantado.

Palavras-chave: Retificação. MQL. Cerâmica avançada. Rebolo de diamante. Sustentabilidade.

ABSTRACT

There is a growing demand for materials capable of operating in high-performance applications requiring high hardness, wear resistance, thermal stability, chemical resistance, and dimensional accuracy. In this context, advanced ceramics, such as alumina, have gained prominence in strategic sectors, including the mechanical, electronics, biomedical, aerospace, and automotive industries. However, owing to their high hardness and brittleness, these materials are difficult to machine, making grinding an essential process for ensuring surface quality, workpiece integrity, and geometric accuracy. Despite its importance, the grinding of advanced ceramics still poses technical, economic, and environmental challenges, particularly those related to diamond grinding wheel wear, the formation of surface defects, and the high consumption of cutting fluid associated with conventional flood cooling. Therefore, this study aimed to evaluate different lubrication and cooling strategies for grinding alumina with a diamond grinding wheel by comparing conventional flood cooling, minimum quantity lubrication (MQL), MQL with diluted cutting fluid, and diluted MQL combined with a wheel cleaning jet (WCJ) system. Variables related to process performance, surface integrity, grinding wheel wear, and sustainability were analyzed, including tangential grinding force, specific grinding energy, grinding power, G-ratio, diametral wheel wear, surface roughness, surface topography, microscopy, costs, and CO_2 emissions. The results showed that diluted MQL applied alone can reduce energy demand and environmental impacts but compromises grinding wheel performance and the quality of the ground surface. In contrast, combining diluted MQL with the WCJ system improved debris removal, reduced wheel loading, and promoted more stable cutting conditions. It was therefore concluded that the WCJ system is essential for improving the effectiveness of diluted MQL in alumina grinding. This strategy provided the best balance among technical performance, grinding wheel preservation, surface integrity, cost reduction, and lower environmental impact, demonstrating its potential as an alternative to conventional flood cooling in the diamond grinding of advanced ceramics.

Keywords: Grinding. Diamond wheel. Advanced ceramic. MQL. Sustainability.

LIST OF FIGURES

Figure 1. Morphology of scratches produced under different load intensities (adapted from Malkin and Ritter, 1989; Zhang, 1990). 29
Figure 2. Influence of the applied load on the wear of ceramic materials (Gueroult and Cherif, 1994). 30
Figure 3. Effect of scratching speed on the fracture stress of scratched glass (Holland and Turner, 1937, cited by Swain, 1979). 31
Figure 4. Illustration of grinding defects on a ceramic surface (Tönshoff, 1989). 32
Figure 5. Chip formation during grinding (Malkin and Ritter, 1989). 33
Figure 6. Specific grinding energy as a function of material removal rate (Malkin and Ritter, 1989). 35
Figure 7. (A) Experimental setup; (B) Workpieces; (C) WCJ Nozzle; (D) MQL Nozzle. (E) Workpiece fixed in dynamometer. 55
Figure 9. Tangential grinding force for various conditions. 63
Figure 10. Specific grinding energy (real and theorical) compared with tangential grinding force for various conditions 64
Figure 11. SEM images of the workpiece ground with conventional condition, a) 1000 x and b) 5000X 66
Figure 12. SEM images of the workpiece ground with MQL, a) 1000 x and b) 5000X. 67
Figure 13. SEM images of the workpiece ground with MQL 1:5, a) 1000 x and b) 5000X... 67
Figure 14. SEM images of the workpiece ground with MQL 1:5 + WCJ, a) 1000x and b) 5000X. 68
Figure 15. 3D profilometer images of the ground surfaces: a) Conventional, b) MQL, c) MQL 1:5, d) MQL 1:5 + WCJ 70
Figure 16. Sa parameter 71
Figure 17. Morphological space of skewness and kurtosis for different machining processes, including the results obtained in the present study. Adapted from ((Whitehouse, 1994)). 72
Figure 18. Abbott-Firestone curves of the ground surfaces: a) Conventional, b) MQL, c) MQL 1:5, d) MQL 1:5 + WCJ 73
Figure 19. Vvv parameter 74
Figure 20. Sdq and Sdr parameters 75
Figure 21. Ra values for each lubrication-cooling condition. 77
Figure 22. Percentage area distribution of the ground surfaces according to height thirds: a) conventional, b) MQL, c) MQL 1:5 and d) MQL 1:5 + WCJ 78
Figure 23. Histogram of peaks: a) conventional, b) MQL, c) MQL 1:5 d) MQL 1:5 + WCJ. 81
Figure 24. Peak and valley volume: a) conventional, b) MQL, c) MQL 1:5 and d) MQL 1:5 + WCJ 82
Figure 25. Diametral wheel wear of the diamond grinding wheel for each lubrication-cooling condition. 83
Figure 26. (A) Grinding wheel surface after one machining operation. (B) Grinding wheel surface after application of the wheel cleaning jet for 10 seconds. 86
Figure 27. Grinding Power for various conditions. 87

Figure 28. Average G-ratio for various conditions..... 87
Figure 29. Confocal images of workpieces: a) conventional, b) MQL, c) MQL 1:5 and d) MQL 1:5 + WCJ..... 89
Figure 30. Grinding cost analysis for each lubrication-cooling condition. 91
Figure 31. Carbon Emission for each lubrication-cooling condition. 92

LIST OF SYMBOLS

Symbol	Description	Unit
μ	Coefficient of friction	[–]
A	Mean area at the abrasive grain tips	[mm²]
a	Actual depth of cut	[mm]
a_p	Depth of cut	[mm]
b	Grinding wheel width	[mm]
c_a	Radial depth of cut	[mm]
d_s	Grinding wheel diameter	[mm]
d*w*	Workpiece diameter	[mm]
e*c*	Specific grinding energy	[J/mm³]
F_t*c*	Tangential grinding force	[N]
G	G-ratio	[–]
h_eq	Equivalent chip thickness	[µm]
K	Unit cutting force	[N]
l*c*	Contact length	[mm]
n_s	Grinding wheel rotational speed	[rpm]
n*w*	Workpiece rotational speed	[rpm]
P	Grinding power	[W]
Q*w*	Material removal rate	[mm³/s]
Q′*w*	Specific material removal rate	[mm³/(mm·s)]
R_a	Arithmetic mean roughness	[µm]
R*z*	Maximum height of the roughness profile	[µm]
v_s	Grinding wheel peripheral speed or cutting speed	[m/s]
v*w*	Workpiece speed	[m/s]
Z_s	Volume of grinding wheel wear	[mm³]
Z*w*	Volume of material removed	[mm³]
MQL	Minimum quantity lubrication	[–]

TABLE OF CONTENTS

1. INTRODUCTION 17
1.1. Motivation 21
1.2. Objectives 22
2. LITERATURE REVIEW 23
2.1. Grinding Process 23
2.2. Thermal Damage Caused by Grinding 24
2.2.1. Chip Formation Mechanisms 24
2.3. Advanced Ceramics 25
2.4. Crack Formation Mechanisms in Ceramic Materials 26
2.5. Material Removal Mechanisms in Ceramic Materials 27
2.6. Defects and Material Removal Mechanisms in the Grinding of Ceramic 31
2.7. Material Removal Mechanisms in the Grinding of Polycrystalline Ceramics 34
2.8. Influence of Grinding Parameters on Defect Formation 34
2.9. Grinding Wheel 36
2.9.1. Grinding Wheel Grade 36
2.9.2. Grinding Wheel Structure 37
2.9.2.1. Abrasives 37
2.9.2.2. Abrasive Grain Size 38
2.9.2.3. Friability 39
2.10. Types of Abrasives 39
2.10.1. Diamond 40
2.11. Bond Materials 41
2.11.1. Resinoid Bonds 42
2.12. Dressing 43
2.13. Grinding Fluid 46
2.13.1. Problems Associated with the Use of Grinding Fluids 48
2.13.2. Costs Associated with Grinding Fluids 49
2.13.3. Maintenance and Disposal 49
2.13.4. Minimum Quantity Lubrication - MQL 51
2.13.5. Wheel Cleaning Jet - WCJ 52
3. METHODOLOGY 54
4. RESULTS AND DISCUSSION 62
4.1. Tangential force and specific grinding energy 63
4.2. Surface Roughness and Topograph 69

4.2.1. Sa parameter and 3D profilometer images 69
4.2.2. Abbott-Firestone curves 71
4.2.3. Vvv, Sdq and Sdr Parameters 74
4.2.4. Ra parameter 77
4.2.5. Analyses based on height distribution 78
4.2.6. Histogram of peaks 80
4.2.7. Peak and valley volumes 81
4.3. Diametral Wheel Wear 83
4.4. Grinding Power and G-Ratio 86
4.5. Cost Analysis 90
4.6. CO_2 Emission 91
5. CONCLUSIONS 93
SCIENTIFIC PRODUCTION 95
SUGGESTIONS FOR FUTURE WORK 96
REFERENCES 99

1. INTRODUCTION

The growing demand for components with high reliability and surface integrity makes defects induced by abrasive processes a critical factor capable of generating significant technical and economic losses (Rowe, 2013). In this context, grinding emerges as a high-precision abrasive process, generally applied as a final stage after forming and machining, in which material removal occurs through a grinding wheel composed of abrasive grains, bond material, and pores (Patra; Swain, 2022). The efficiency of this process is often evaluated by the G-ratio, defined as the ratio between the volume of material removed from the workpiece and wheel wear (Gerling, 1967). Among the abrasive properties that directly influence this performance, friability stands out and is characterized by the grain's ability to fracture and generate new cutting edges during the process (Groover, 2010).

Although friability is desirable for wheel self-sharpening, one of the main operational challenges in grinding lies in controlling the thermal effects generated in the contact zone, which can drastically compromise the surface integrity and the quality of the workpiece (Malkin; Guo, 2007). As demonstrated by Wei et al. (2023), the amount of heat transferred to the workpiece is strongly dependent on the abrasive type and the cutting conditions employed. This relationship becomes even more critical in advanced ceramic materials, whose high brittleness makes them particularly susceptible to crack propagation induced by thermal gradients.

Advanced ceramics have a carefully controlled chemical composition and microstructure, which allows them to perform exceptionally well under severe mechanical, thermal, and chemical stress conditions. Among these materials, aluminum oxide (α-Al_2O_3), commonly known as corundum or alumina, is one of the most widely used engineering ceramics. It is characterized by a hexagonal close-packed crystal structure, which contributes to its high stiffness, hardness, wear resistance, chemical stability, and favorable cost-to-performance ratio (Krishnan et al., 2021)

The combination of high hardness and wear resistance makes alumina suitable for applications such as gears, bearings, shafts, cutting tools, and dies (Žmak et al., 2025). However, its low fracture toughness, typically ranging from 2 to 6 $MPa \cdot m^{1/2}$, makes it susceptible to crack initiation and propagation in the presence of surface or subsurface defects, which act as stress concentrators during abrasive processes (Carter; Norton, 2007; Fathalian et al., 2024; Marinescu, 2007). Furthermore, the interaction between abrasive grains

and the workpiece occurs predominantly through brittle fracture mechanisms based on the indentation model, involving median and lateral cracks (Javaroni et al., 2019). The extent of these mechanisms is influenced by parameters such as feed rate and grinding wheel characteristics (Chen et al., 2010; Ribeiro et al., 2020a).

This fracture-based material removal mechanism, unlike that observed in metallic materials, makes alumina grinding compatible with diamond wheels. Although diamond undergoes graphitization and accelerated wear when in contact with ferrous materials at high temperatures, this phenomenon is not significant during ceramic machining, allowing its high hardness and wear resistance to be exploited (Jiang et al., 2020). In fact, Choudhary and Paul (Choudhary; Paul, 2020) did not observe significant evidence of this effect after grinding alumina. Resin-bonded diamond wheels are widely used in advanced ceramic grinding because they provide good grain retention and greater conformability during contact with the workpiece, although their low porosity limits lubricant penetration into the cutting zone (Emami; Sadeghi; Sarhan, 2013b; Javaroni et al., 2019).

However, even with the use of an appropriate abrasive, alumina grinding still presents challenges related to surface integrity (Chen et al., 2010; Choudhary; Naskar; Paul, 2018). Its low thermal conductivity, approximately 30 $W \cdot m^{-1} \cdot K^{-1}$ (Kingery; Bowen; Uhmann, 1976), promotes heat concentration in the contact zone, intensifying damage mechanisms such as burning, residual stresses, and cracks, which compromise the mechanical strength and durability of the component (Bianchi et al., 2000; Choudhary; Naskar; Paul, 2018). Additionally, chipping resulting from unstable crack propagation and phenomena associated with the tribological behavior of the grinding wheel, such as pore loading by debris generated during material removal, may occur (Choudhary; Paul, 2020; Javaroni et al., 2019). Therefore, thermal and tribological control of the process strongly depends on the efficient application of the cooling and lubrication system.

The cutting fluid is directed toward the interface between the grinding wheel and the workpiece, acting simultaneously on the lubrication and cooling of the cutting zone (Marinescu et al., 2016). Part of the energy generated during the process is dissipated by the wheel-fluid interaction (Malkin; Guo, 2008a). Thus, the cutting fluid reduces heat generation and shear resistance in the contact zone by forming a thin lubricating film and contributing to heat dissipation, especially in the case of water-based fluids (Sales; Diniz; Machado, 2001). Furthermore, its ability to transport and remove debris generated during grinding directly influences process efficiency.

The conventional flood method uses large volumes of fluid; however, the air barrier formed at high wheel speeds limits its penetration into the cutting interface, reducing cooling efficiency even under high flow rates (Choudhary; Naskar; Paul, 2018; Javaroni et al., 2019). Although these fluids provide good lubrication and cooling properties, their emulsion-based composition makes them susceptible to bacterial contamination and may pose health risks to operators (Farfan-Cabrera et al., 2023). At the end of their useful life, they are classified as hazardous waste, requiring proper disposal (Soković; Mijanović, 2001). Furthermore, their adhesion to the workpiece and chips results in fluid losses and contamination, while the generation of toxic mists during the process exposes operators to respiratory problems (Benedicto; Carou; Rubio, 2017; Li et al., 2003). Although this method provides good results in terms of surface finish and wheel wear, its environmental and occupational impacts have encouraged the search for more sustainable alternative (Javaroni et al., 2020; Lopes et al., 2019, 2020; Ribeiro et al., 2020b).

In this context, the minimum quantity lubrication (MQL) technique has gained prominence by combining technical performance with environmental benefits (Silva et al., 2005). MQL consists of applying a jet composed of compressed air and a very small amount of oil delivered in the form of droplets toward the cutting zone (Mali; Shinde; Khankal, 2019). The oil flow rate in this system typically ranges from 10 to 500 mL/h, in contrast to the much higher volumes used in conventional lubrication, which may reach 300,000 to 1,200,000 mL/h (Stachurski et al., 2022). In addition to the significant reduction in fluid consumption and operating costs, which may account for 16 to 20% of manufacturing costs (Sreejith; Ngoi, 2000), MQL can reduce cutting forces, surface roughness, tool wear, and temperature during grinding, provided that parameters such as flow rate, pressure, and nozzle positioning are properly adjusted (Emami; Sadeghi; Sarhan, 2013b; Qu et al., 2020; Ribeiro et al., 2020a; Said et al., 2019).

On the other hand, although MQL presents significant advantages, its application in grinding may be limited by its lower efficiency in debris removal compared with the conventional method (Patra; Swain, 2022). Ceramic fragments may remain trapped in the wheel pores, promoting wheel loading, which prevents the exposure of new cutting edges and favors increased forces and temperature in the contact zone, potentially resulting in thermal damage to the workpiece (Agarwal, 2019). In ceramics such as alumina, this limitation becomes even more relevant due to the high hardness of the fragments generated during material removal. Soluble oils tend to promote chip adhesion, whereas neat oils reduce this effect (Choudhary; Paul, 2020).

Furthermore, the retention of chips and abrasive fragments at the wheel-workpiece interface may alter the tribological mechanisms involved in the process. Particles trapped between two surfaces in relative motion can act as free abrasives, corresponding to three-body abrasion mechanisms. In the context of alumina grinding with MQL, this phenomenon is critical because ceramic debris, due to its high hardness, tends to remain adhered to the wheel pores as a consequence of the limited debris evacuation capacity of MQL (Agarwal, 2019). This debris accumulation acts as free abrasive particles between the wheel and the workpiece, promoting excessive wheel wear, increased cutting forces, and deterioration of surface finish (Ávila et al., 2023; Rodrigues et al., 2024; Sato et al., 2020; Talon et al., 2022). Therefore, the efficiency of MQL in alumina grinding is directly dependent on its ability to remove this debris from the cutting zone.

Given these limitations, complementary strategies to MQL have been investigated. Among them, the combination with the wheel cleaning jet (WCJ) has emerged as a promising approach to reduce wheel loading through the application of compressed air in the opposite direction to wheel rotation, acting directly on the removal of accumulated debris (Moretti et al., 2023). This technique contributes to reducing cutting temperatures and increasing wheel life (Ribeiro et al., 2020a). The effectiveness of the system, in turn, depends on nozzle positioning, with a superior surface finish compared with conventional MQL being reported when the nozzle was positioned at 30° from the grinder base (Oliveira et al., 2012a). By reducing wheel loading and three-body abrasion, WCJ enables the application of MQL without compromising workpiece surface integrity or wheel cutting ability.

The relevance of WCJ for advanced ceramic grinding is further supported by recent investigations. In alumina grinding with a diamond wheel, the combination of MQL and WCJ resulted in an approximately 40% improvement in the G-ratio compared with MQL without the cleaning jet, in addition to reducing the cost per piece to only 24% of that associated with the conventional flood method (Fernandes et al., 2023). Additional results demonstrated performance close to the conventional method, even surpassing it in terms of diametrical wheel wear and G-ratio when combined with cooled air (De Moraes et al., 2021). Furthermore, it was observed that the combination of WCJ and MQL contributes to reducing the environmental impact of the process (De Moraes et al., 2024).

In addition to strategies aimed at wheel cleaning, modifications to the cutting fluid properties through water dilution have also been investigated. Such changes affect viscosity and flow behavior, with direct implications for fluid penetration into the cutting zone and particle transport. In tests with SAE 52100 steel, dilution at a 1:5 ratio provided a reduction of

up to 53% in surface roughness (De Moraes et al., 2019). In the case of alumina, the addition of water to MQL, combined with a high-pressure water jet (WCJ), proved effective in reducing wheel wear, operating costs, and CO_2 emissions, although it negatively affected surface roughness and roundness deviation under certain conditions (Lopes et al., 2018b). However, the effects on ceramics remain poorly explored, particularly regarding debris removal, as well as comparative studies between WCJ and fluid dilution in MQL.

Given these considerations, this work aims to investigate the influence of different lubrication-cooling strategies on the grinding of Al_2O_3 using a diamond wheel, with particular emphasis on evaluating the role of WCJ associated with MQL. For this purpose, conventional flood cooling, pure MQL, MQL with diluted fluid (1:5), and MQL diluted combined with WCJ conditions were compared. The central hypothesis is that the efficient removal of debris through WCJ constitutes the main mechanism enabling the application of MQL in alumina grinding by reducing the harmful effects of three-body abrasion and preserving the surface quality of the workpiece. Parameters such as tangential grinding force, specific grinding energy, three-dimensional surface roughness, Abbott-Firestone parameters, diametrical wheel wear, SEM images, grinding power, G-ratio, confocal microscopy images, surface roughness parameters, height distribution, peak histogram, peak and valley volumes, cost analysis, carbon emissions and qualitative wheel-cleaning images were evaluated.

1.1. Motivation

Advanced ceramics are becoming increasingly important in industrial applications owing to their specific properties, such as corrosion resistance, heat resistance, high hardness, and wear resistance. However, the design of ceramic components is complex because their theoretical mechanical strength may differ significantly from their actual strength due to defects in their microstructure. Therefore, studying the manufacturing processes of advanced ceramics is essential, since inappropriate processing conditions may compromise the physical integrity and geometric accuracy of the workpiece.

Because of their high hardness, advanced ceramics are commonly ground using diamond grinding wheels. These tools are expensive, making the grinding process costly. Furthermore, although diamond has high thermal conductivity, excessive heat generation in the grinding zone can accelerate wheel degradation and significantly reduce tool life.

Therefore, the application of cutting fluids is necessary to provide adequate cooling and lubrication. Nevertheless, the use of these fluids raises important concerns regarding their

environmental impacts and potential risks to human health. Consequently, alternatives to conventional flood cooling have been investigated to reduce cutting-fluid consumption and help companies meet the growing demand for more sustainable manufacturing practices. Minimum quantity lubrication (MQL) has emerged as a promising strategy for addressing these concerns, improving the environmental performance of machining processes and generally reducing operating costs.

However, bibliometric studies conducted using international databases, including Scopus, Google Scholar, and ScienceDirect, have revealed a lack of research on the diamond grinding of advanced ceramics under MQL conditions and Wheel Cleaning Jet (WCJ).

Thus, although the industrial use of advanced ceramics and society's demand for more sustainable processes are both increasing, relatively few studies have investigated sustainable manufacturing strategies for these materials.

In this context, the present research aims to expand scientific knowledge in this field while providing relevant information for an industry undergoing continuous development and expansion.

1.2. Objectives

General Objective:

- To evaluate the technical, economic, and environmental performance of alumina surface grinding with a diamond wheel under conventional lubrication, MQL, diluted MQL (1:5), and diluted MQL assisted by a wheel-cleaning jet (MQL 1:5 + WCJ).

Specific Objectives

- To compare the grinding force, power, and specific grinding energy obtained under the four conditions.
- To assess diametral wheel wear, G-ratio, wheel loading, and wheel surface condition.
- To characterize the surface integrity of the ground alumina using roughness parameters, three-dimensional topography, Abbott–Firestone curves, confocal microscopy, and scanning electron microscopy.
- To estimate the grinding cost and CO_2 emissions per workpiece.

- To correlate the results and identify the condition that provides the best balance between process performance, wheel preservation, surface integrity, cost, and environmental impact.

2. LITERATURE REVIEW

This chapter presents a literature review of the main topics addressed in this study, including the grinding process, the characteristics of diamond grinding wheels, abrasive grain friability, advanced ceramics, output variables in grinding, and other topics related to this research.

2.1. Grinding Process

Abrasive machining is a process in which the cutting edges are randomly distributed and oriented. In grinding, the tool has undefined cutting-edge geometry, unlike turning and milling tools, because the abrasive grains have irregular cutting edges (Marinescu et al., 2013a).

Material removal in the grinding process is performed by the grinding wheel, a tool in which the abrasive grains are irregularly distributed (Rasim; Mattfeld; Klocke, 2015). Material removal occurs through friction, deformation, and shearing. Shearing is responsible for chip formation, whereas friction and deformation consume energy without effectively removing material (Sinha et al., 2016).

Grinding is typically one of the final operations in the manufacturing of a workpiece and is employed to achieve the required surface finish and dimensional tolerances. At this stage, the workpiece already has considerable added value; therefore, any error may result in substantial losses. Consequently, grinding parameters must be carefully selected and controlled (Anderson; Warkentin; Bauer, 2008).

According to Sinha et al. (2016), grinding is a complex and dynamic process widely employed in the manufacture of high-quality components requiring tight dimensional tolerances and excellent surface finish. Silva et al. (2020) stated that grinding is a highly complex process involving numerous variables and is therefore highly sensitive to changes in machining conditions, the working environment, and even operator skill.

In grinding, the abrasive tool operates at a higher peripheral speed than cutting tools used in other machining processes, such as turning and milling. Conventional grinding wheel

speeds typically range from 20 to 45 m/s, whereas high-speed grinding may reach 140 m/s or more (Marinescu et al., 2013a).

Hassui and Diniz (2003) The authors stated that most machining researchers regard grinding as a difficult process to investigate because it involves numerous variables, is highly sensitive to slight changes in their values, and employs a tool with irregular cutting-edge geometry.

2.2. Thermal Damage Caused by Grinding

In grinding, many abrasive grains are in contact with the workpiece at any given instant; however, only a fraction of them effectively cut and remove material. The remaining grains merely slide over the workpiece surface, generating considerable friction and, consequently, high temperatures (Tawakoli et al., 2009).

The high temperatures generated during grinding may cause visible grinding burns on the workpiece, such as staining or discoloration, as well as microstructural damage resulting from changes in the material microstructure. These changes may reduce surface hardness, increase residual stresses, and consequently decrease fatigue strength. Tempering or rehardening of the material may also occur. Furthermore, uncontrolled thermal expansion can lead to dimensional and form errors, typically roundness error, as well as crack formation. (Da Silva et al., 2007; Irani; Bauer; Warkentin, 2005).

2.2.1. Chip Formation Mechanisms

The three phases required for material removal. In the first phase, only elastic deformation occurs in the workpiece material. Consequently, the energy supplied to the process is consumed by friction, heat generation, and deformation.

In the second phase, as the abrasive grains continue to penetrate the workpiece, plastic deformation, lateral material flow, and recovery of the elastic deformation produced in the previous phase occur. As grain penetration increases, the frictional force also increases. Consequently, most of the energy continues to be dissipated through deformation, friction, and heat generation.

Finally, in the third phase, the cutting edge reaches a penetration depth at which chip formation begins. Consequently, a large proportion of the energy is consumed by material shearing.

2.3. Advanced Ceramics

According to Rodríguez et al. (2022), advanced ceramics are currently employed in a wide range of structural and functional applications. High strength is a fundamental requirement for structural applications, such as cutting tools, rotors, and valves. Functional ceramics, in contrast, exhibit a variety of electrical, magnetic, biological, and optical properties that enable their use in different applications.

Shareef et al. (2022) added that engineering ceramics exhibit several relevant properties, including heat resistance, thermal insulation, abrasion resistance, high strength, self-lubrication, dimensional stability, electrical insulation, nonmagnetic behavior, dielectric properties, ionic conductivity, electron emission, fluorescence, transparency, polarization, photosensitivity, absorptivity, biocompatibility, catalytic activity, and corrosion resistance. The combination of these properties makes ceramics suitable for a wide variety of applications, including engines, mechanical seals, turbine blades, cutting tools, abrasives, watches, heaters, gas sensors, transformers, batteries, laser diodes, artificial bones and teeth, heat exchangers, nuclear and fusion reactor materials, and nuclear fuels.

The main advanced ceramics include zirconia, silicon carbide, alumina, and silicon nitride. Although the properties of these materials are highly desirable for applications in extreme environments, their inherently high brittleness and low shear strength represent significant challenges to their machinability. Ceramic machining is also hindered by surface damage and excessive tool wear (Bharathi et al., 2021).

Ceramics are inherently brittle materials with low fracture toughness. Ceramic components fail under tensile loading because of flaws introduced during processing and/or machining. In optimized materials, these flaws may be so small that they cannot be detected using currently available nondestructive evaluation techniques. Because the size, shape, and orientation of the flaws vary, ceramic strength may also vary considerably, making statistical design approaches essential. Two types of defects may be present in ceramics. Intrinsic defects, such as grain boundaries, pores, agglomerates, and inclusions, are distributed throughout the bulk of the component. Extrinsic defects associated with forming or machining processes are located on the surface (Rodríguez et al., 2022).

Because defect distribution is determined by the processing method, evaluating ceramic manufacturing processes, including grinding, is essential.

In this context, Shareef et al. (2022), stated that the commercial application of advanced ceramics has been hindered by the lack of efficient and cost-effective machining

processes. According to the same authors, two of the most important requirements for making ceramic machining economically viable are achieving sufficiently high material removal rates and developing a machining process that does not cause surface or subsurface damage to the ceramic component. Therefore, machining processes capable of efficiently and reliably processing advanced ceramics must be investigated in depth.

Choudhary et al. (2018) investigated the diamond grinding of alumina by comparing conventional flood cooling with MQL. The authors concluded that alumina exhibited greater plastic deformation under MQL conditions, whereas conventional flood cooling resulted in more extensive brittle fracture. Furthermore, lower workpiece surface roughness was obtained using conventional flood cooling. The authors attributed this behavior to the low friction provided by straight oil under MQL conditions, which increased plastic deformation and helped preserve the peaks and valleys on the workpiece surface. This increased plastic deformation also resulted in higher residual stresses in the workpiece.

Therefore, investigating the grinding of advanced ceramics is essential to meet the growing demand for ceramic components in engineering applications. However, several aspects must be evaluated because ceramic grinding is a complex machining process.

2.4. Crack Formation Mechanisms in Ceramic Materials

In the doctoral thesis by Sanchez (1997) the author reported that material removal during the machining of brittle materials may occur predominantly in either the ductile or brittle regime. In general, the ductile mode is characterized by a removal mechanism dominated by plastic deformation, leaving the workpiece with few surface and subsurface defects. In contrast, in the brittle mode, removal occurs through fracture and consequently leaves surface and/or subsurface defects in the workpiece.

These defects, which are commonly caused by machining - particularly by grinding, the most important and almost exclusive machining process used for ceramics - have a decisive influence on the mechanical strength of the finished components.

Nevertheless, owing to the complexity of the variables involved in grinding, which results from the large number of simultaneous interactions between abrasive grains and the ground workpiece surface, researchers have sought to understand the removal mechanisms by simplifying the process through the analysis of a single cutting edge represented by an indenter.

In ceramic materials, removal may occur on a small scale through plastic deformation and, more predominantly, through fracture mechanisms involving crack initiation and propagation. Crack behavior, in turn, is strongly influenced by the material structure. In general, single-crystal and amorphous ceramic materials, such as glass, develop long cracks, which are also common in some polycrystalline ceramics. Polycrystalline ceramics, however, preferentially exhibit short cracks at the grain scale (Hu; Chandra, 1993; Malkin; Ritter, 1989; Tonshoff; Wobker; Lierse, 1994).

These defects, which are typical of grinding, are investigated using simpler fracture models, such as indentation and scratching, in which contact analogous to abrasive grain-workpiece contact is produced by an indenter acting on a ceramic surface.

The following discussion reviews defect formation and material removal mechanisms in ceramics in a progressive manner, according to the complexity of the models used to more closely represent the grinding process. The influence of the parameters employed and their deleterious effects on the mechanical strength of the finished components are then examined.

2.5. Material Removal Mechanisms in Ceramic Materials

At low loads, scratches are produced entirely through plastic removal mechanisms, as typically occurs in metals, without the formation of surface or subsurface cracks. According to several authors, including Swain (1979) and Marinescu and Zeng, (1996), the accumulation of a large number of events of this nature produces the surface finish characteristic of mechanical lapping operations.

Figure 1a illustrates material removal in alumina and silicon nitride under the conditions described above, as reported by Malkin and Ritter (1989), Kitajima et al. (1992), and Zhang (1990). In both materials, the scratch has a smooth appearance along its entire length, and its depth, width, and cross-sectional profile correspond to the indenter geometry.

At intermediate loads, the scratch surface is plastically deformed, as in the previous condition, and remains free of subsurface defects. However, median and lateral cracks are observed, and the latter may intersect the workpiece surface.

Figure 1b illustrates the scratch morphology described above, showing lateral ridges formed by the flow of plastically deformed material. Neither the ridges nor the scratch profile are uniform, which prevents the indenter profile geometry from being accurately reproduced on the workpiece.

Under high loads, as under intermediate loads, median and lateral cracks are present. Radial cracks and surface microcracks caused by crushing of the material at the indenter-workpiece contact are also observed. These microcracks fragment the material, which is then removed by the tangential component of the friction force. According to Swain (1979), this mechanism corresponds to typical wear operations. It is characterized by rapid material removal and invariably produces a rough surface.

Figure 1c represents the possible defects resulting from this condition. The scratch surface is irregular, and the material removal mode alternates between plastic deformation and brittle fracture. Brittle removal includes crushing, the generation of small flake-like chips caused by radial cracks, and larger-scale chipping caused by lateral cracks that are deeper and more extensive than the former.

With further reference to Figure 1, Zhang (1990) observed that the total scratch width becomes greater than the corresponding indenter dimensions and that the plastic-zone region decreases. This behavior results from the extensive material removal promoted mainly by lateral cracks.

Using a similar approach and pursuing the same objective as the tests described above, other studies, including those by Nakajima et al. (1989), Tonshoff et al. (1994), Tsukuda et al. (1995), and Wang and Hsu (1996), varied the depth of cut to identify regions containing different types of defects. Most of these studies used a diamond tip, generally an indenter, fixed to the periphery of a rotating disk, analogous to a single-grain grinding wheel. This configuration produces a semicircular scratch on the workpiece surface, creating regions ranging from completely defect-free areas to severely deteriorated areas when the maximum depth is reached.

Tonshoff et al. (1994), shows the sequence of a scratch produced in alumina at progressively increasing depths. At the beginning of contact between the tool cutting edge and the workpiece, no material removal is observed, characterizing a region of elastic deformation without groove formation. As the depth of cut increases, plastic deformation begins, as indicated by the formation of lateral ridges. Beyond a threshold depth, cracks develop and the material is then removed by brittle fracture.

Regarding the volume removed from brittle materials, Gueroult and Cherif (1994) identified plastic deformation and lateral cracking as the most important mechanisms involved in the process and related their magnitude to mechanical properties such as hardness and toughness.

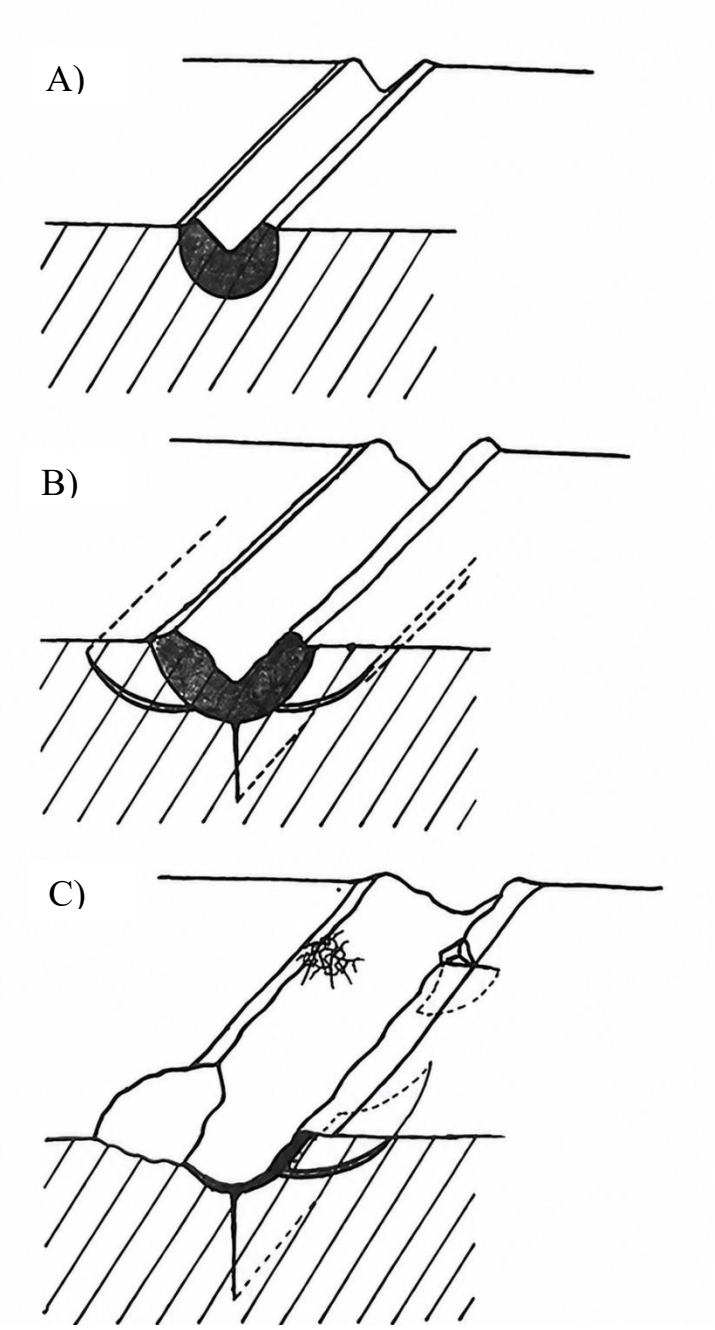


Figure 1. Morphology of scratches produced under different load intensities (adapted from Malkin and Ritter, 1989; Zhang, 1990).

Gueroult and Cherif (1994) investigated the wear behavior of ceramic materials. Their results showed that the wear mechanism changes from plastic to brittle removal as the applied load progressively increases, as shown in Figure 2.

In Figure 2, region A represents plastic wear and region B represents brittle wear, whereas the transition interval between these regions exhibits both removal modes simultaneously. These regions naturally vary according to the mechanical properties of the

material and the coefficient of friction, which changes the magnitude of the tangential force and therefore also modifies the tensile stress field behind the moving indenter.

Regarding scratching speed, few studies have addressed its influence on defect formation and, consequently, on material removal mechanisms. However, Swain (1979) cited the effect of scratching speed on glass was related to fracture strength. Flexural strength tests were performed after each scratch, making it possible to obtain the graph in Figure 3.

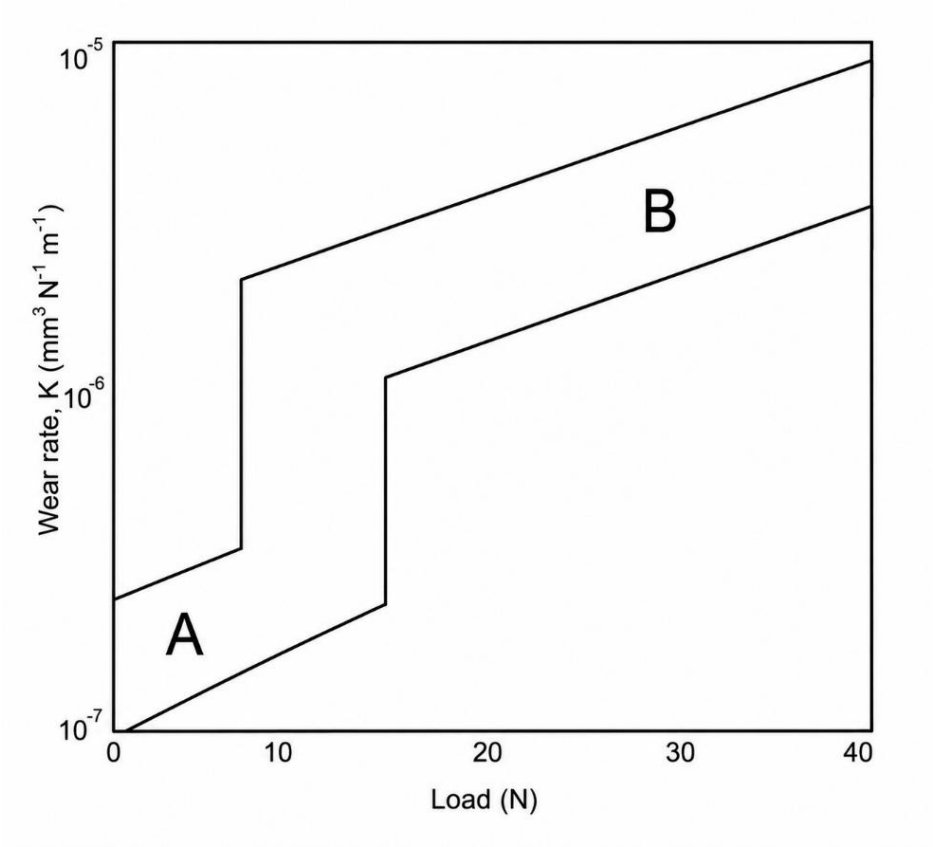


Figure 2. Influence of the applied load on the wear of ceramic materials (Gueroult and Cherif, 1994).

The results presented in Figure 3 were obtained under constant load and show that fracture strength decreases as scratching speed increases. According to Swain (1979), this behavior provides further evidence of residual stresses generated during the scratching of brittle materials.

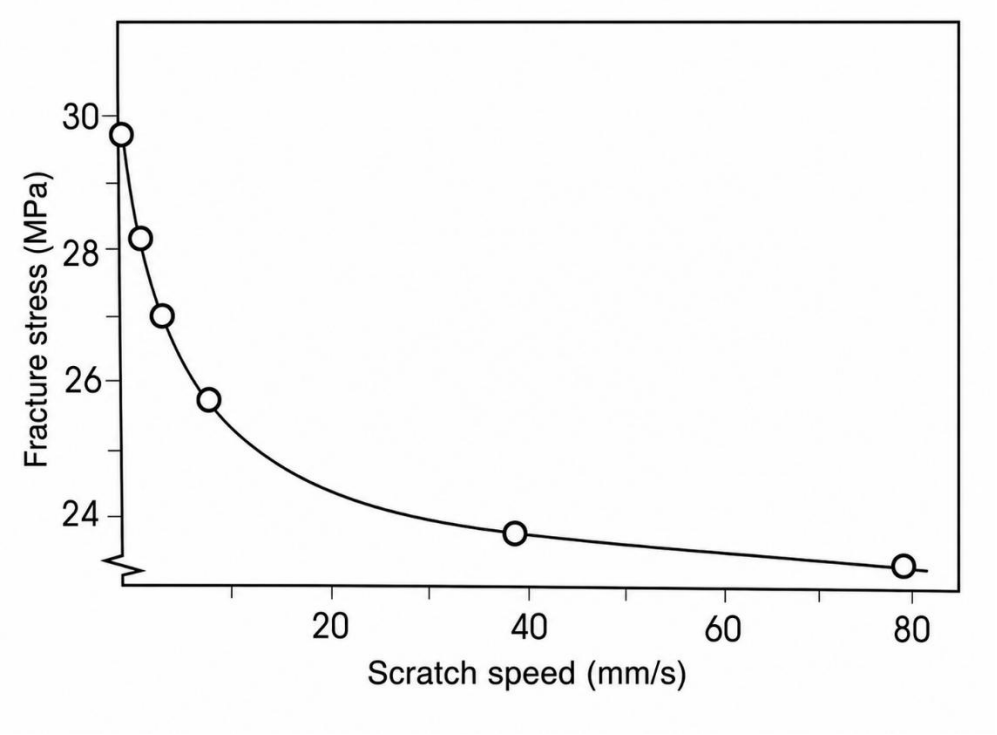


Figure 3. Effect of scratching speed on the fracture stress of scratched glass (Holland and Turner, 1937, cited by Swain, 1979).

2.6. Defects and Material Removal Mechanisms in the Grinding of Ceramic

Compared with indentation and scratching, grinding involves additional factors that must be considered in order to study the process more thoroughly.

The first consideration concerns the effects caused by interactions among the numerous adjacent scratches. The second is that, unlike in scratching, an abrasive grain held in the grinding wheel does not follow a linear path at a constant depth. Finally, the nearly simultaneous action of the abrasive grains in contact with the workpiece creates a high-temperature grinding zone (Malkin; Ritter, 1989).

Regarding interactions between neighboring scratches, Tonshoff et al. (1994), presented in Figure 4 a schematic illustration of a ground surface containing the main defects associated with the mechanical degradation of a workpiece. These include the median and radial cracks already described in the two preceding fracture models - indentation and scratching - and apply to ceramic materials with different structures.

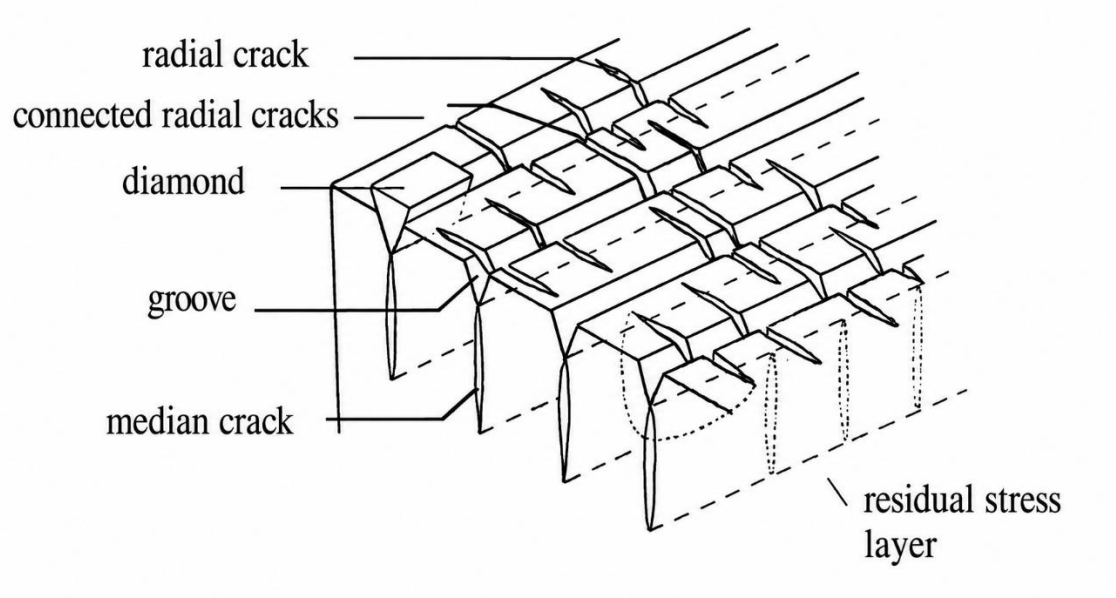


Figure 4. Illustration of grinding defects on a ceramic surface (Tönshoff, 1989).

The illustration shows the overlap of radial cracks extending from one scratch to another, thereby intensifying surface deterioration. Beneath the surface, median cracks and the residual-stress layer are represented; both govern the mechanical strength of the finished workpiece (Hu; Chandra, 1993).

The model proposed in Figure 4 presents the defects that normally accompany material removal, but it does not represent the removal phenomenology observed during grinding. To explain material removal during the grinding of ceramic materials, Malkin and Ritter (1989), Fawcett and Dow (1991), and Warnecke and Rosenberger (1995) used the classical chip-formation model illustrated in Figure 5.

This model focuses exclusively on the grinding zone and shows the theoretical formation of a fully ductile chip along the cutting direction, from zero chip thickness at the entrance to the grinding zone to a maximum chip thickness near the workpiece exit. However, the formation of a chip typical of metallic materials occurs only after a region governed entirely by plastic deformation, identified by the accumulation of material along the lateral edges of the groove. Beyond this region, which is bounded by the critical chip thickness, physical chip formation begins. From this point onward, material may be removed by plastic deformation, with the formation of a ductile chip, or by fracture, with brittle chips detaching as fragments.

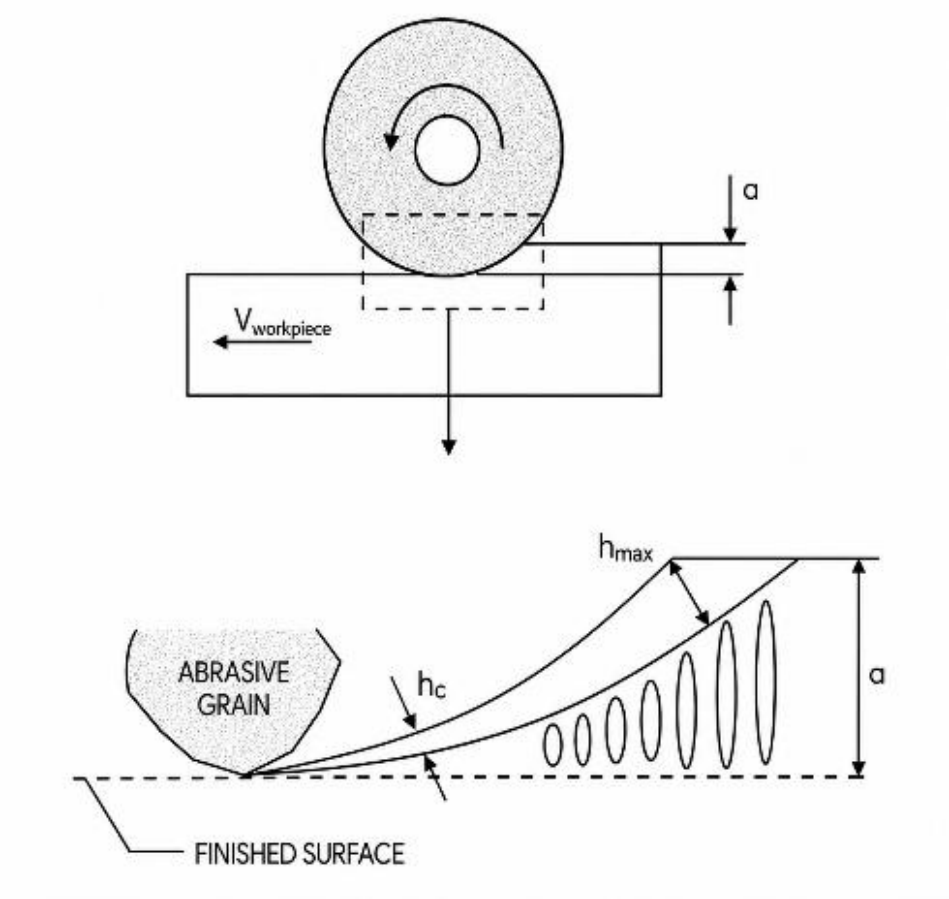


Figure 5. Chip formation during grinding (Malkin and Ritter, 1989).

The latter condition progressively prevails over the former as chip thickness increases along the cut. Nevertheless, Blackley and Scattergood (1994) stated that the presence of fracture-based removal mechanisms does not necessarily mean that grinding is occurring in the brittle regime. This classification applies only when the defects extend below the final workpiece surface; otherwise, the regime may still be considered ductile.

Depending on the material properties, particularly fracture toughness, the critical chip thickness may need to be reduced in order to minimize surface defects. For such a material, the critical chip thickness moves closer to the beginning of the grinding zone, reducing the region in which deformation is exclusively plastic. At the same time, defects begin to form earlier within a narrower region between the grain trajectory and the final workpiece surface, thereby limiting the possibility of grinding in the ductile regime (Blackley; Scattergood, 1994).

2.7. Material Removal Mechanisms in the Grinding of Polycrystalline Ceramics

Investigations by Tonshoff et al. (1994) into the influence of microstructure on material removal mechanisms during the grinding of polycrystalline ceramics showed that plastic deformation predominates over brittle fracture when fine-grained materials are used. Consequently, the surfaces of these ceramics are more regular and exhibit a deeper plastic zone than coarse-grained ceramics, although long cracks may still be present inside the component, as observed in scratching.

In general, a ground workpiece exhibits layers with distinct morphological characteristics. At the surface is a layer of material that has been plastically deformed and displaced laterally by the passage of abrasive grains. The thickness of this layer normally ranges from 0.1 to 1 μm in both fine- and coarse-grained ceramics. Successively deeper layers contain a plastic zone extending from 10 to 30 μm and median cracks whose length may reach 50 μm.

Many studies of brittle material removal attribute the removal of polycrystalline ceramics exclusively to lateral cracking. More recent studies, however, consistently with scratch-test simulations, identify up to three basic removal processes during grinding: (1) individual grain pullout resulting from intergranular microcracks distributed throughout a damaged zone; (2) removal of a portion of material through classical lateral cracks; and (3) fragmentation of part of a crystalline grain as a result of intragranular microcracking (Xu; Jahanmir; Ives, 1996).

The presence of one or more removal processes depends on the machining conditions and, above all, on the strength of the bonds between the grains. Ceramics with strong bonding, such as fine-grained, homogeneous polycrystalline materials - analogous to glasses - develop median, radial, and lateral cracks, which under severe grinding conditions enable removal by transgranular cracking. Nevertheless, grain pullout also occurs.

2.8. Influence of Grinding Parameters on Defect Formation

As in conventional metal grinding, the final quality of a ground ceramic component depends on process variables such as grinding force and energy. These variables ultimately reflect the behavior generated by the input parameters of the grinding system, which comprises the machine tool, the cutting tool, the machining conditions, and the workpiece material (Subramanian; Ramanath; Matsuda, 1990).

Scratch and indentation models show that ceramics can be machined in the ductile regime provided that the deformation scale is kept at a level at which plastic deformation becomes energetically more favorable than fracture (Kendall, 1978).

Grinding efficiency requires the machining conditions to be identified and controlled in order to maximize the removal rate without compromising workpiece quality. In this respect, an important parameter in grinding theory is specific grinding energy. Specific grinding energy assumes higher values at minimum removal rates, that is, under conditions favorable to a predominantly ductile regime. Conversely, in the presence of brittle-fracture mechanisms, specific energy decreases as the removal rate increases. This trend can be observed in Figure 6 for the grinding of silicon nitride (Subramanian; Ramanath; Matsuda, 1990).

Although specific energy is a useful parameter for identifying the material removal regime, it is difficult to measure in grinding operations that require methods more complex than plunge grinding. In the test described above, abrasive-grain depth of cut was estimated and therefore did not correspond exactly to the actual value (Bifano; Fawcett, 1991).

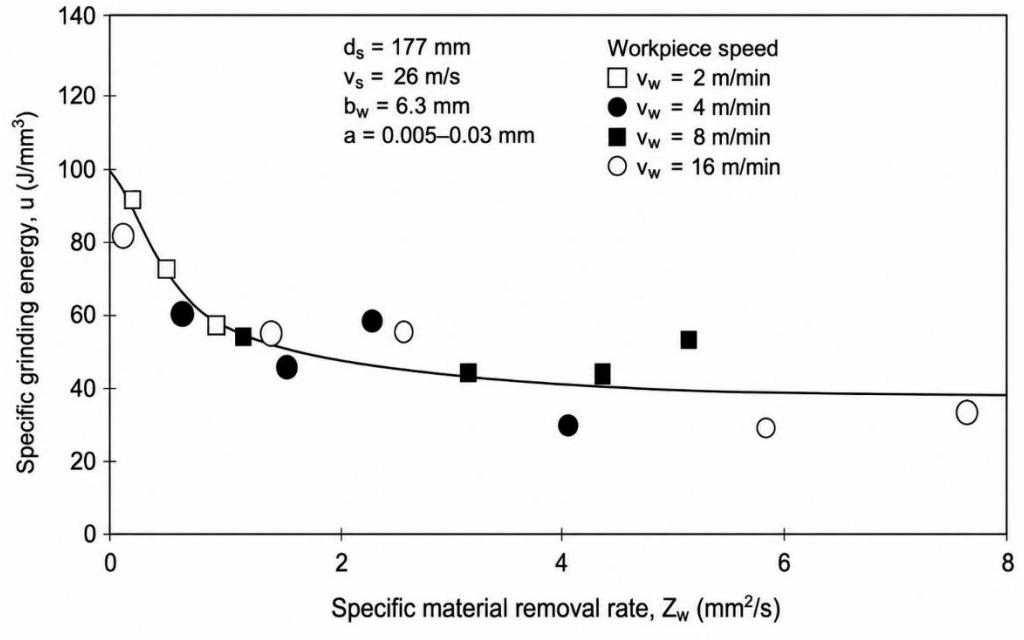


Figure 6. Specific grinding energy as a function of material removal rate (Malkin and Ritter, 1989).

Ceramic materials generally have properties such as a high elastic modulus and hardness that result in less deformation during grinding than in metallic materials. Ceramic workpieces can consequently be produced with better dimensional, geometric, and surface

quality than metals. On the other hand, the forces involved in grinding are higher, increasing the elastic deformation of the machine structural components and the grinding wheel. The resulting force variations may adversely affect workpiece accuracy, cause irregular wheel wear, and generate different material removal mechanisms (Li; Low, 1991).

2.9. Grinding Wheel

According to Rasim et al. (2015), a grinding wheel is a circular tool containing numerous randomly distributed abrasive grains with irregular shapes.

The abrasive grains are held together by a bonding matrix. The combination of these two components produces controlled and defined pores, which are essential for accommodating chips and transporting grinding fluids. The grinding wheel can be considered a tool with undefined cutting-edge geometry because its abrasive grains have randomly shaped cutting edges (Malkin; Bitter, 1989) .

The same authors also stated that grinding wheel performance is directly related to three important characteristics: abrasive grain type and size, the properties of the bond material, and the porosity of the wheel structure.

According to Winter et al. (2015) in addition to the abrasive grains, bond, and pores, the material used for the wheel core is another relevant characteristic, depending on the wheel design. Webster and Tricard (2004) explained that grinding wheel design depends on its profile, thickness, core material when the wheel is not entirely composed of abrasive grains, bond, and pores, ability to withstand rotational stresses, accuracy, and resistance to chemical attack.

A grinding wheel may be entirely composed of a mixture of abrasive grains, bond, and pores or may contain only a thin layer of this mixture, depending on the type of abrasive grain and bond employed.

2.9.1. Grinding Wheel Grade

Grinding wheel grade is defined as the ability of the wheel to resist abrasive grain dislodgement, that is, the ability of the bond to retain the abrasive grains. Therefore, the higher the wheel grade, the fewer abrasive grains will be released (Malkin; Guo, 2008a).

However, according to Rowe (2014a), because harder-grade grinding wheels retain abrasive grains for longer periods, the grains tend to lose their sharpness, increasing the

likelihood of surface burn on the workpiece. In contrast, softer-grade grinding wheels can release worn abrasive grains, thereby exposing new cutting edges and maintaining wheel sharpness.

The same author also stated that grinding wheel grade generally indicates how the wheel will wear. A softer-grade grinding wheel wears more rapidly than a harder-grade wheel because this characteristic depends on the volume of bond within the wheel. Therefore, a higher bond volume results in lower porosity and a harder grinding wheel. The grade is an intrinsic characteristic of the grinding wheel and cannot be altered.

According to Marinescu et al. (2007), the abrasive must be harder than the material being ground. Abrasive hardness can be determined using the Knoop hardness test, which is based on resistance to static indentation.

2.9.2. Grinding Wheel Structure

According to Rowe (2014a), grinding wheel porosity and structure are closely related. A highly porous grinding wheel has an open structure and a lower proportion of bond than a conventional wheel with the same structure. In addition, a highly porous wheel tends to have a softer grade, whereas a wheel with low porosity tends to have a harder grade.

According to the same author, open-structure grinding wheels are essential for high material removal rate operations because they contain a large volume of pores in which chips can be accommodated. In this type of grinding, porosity also facilitates grinding fluid transport, which is particularly important because of the considerable amount of heat generated.

Marinescu et al. (2007) stated that porosity is necessary to achieve effective cutting action. However, it reduces the maximum permissible grinding wheel speed because greater porosity decreases the wheel's mechanical strength. Porosity also facilitates the release of abrasive grains from the grinding wheel.

2.9.2.1. Abrasives

According to Malkin and Guo (2008a), abrasives may be natural or synthetic and must be considerably harder than the materials to be machined.

According to Marinescu et al. (2007), abrasives can be considered cutting tools with undefined geometry, high hardness, cutting edges, and good cutting ability. The sharpness of

abrasive grains is described in terms of the cutting-edge radius and apex angle, while their cutting ability depends on factors such as grain structure and friability.

Grinding generates high temperatures. Therefore, a suitable abrasive must retain its hardness, exhibit low chemical reactivity, and resist diffusion into the workpiece material. Furthermore, the thermal properties of abrasives are extremely important for their wear resistance.

The same authors also stated that increasing temperature reduces the hardness of most abrasives, except for abrasive material, which transforms into a harder structure at high temperatures. Therefore, the thermal properties of the abrasive and the temperature at which grinding occurs must be considered to prevent premature abrasive wear.

Klocke (2009) also stated that an abrasive must possess high hardness and mechanical strength to facilitate chip formation and maintain sharp cutting edges for a considerable period.

According to Sinha et al. (2016), abrasive wear can be attributed to the following factors:

- Friction between the workpiece and the abrasive
- Plastic deformation at high temperatures
- Fracture caused by mechanical impact
- Chemical reactions between the abrasive and the workpiece at high temperatures

2.9.2.2. Abrasive Grain Size

The dimensions and size uniformity of abrasive grains can be classified according to the American standard ANSI B74.12-1977, Specification for Size of Abrasive Grain. This standard specifies grain size in mesh, defined as the number of openings per linear inch of the sieve on which the grains are retained during the classification process. It is commonly applied to conventional abrasive grains (Marinescu et al., 2007).

According to the same authors, superabrasive grains are classified according to the European FEPA standard (Federation of European Producers of Abrasives), which specifies the theoretical grain diameter. Table 1 presents the correspondence between the FEPA and ANSI standards.

Coarse abrasive grains should be used for:

- Ductile or fibrous materials, such as low-carbon steels and aluminum alloys

- High material removal rates during rough grinding
- Workpieces without strict surface quality requirements
- Large contact areas

Fine abrasive grains should be selected for:

- Hard or brittle materials, such as cemented carbide and glass
- Workpieces requiring a high-quality surface finish
- Small contact áreas

2.9.2.3. Friability

Marinescu et al. (2007) defined friability as the tendency of an abrasive grain to disintegrate into small fragments when subjected to pressure. According to Nascimento et al. (2016), friability is an essential characteristic for evaluating an abrasive material.

The greater the friability of a grain, the more readily it fractures and produces new cutting edges. Therefore, friability is advantageous for maintaining grinding wheel sharpness. However, this characteristic is also associated with grinding wheel wear because greater friability results in more frequent grain fracture and, consequently, greater wheel wear (Rowe, 2014).

Regarding grain strength, a stronger grain is less likely to fracture upon contact with the workpiece. Conversely, the more friable and less resistant the grain, the greater its tendency to fracture and generate new cutting edges. Consequently, the grinding wheel undergoes self-sharpening during the grinding process (Malkin; Guo, 2008a).

Acoording to Marinescu et al. (2007) the larger the crystal, the more friable it becomes, and lower cooling rates result in larger crystals. Therefore, friable grains are obtained when the material is cooled rapidly.

2.10. Types of Abrasives

Marinescu et al. (2007) classified abrasive materials into two groups:

- Conventional abrasives, such as silicon carbide (SiC) and aluminum oxide (Al_2O_3).
- Superabrasives, such as diamond and cubic boron nitride (CBN)

There is a considerable difference in hardness between the materials belonging to these two groups. This results in different grinding wheel wear behaviors and directly influences the grinding process. Cost is another factor that distinguishes conventional

abrasives from superabrasives, as a superabrasive grinding wheel may be 10 to 100 times more expensive than a conventional abrasive wheel (Marinescu et al., 2007)

In some cases, grinding is only feasible with superabrasives because they are harder and more resistant to wear. Consequently, longer intervals between dressing operations can be employed, reducing operating costs and making the investment in superabrasives economically advantageous despite their higher initial cost (Rowe, 2014a).

According to Marinescu et al. (2007), superabrasive grinding wheels are generally manufactured with only a thin abrasive layer around their periphery, while the wheel core is made of materials such as polymers or metals. This design reduces the amount of abrasive material required and, consequently, the cost of the grinding wheel. Furthermore, it enables high material removal rates because the wheel can operate at high rotational speeds.

2.10.1. Diamond

Diamond is the hardest known material and is therefore used to grind extremely hard materials, including the hardest ceramics. It also exhibits one of the highest thermal conductivities at room temperature, which contributes to reducing grinding temperatures. However, its thermal conductivity decreases at elevated temperatures (Rowe, 2014).

According to Marinescu et al. (2007), diamond hardness is difficult to measure because diamond undergoes almost no deformation at room temperature. Furthermore, because hardness tests use a diamond indenter, producing deformation in the diamond specimen is particularly difficult.

At room temperature, diamond has the highest thermal conductivity of any material, ranging from 600 to 2,000 W/(m·K). However, this value decreases to approximately 70 W/(m·K) at 700 °C.

Marinescu et al. (2007) stated that diamond occupies a unique position in industry because it is the only material capable of dressing any type of grinding wheel.

Nascimento et al. (2016) stated that diamond is thermally stable up to 800 °C in air and above 1,400 °C under vacuum. Therefore, it is an abrasive with good hardness retention at elevated temperatures. Rowe (2014a) stated that because diamond is composed of carbon, it is unsuitable for grinding steels. Carbon has a strong chemical affinity for the iron present in steel, resulting in excessive abrasive wear and a considerable increase in temperature.

Marinescu et al. (2007) explained that diamond, which is metastable at atmospheric pressure, tends to transform into graphite at relatively low temperatures—approximately 700

°C in air and 1,500 °C in an inert atmosphere. This transformation facilitates chemical wear and the formation of compounds such as Fe3C, resulting in premature wear of the diamond grains. Consequently, diamond is particularly suitable for grinding ceramic materials.

Rowe (2014) further explained that another source of diamond abrasive wear is its exposure to oxygen at elevated temperatures. Diamond remains thermally stable up to approximately 760 °C in air and 1,400 °C under vacuum before oxidation begins.

Natural diamonds used in industry are generally those rejected by the jewelry market because they do not meet the required standards for shape, color, or size or because they contain crystalline defects. However, most diamonds used for industrial applications are synthetic because synthetic diamond is less expensive than natural diamond. Most industrial diamonds are used in grinding wheels or single-point dressing tools (Marinescu et al., 2007).

The shape and size of natural diamonds are determined by geological conditions during their formation (Malkin; Guo, 2008a). They predominantly grow in an octahedral form and exhibit sharp points that are particularly suitable for single-point diamond tools. Therefore, synthetic diamond predominates in grinding wheel production, whereas natural diamond is commonly used in dressing tools (Marinescu et al., 2007).

Synthetic diamonds are produced by subjecting graphite to high temperatures and pressures in the presence of a catalyst, such as nickel or another transition metal. Crystal size and structure vary according to the temperature, pressure, and processing time (Malkin; Guo, 2008a) .

According to Marinescu et al. (2007), the catalyst reduces the temperature and pressure required to transform carbon into diamond, thereby making the manufacturing process more flexible. Furthermore, controlling the processing time and nucleation density makes it possible to produce high-quality grains with specific morphologies: cubic at low temperatures, cuboctahedral at intermediate temperatures, and octahedral at high temperatures.

2.11. Bond Materials

Bond materials play an essential role in the grinding wheel structure because they hold the abrasive grains in place. They must withstand grinding forces, elevated temperatures, centrifugal forces generated by high wheel rotational speeds, and chemical attack resulting from the use of grinding fluids. In addition, the bond must provide rigidity to the grinding wheel and maintain the abrasive grains in position (Malkin and Bitter, 1989).

Rowe (2014a) classified the bond materials used in grinding wheels into three main categories: resinoid, vitrified, and metallic bonds.

According to Marinescu et al. (2007), the bond must be capable of:

- Providing adequate grain retention without allowing premature abrasive grain dislodgement
- Undergoing controlled erosion to expose the cutting edges of the abrasive grains
- Having sufficient strength to transfer grinding forces from the spindle to the workpiece
- Providing adequate heat dissipation during the grinding process

Most conventional abrasive grinding wheels use vitrified or resinoid bonds, whereas most superabrasive grinding wheels use resinoid or metallic bonds. However, vitrified bonds are also used in CBN grinding wheels (MALKIN; GUO, 2008a).

Jackson et al. (2001) stated that grinding wheel size, operating conditions, wheel life, and manufacturing cost should be considered when selecting a bond material. Furthermore, the bond is directly related to the aggressiveness of a grinding wheel (Bianchi et al., 2011).

2.11.1. Resinoid Bonds

Grinding wheels with resinoid bonds tend to be more elastic than wheels containing other types of bonds. Therefore, elasticity is a determining factor when selecting a resinoid bond. This property can be useful in two situations: ensuring operational safety at high speeds and allowing the application of pressure to produce a more polished surface. Resinoid bonds are mainly used with conventional abrasives; however, when combined with superabrasive grains, they can also produce extremely low surface roughness values. An important limitation is that, because of their organic nature, resinoid-bonded grinding wheels have a limited shelf life, even when they are not used (Rowe, 2014)

Resinoid-bonded grinding wheels are the most widely used type. In some applications, they are combined with diamond grains for grinding cemented carbides and ceramics, as well as with CBN superabrasive grains for grinding cutting tools (Webster; Tricard, 2004).

Malkin e Guo (2008a) stated that resinoid-bonded wheels containing conventional abrasives are widely used for heavy-duty grinding because of their high strength and ability to withstand impact. However, resinoid bonds are susceptible to chemical attack by alkaline grinding fluids, particularly when exposed to high temperatures for prolonged periods.

According to Rowe (2014a), all resinoid bonds undergo excessive wear when exposed to elevated temperatures.

Resinoid-bonded grinding wheels are manufactured by mixing abrasive grains with synthetic resins and plasticizers. The mixture is then molded into the final wheel geometry and cured in a furnace at temperatures ranging from 150 to 200 °C (Malkin; Guo, 2008a).

Another application of resinoid bonds is in cut-off wheels, which are reinforced with fiberglass to increase their strength and enable operation at high cutting speeds of up to 100 m/s (Webster; Tricard, 2004).

Marinescu et al. (2007) classified resinoid bonds into three types:

- Plastic: The softest type and commonly used with conventional abrasives. This bond is employed in double-disc and grinding. In superabrasive wheels, plastic bonds are used for high-precision grinding, typically with diamond micrograins in the glass and ceramics industries.
- Phenolic resin: The second most widely used bond material and the predominant type in rough-grinding operations. This type of bond was formerly known as Bakelite.
- Polyimide resin: This bond exhibits greater strength, higher thermal resistance, and lower elongation than phenolic resins. Therefore, it can retain abrasive grains for longer periods at elevated temperatures.

2.12. Dressing

Dressing is the process of creating and exposing new cutting edges on the grinding wheel surface, thereby restoring the cutting ability of the tool (Srivastava et al. 1988).

According to Marinescu et al. (2007), dressing aims to make the grinding wheel perfectly circular and concentric with its axis of rotation, remove workpiece material embedded in the wheel surface, expose new abrasive grains with sharp cutting edges, and remove the bond surrounding the grains to increase their exposure.

In principle, a grinding wheel should self-sharpen as it wears. Worn abrasive grains should either fracture and generate new cutting edges or be released by the bond, thereby exposing new grains. However, this process is not always effective, and dressing is therefore required to restore the cutting characteristics of the tool (Jackson et al., 2007) .

According to Rowe (2014), dressing is a grinding wheel preparation operation with the following functions:

- Correct deviations in the grinding wheel geometry

- Produce and standardize sharp cutting edges
- Remove the bond surrounding the abrasive grains to create a more open wheel surface, particularly in resinoid- and vitrified-bonded wheels
- Remove the abrasive layer loaded with chips generated during machining

During grinding, approximately 10% of the grinding wheel is consumed while machining the workpiece, whereas approximately 90% is consumed during dressing. Nevertheless, this sharpening process is essential because the cutting edges of the abrasive grains become rounded during grinding, increasing the grinding forces. Wheel loading may also occur when workpiece material clogs the pores of the wheel. Without dressing, the grinding wheel loses its cutting ability, and the surface quality of the workpiece deteriorates (Jackson et al., 2007).

The application of grinding fluid during dressing is essential to maintain the diamond at a low temperature. The fluid must be supplied before dressing begins to prevent thermal shock in the dressing tool (Rowe, 2014).

Grinding wheel irregularities such as surface roughness, waviness, wear, and profile loss are classified as macroscopic defects. These defects cause problems during grinding and reduce the dimensional accuracy of the machined workpieces. In contrast, the loss of cutting ability of the abrasive grains is considered a microscopic defect. This condition increases the grinding forces and the required power. These defects also increase the risk of thermal damage to the workpiece. Therefore, dressing aims to establish the conditions required for efficient grinding wheel operation (Klocke, 2009).

According to the same author, dressing is necessary both before the first use of the grinding wheel and throughout the grinding process to maintain workpiece quality. Oliveira et al. (2009) defined the concept of the dressing point as the appropriate moment to perform this operation, when the abrasive grains have lost their cutting edges and can no longer remove material efficiently. If dressing is performed too late, the risk of surface burn, cracking, and workpieces outside dimensional tolerances increases. Conversely, premature dressing causes unnecessary wheel wear and production downtime.

The dressing method is selected according to economic and quality requirements, as well as the type of abrasive, bond, and grinding wheel geometry. These parameters determine the suitable dressing methods and tools (Klocke, 2009).

Marinescu et al (2007) classified dressing tools into two basic categories: stationary and rotary dressers. According to Rowe (2014) stationary dressers can be further divided into single-point and multipoint dressers.

During mechanical dressing with a stationary tool, the dresser does not move in the peripheral direction of the grinding wheel. Instead, the wheel profile is generated by the axial movement of the dresser across the wheel contour, which explains why this process is often compared with turning (Klocke, 2009).

Single-point diamond dressers consist of an octahedral diamond mounted in a steel holder (Klocke, 2009), with approximately one-third of the diamond remaining exposed after mounting (Marinescu et al., 2007).

Rowe (2014) stated that the dresser should be periodically rotated to present a different cutting edge during dressing. Otherwise, the diamond wears predominantly along a single edge, reducing process efficiency because of the resulting increase in dressing forces.

Dressing with a single-point diamond dresser produces both macro- and micro-effects. The macro-effect results from the dresser geometry and dressing conditions and determines the arrangement of the cutting edges within the grinding wheel topography. In other words, it produces a thread-like pattern on the wheel surface through the combination of the relative movements between the dresser and the grinding wheel. The micro-effect was defined by Malkin (1989), as the removal or fracture of worn abrasive grains from the bond, thereby generating new cutting edges.

Regarding the dressing micro-effect, Rowe (2014) stated that grinding wheel smoothness depends on the dressing overlap ratio Ud, which is defined as the number of times a point on the grinding wheel surface is covered by the dresser. The overlap ratio can be expressed as follows:

$$U_d = \frac{b_d}{s_d} \qquad (1)$$

where: b_d is the effective dresser width and s_d is the dressing lead per wheel revolution.

Rowe (2014) also emphasized that increasing the dressing overlap ratio produces a smoother grinding wheel surface, thereby increasing the grinding forces and specific grinding energy. A low overlap ratio produces a sharper but rougher wheel surface. Multipoint dressers contain several cutting points, resulting in a longer service life. Furthermore, they can be manufactured in different geometries to accommodate different types of grinding wheels. The spatial arrangement of the abrasive grains allows higher dressing feed rates and greater dressing widths. However, under these conditions, the dressing results may be less predictable (Rowe, 2014).

According to the same author, rotary dressers have a longer service life than single-point dressers because they contain a larger quantity of diamond. Two main configurations may be employed: a narrow disc with a diamond layer around its periphery or a cup-shaped dresser with a diamond layer along its rim. The latter can replace a single-point dresser and is used similarly by traversing the dresser across the grinding wheel surface.

Because rotary dressers are narrower than the grinding wheels being dressed, they must move laterally across the wheel surface Klocke (2009). Cup-shaped dressers are generally used for dressing grinding wheels in serial production but are limited to wheels with simple profiles. Grinding wheels with nonlinear profiles are typically dressed using rotary diamond discs.

2.13. Grinding Fluid

During the relative cutting motion between the workpiece and the tool, nearly 99% of the energy supplied to the machine is converted into heat. When machining ferrous materials, the temperature increases with cutting speed, while tool strength decreases, resulting in accelerated tool wear and potentially leading to tool failure (Bruni et al., 2006).

Barczak et al. (2010) emphasized that material removal in abrasive processes is challenging because of the high temperatures generated. Therefore, effective lubrication and cooling are essential to prevent excessive temperatures. Oliveira et al. (2012) stated that grinding fluids reduce both temperature and friction, thereby minimizing forces and residual stresses in the workpiece.

According to Debnath et al. (2014) grinding fluids also improve the final quality of the workpiece by providing better dimensional control and surface quality. Surface quality is not merely related to appearance, as low surface roughness improves the corrosion resistance of the workpiece and reduces residual stresses. Grinding fluids also remove chips from the cutting zone.

High-speed machining provides greater productivity; however, the resulting high temperatures limit the cutting speed because of accelerated tool wear. The use of a worn tool increases energy consumption and reduces the surface quality of the workpiece. Therefore, the cutting zone must be cooled to extend tool life and maintain the desired surface finish (Sharma; Tiwari; Dixit, 2016). Similarly, Sanchez et al. (2010) emphasized that large amounts of thermal energy must be removed from the process; otherwise, workpiece burn and thermally induced deformation may occur.

Regarding the temperature increase in the cutting zone, Malkin & Guo (2008) stated that several types of thermal damage may occur, including workpiece burn, phase transformations, changes in surface hardness, unfavorable surface residual stresses, cracking of the workpiece and grinding wheel, and reduced fatigue strength.

Grinding fluids are employed to improve the tribological conditions that are invariably present at the contact interface between the workpiece and the tool. Therefore, they generally improve the efficiency of the production system in which they are employed (Soković; Mijanović, 2001).

According to Irani et al. (2005), thermal damage is one of the primary limiting factors in grinding. This damage can be reduced through the application of grinding fluids because they decrease the temperature in the cutting zone through heat transfer.

In general, grinding fluids cool the cutting zone, lubricate the contact between the workpiece and the tool—thereby reducing friction—and remove chips from the cutting zone. Klocke (2009) also stated that grinding fluids protect both the grinding machine and the workpiece against corrosion. In many cases, their formulations are specifically designed for this purpose through the addition of anticorrosion additives.

The same author stated that viscosity is the primary physical property of a grinding fluid because it is directly related to its two main functions: lubrication and cooling. Low-viscosity fluids generally provide greater cooling capacity and are easier to remove from the workpiece and filter. However, they also tend to generate more vapor and mist, which may cause skin irritation and respiratory disorders.

Grinding fluids reduce temperature by directly removing heat from the process and maintaining the cutting efficiency of the grinding wheel through friction reduction, thereby decreasing the specific grinding energy (Rowe, 2014).

As a consequence of these fundamental functions, grinding fluids reduce the power required for material removal and overall energy consumption, extend tool life, and improve the surface finish of the machined workpiece. However, the costs associated with their use have been shown to represent a significant portion of the total manufacturing cost of the workpiece (Bruni et al., 2006).

Therefore, according to Barczak et al. (2010), controlling heat generation during grinding is essential to ensure the quality and thermal integrity of the finished workpiece. Owing to friction, elastic deformation, and chip formation, temperatures in the cutting zone may reach approximately 1,800 °C. However, these temperatures persist for only a few milliseconds and are proportional to the cutting speed. The authors also noted that the most

widely used industrial method is conventional flood cooling, in which grinding fluid is supplied abundantly to the cutting zone at a relatively low velocity.

2.13.1. Problems Associated with the Use of Grinding Fluids

Despite the economic benefits associated with grinding fluids, their improper use and disposal can severely affect human health and the environment. Furthermore, grinding fluids account for approximately 16% to 20% of total manufacturing costs in the production industry (Sharma et al. 2016).

The various substances present in these fluids may affect machine operators through skin contact, accidental ingestion, inhalation, and exposure to irritating fluid mists generated by evaporation. After use, grinding fluids may be treated and disposed of internally by the company or externally by a specialized waste-management company (Soković; Mijanović, 2001).

According to Bruni et al. (2006), the quality of the fluid and the manner in which it is disposed of may result in water, soil, and air pollution. In Brazil, CONAMA Resolution No. 430/2011 establishes regulatory limits for the discharge of mineral, animal, and vegetable oils in effluents, requiring industries to adopt appropriate procedures for grinding fluid treatment and disposal. However, proper disposal considerably increases operating costs.

During use, the fluid undergoes changes because new substances are formed or incorporated into it, including foreign matter and microorganisms. Although the original fluid already poses health risks, these risks may increase throughout its service life (Soković; Mijanović, 2001)

Considering the negative effects of grinding fluids on human health and the environment, increasingly stringent criteria have been adopted for their selection. These fluids must provide adequate process performance, minimize environmental impacts, and comply with applicable regulations. Environmental requirements are therefore imposing new constraints on machinability parameters, making the development and adoption of high-performance, environmentally friendly fluids a common interest (Soković; Mijanović, 2001)

Under these circumstances, industry has increasingly sought to comply with more environmentally conscious sustainability standards (Umeda et al., 2012). Following this trend, scientific research has increasingly focused on evaluating and improving the sustainability of abrasive processes (Aurich et al., 2008) .

2.13.2. Costs Associated with Grinding Fluids

Total machining costs depend on expenses related to the machine—including wear, labor, grinding fluids, and maintenance—as well as facilities and energy consumption (Winter; Herrmann, 2014).

Walker (2013), stated that the cost of grinding fluids applied through conventional flood cooling is high compared with other manufacturing expenses. These costs include fluid acquisition, maintenance, and disposal. It is estimated that grinding fluid expenses account for approximately 8% to 16% of total production costs and may even exceed expenditures on cutting tools (Dhar; Kamruzzaman; Ahmed, 2006). Therefore, reducing grinding fluid consumption is economically justified (Walker, 2013).

According to Alberdi et al. (2011), in addition to the factors previously mentioned, recycling, safety measures, and other operational requirements also contribute to the costs associated with grinding fluids. In the automotive industry, expenditures related to grinding fluids may represent between 15% and 30% of total manufacturing costs (Rabiei et al., 2015).

2.13.3. Maintenance and Disposal

During the use of grinding fluids in machining operations, small quantities of material, such as grinding wheel debris and chips, inevitably accumulate in the fluid. Owing to the high concentration of organic compounds in its composition, this contamination promotes microbial proliferation. Consequently, the chemical composition of the fluid changes, altering its fundamental properties and potentially increasing tool wear and the production of defective workpieces (Oliveira et al., 2012).

Monitoring and maintaining grinding fluid quality are essential for successfully reducing fluid consumption at the source. The most relevant monitoring practices include system inspections; periodic measurement and adjustment of parameters such as concentration, pH, and microbial growth; appropriate biocide dosing; and the removal of tramp oil and chips.

Regarding storage, grinding fluid quality control begins with appropriate storage conditions, with temperature being a particularly important parameter. Extreme temperatures should be avoided. Furthermore, water-soluble grinding fluids require greater care during storage than straight oils because of the complex chemical composition of emulsifiable fluids, which makes them more susceptible to physical changes caused by extreme storage temperatures.

Specific regulations establish requirements for the proper handling of grinding fluids. Brazilian Ministry of Transport Ordinance No. 204/1997 regulates the transportation of contaminated fluids, whereas ANTT Resolution No. 420 of February 12, 2004, provides supplementary instructions to the regulations governing the inland transportation of hazardous products.

The disposal of grinding fluids has become increasingly important in industrial environments. This is primarily due to increasingly stringent environmental legislation, which requires specific procedures for disposing of different types of fluids (Lauer-Schmaltz and König, 1980). Some of these procedures, as described by (Lauer-Schmaltz; König, 1980). Sokovic & Mijanovic (2001) are presented below.

Straight oils can be sold for rerefining or recycled by the fluid manufacturer or specialized companies. These oils may also be incinerated in boilers, provided that environmental regulations are observed. For this purpose, the oil must be free of impurities, dry, and contain low concentrations of sulfur and chlorine.

For water-soluble grinding fluids, the oil and other chemicals dissolved in the water must be separated. Even after this separation, the fluids cannot be discharged directly into the sewage system.

Emulsion disposal processes can be classified as chemical, physical, or physicochemical. The selection of the most appropriate procedure depends on the condition and composition of the emulsion, as well as the associated processing costs. These procedures generally involve three stages: emulsion breaking, oil separation, and water treatment. The resulting aqueous phase must comply with applicable legislation before its final disposal.

The most widely used physical processes include ultrafiltration and thermal separation. In ultrafiltration, the emulsion circulates through permeators containing tubular membranes whose pores prevent oil molecules from passing through, thereby separating the emulsion phases. In thermal separation, the oily phase is separated from the aqueous phase by heating the emulsion and evaporating the water.

Recycling can therefore be a suitable alternative for grinding fluids because pollutants are separated and removed, allowing the treated fluid to be reused together with fresh fluid. This reduces the frequency of disposal and directly lowers process costs.

The procedures required for using cutting oils make their application particularly costly. This is mainly associated with nonbiodegradable products, which generate additional treatment and disposal expenses (Shokrani; Dhokia; Newman, 2012). Furthermore, the

improper disposal of oil-based grinding fluids may contaminate surface water and groundwater and cause air and soil pollution (Hadad, 2015) .

Considering that grinding fluid disposal considerably increases process costs, the adoption of alternative lubrication and cooling techniques is particularly advantageous.

2.13.4. Minimum Quantity Lubrication - MQL

Bianchi et al. (2012) explained that the minimum quantity lubrication (MQL) technique essentially consists of applying a compressed-air jet containing a minimum amount of grinding fluid directly to the cutting zone. However, the amount of fluid supplied must be sufficient to reduce friction and prevent material adhesion.

According to the same authors, this technique employs a small quantity of lubricating oil combined with a compressed-air flow. This mixture forms a mist that is directed toward the contact region between the workpiece and the grinding wheel. Because the targeted application of the lubricant mist reduces friction in the wheel–workpiece contact zone, less heat is generated during grinding, thereby helping to preserve the integrity of both the tool and the workpiece against thermal damage.

According to Malkin and Guo (2008b), conventional flood cooling is not highly efficient in grinding because the fluid may not adequately penetrate the contact zone between the workpiece and the grinding wheel. Furthermore, the large volume of fluid employed may adversely affect human health and the environment.

Emami et al. (2013a), stated that MQL reduces production costs because of the smaller volume of grinding fluid required, potentially decreasing the total process cost by up to 20%. In addition, it can eliminate or reduce respiratory and dermatological problems and decrease soil and water contamination resulting from improper fluid disposal. In this context, the development of alternative lubrication and cooling techniques is clearly important.

Lopes et al. (2018a) concluded that MQL combined with grinding wheel cleaning is a viable alternative to conventional flood cooling in grinding. The authors evaluated several output variables and found that, although this technique resulted in poorer performance for some of them, its application was associated with a considerable reduction in costs.

Ruzzi et al. (2020), investigated the grinding of AISI 4340 steel using an aluminum oxide grinding wheel. The authors reported that MQL improved the average surface roughness at higher plunge speeds, producing lower values than conventional flood cooling. According to the authors, this behavior may be explained by the ability of the compressed-air

jet employed in MQL to disrupt the air barrier formed around the grinding wheel during operation. Under conventional flood cooling, this air barrier may remain around the wheel because the pressure of the grinding fluid is lower than that of the compressed air used in MQL, unless the fluid jet velocity exceeds the grinding wheel peripheral speed. MQL also provided advantages in terms of diametral wheel wear, outperforming conventional flood cooling at all plunge speeds. The authors attributed this result to the superior lubricating capability of MQL. Furthermore, lower grinding power values were recorded with MQL than with conventional flood cooling, also because of the improved lubrication provided by the technique.

2.13.5. Wheel Cleaning Jet - WCJ

According to Choi et al. (2002), a compressed-air jet is an alternative for preventing material adhesion during grinding because the air is directed onto the grinding wheel and removes debris adhering to the tool. The auxiliary grinding wheel cleaning system essentially consists of applying compressed air to the wheel at a point outside the cutting zone. This method helps reduce wheel loading by expelling part of the sludge formed by chips and grinding fluid. Furthermore, the compressed-air jet disrupts the air barrier generated around the grinding wheel by its rotation. Consequently, the grinding fluid can reach the cutting zone more easily, further reducing the clogging of the wheel pores. Therefore, auxiliary cleaning improves lubrication and cooling in the cutting zone and minimizes problems caused by clogged pores.

In this context, investigated the effectiveness of installing an auxiliary cleaning system during the grinding of ABNT 4340 steel with a CBN grinding wheel under MQL conditions. The authors concluded that MQL combined with an auxiliary cleaning system employing a jet impingement angle of 30° relative to the grinding wheel axis effectively produced better results for all the output variables analyzed. They also reported that, even as the cutting speed increased, the superior performance of the MQL system combined with the 30° compressed-air jet was maintained. This makes it possible to increase the specific material removal rate—and consequently reduce the machining time—without compromising the final quality of the workpiece.

It should be emphasized that Oliveira et al. (2012a) observed that MQL combined with cleaning of the grinding wheel cutting surface produced surface roughness comparable to that obtained using conventional flood cooling.

Ruzzi et al. (2017b) concluded that all surface roughness values decreased when the grinding wheel cutting surface was cleaned, regardless of the grinding fluid dilution employed under MQL conditions. This occurred because the cleaning system minimized the clogging of the pores on the grinding wheel cutting surface, thereby improving grinding efficiency. The authors also observed that workpiece roundness deviations decreased when the wheel cutting surface was cleaned. Once again, this was attributed to the ability of the cleaning method to reduce wheel loading, thereby decreasing friction, heat generation, and thermal distortion.

In the study conducted by Ruzzi et al. (2020), MQL combined with wheel cleaning produced the lowest average surface roughness values at all plunge speeds. At higher material removal rates, the resulting roughness was considerably lower than that obtained using conventional flood cooling. This behavior can be explained by the removal of material clogging the grinding wheel pores, which consists of a mixture of chips, grinding fluid, and worn abrasive grains generated during grinding. Cleaning the grinding wheel pores improves contact between the abrasive grains and the workpiece surface, chip formation, and lubricant penetration into the cutting zone. Furthermore, MQL combined with wheel cleaning resulted in the lowest diametral wheel wear among the conditions tested, highlighting the effectiveness of the cleaning system. However, the authors evaluated grinding power under the three lubrication and cooling conditions and observed that power consumption increased when the cleaning system was employed. The air jet applied at an impingement angle of 30° generates a reaction force on the wheel cutting surface that removes the adhered sludge but also produces a force component opposing wheel rotation, thereby increasing the power required to maintain its rotation.

Bianchi et al. (2018b) evaluated the grinding of AISI 4340 steel with an aluminum oxide grinding wheel using MQL and MQL combined with wheel cleaning. Because MQL with wheel cleaning resulted in lower surface roughness than conventional MQL, the authors stated that the cleaning jet improved chip evacuation from the contact zone, thereby preventing wheel loading. Furthermore, because the material removal mechanism in grinding occurs at the microscale and consists of three stages—rubbing, plowing, and cutting—the rubbing and plowing stages are highly inefficient in terms of material removal, whereas chip formation occurs only during the cutting stage. During rubbing and plowing, a considerable amount of energy is consumed by deformation and friction at the surface being machined and is converted into heat within the grinding zone. When the grinding wheel pores become filled with chips, as observed under conventional MQL conditions, the cutting stage is impaired,

resulting in several adverse effects, including poorer surface finish and greater geometric and dimensional errors.

3. METHODOLOGY

The grinding experiments were performed on a tangential surface grinding machine (Vitor & Buono, model VB-1224). The machine is equipped with a horizontal spindle and a hydraulic reciprocating table measuring 600 × 300 mm. Grinding tests were conducted using a diamond grinding wheel manufactured by Rediam (model 461722), featuring an outer diameter of 300 mm, a width of 10 mm, and an abrasive layer thickness of 6 mm. The abrasive grains consisted of synthetic diamond with a D91 grit size, corresponding to the MESH 170/200 range, and were bonded w a resin bond of grade R hardness. The grinding parameters, including wheel speed, table feed rate, and depth of cut, were adjusted and controlled through the machine system. All grinding tests investigated in this study were carried out using this experimental setup. For each lubrication-cooling condition, five alumina workpieces were ground, and each workpiece was considered an independent grinding test. The results presented in the graphs correspond to the mean values obtained from these five workpieces, and the error bars represent the standard deviation calculated from the five results for each condition. To ensure comparable initial wheel conditions between tests, the grinding wheel was dressed after each workpiece. Dressing was performed using a conglomerate-type multi-granular dresser manufactured by Master Diamond, with a parallelepiped geometry and dimensions of 15 mm × 8 mm × 10 mm. The total dressing depth was 0.2 mm, applied over 50 cycles, corresponding to 0.004 mm per cycle, and the dressing speed was 500 mm/min. The details of this setup are illustrated in Figure 7 (A) and (E). The main grinding conditions and experimental parameters adopted in this study are summarized in Table 1. The workpieces used in the grinding experiments were manufactured from reactive calcined alumina powder (Alumina 1000 SG, Almatis Inc./USA), composed of submicrometric particles with an average size of approximately 0.5 μm.

Granules of #80 mesh size were obtained from slurry drying composed of 30 vol% alumina powder, Poly (vinyl butyral) (PVB) as organic binder 2 wt.% relative to the alumina powder, p-aminobenzoic acid (PABA) of 0,05 wt.% as dispesant and Isopropanol as a vehicle (balance).

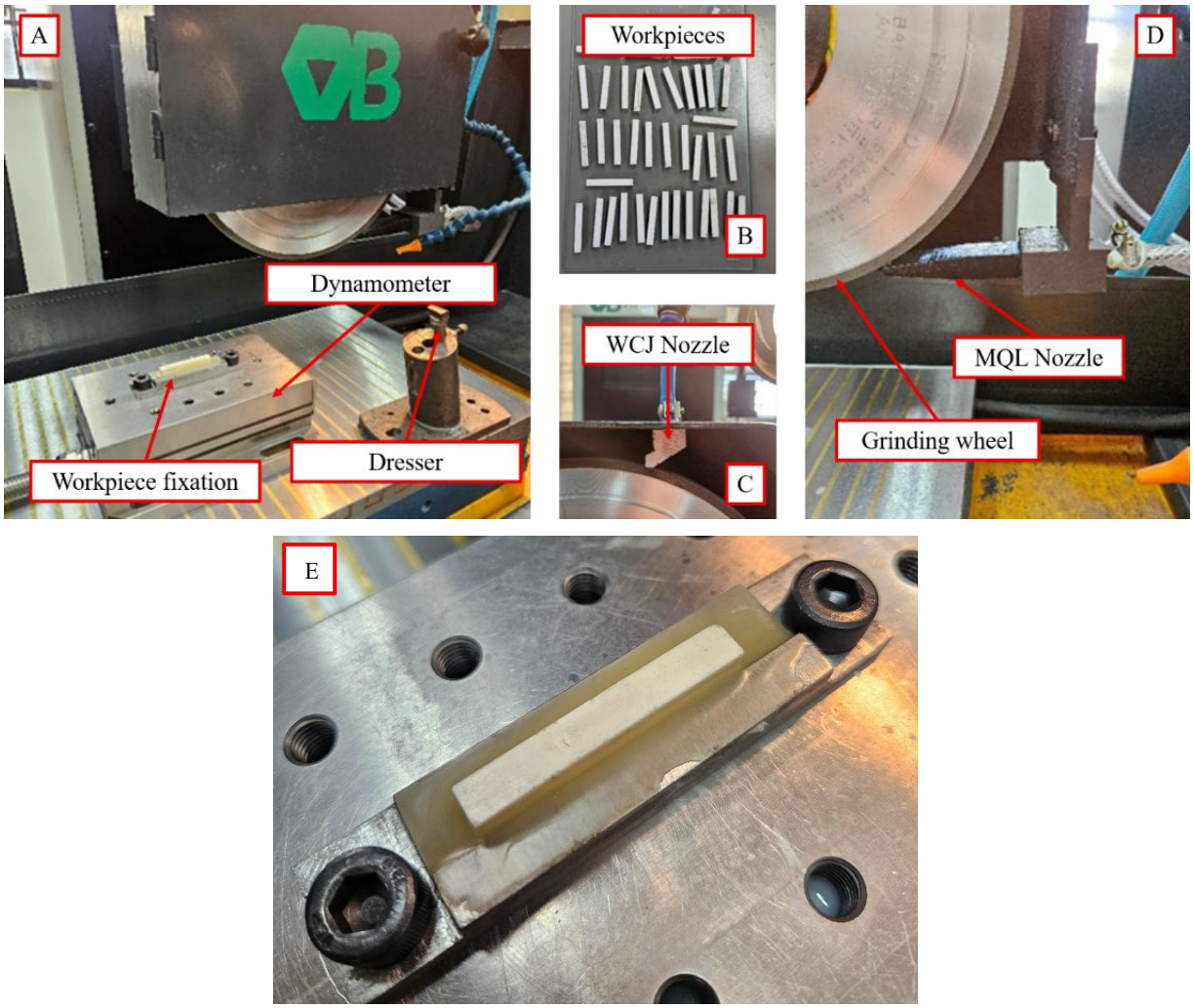


Figure 7. (A) Experimental setup; (B) Workpieces; (C) WCJ Nozzle; (D) MQL Nozzle. (E) Workpiece fixed in dynamometer.

The granules were shaped by uniaxial pressing into a metallic mold under a stress of 100MPa and subsequently subjected to cold isostatic pressing at 200 MPa for 90s to improve uniform high compaction throughout the green bodies. The specimens were then sintered at 1600 °C for 2 h, resulting in highly densified alumina samples. After sintering, the workpieces exhibited a square cross-section of 6 × 6 mm and a length of 40 mm, which were used in all grinding tests. Representative alumina workpieces are shown in Figure 7 (B).

Customized nozzles were designed and manufactured by additive manufacturing to enable the application of MQL and WCJ under the experimental conditions adopted. Both nozzles were produced by fused filament fabrication (FFF) using a Bambu Lab A1 3D printer. Their geometries were defined according to the requirements of the grinding machine and the positioning constraints of the experimental setup. During the WCJ-assisted tests, the cleaning nozzle was positioned at an inclination angle of 30° relative to the grinding wheel surface.

A semisynthetic water-miscible cutting fluid (ME-1, Quimatic Tapmatic, Brazil) was employed in all lubrication and cooling conditions investigated in this study. According to the manufacturer, the fluid is a pre-emulsified semisynthetic formulation designed to provide effective lubrication and cooling during machining operations, presenting good emulsion stability and lubricating properties. For the conventional grinding condition, the fluid was diluted in water at a concentration of 3 vol.% and supplied by the flood method at a flow rate of 7 L/min. In the minimum quantity lubrication (MQL) condition, the fluid was applied in its concentrated form at a flow rate of 170 mL/h. For the diluted MQL conditions, a mixture containing one part of ME-1 and five parts of water (1:5 ratio) was prepared and delivered through the MQL system at the same flow rate of 170 mL/h. The same dilution was adopted for the MQL condition combined with wheel cleaning jet assistance (MQL 1:5 + WCJ). The different lubrication and cooling strategies were selected to evaluate the influence of fluid application and dilution on the grinding performance of alumina ceramics. To enable the application of the minimum quantity lubrication (MQL) and wheel cleaning jet (WCJ) techniques, customized nozzles were designed and manufactured using additive manufacturing. Both the MQL and WCJ nozzles were produced by fused filament fabrication (FFF) on a Bambu Lab A1 3D printer. The nozzle geometries were designed according to the requirements of the grinding machine and experimental setup. During the WCJ-assisted tests, the cleaning nozzle was positioned at an inclination angle of 30° relative to the grinding wheel surface. The configuration adopted for the lubrication and cleaning systems is illustrated in Figure 7 (C) and (D).

After the grinding tests, surface topography measurements were performed using a Taylor Hobson Talysurf Form 60 three-dimensional profilometer. The analyses were conducted to evaluate the surface integrity of the ground alumina specimens under the different lubrication and cooling conditions investigated in this study. Surface texture parameters were determined according to ISO 25178-2:2021, including the height parameters Sa, Sq, Ssk, and Sku; the spatial parameter Str; the functional parameters Spk, Sk, Svk, Smrk1, and Smrk2; the volume parameters Vv, Vvc, and Vvv; and the hybrid parameters Sdq and Sdr. The analysis included the conventional roughness parameter Ra, as well as topographical height parameters such as Sp, Sv, and Sz, which were used to evaluate the maximum peak height, maximum valley depth, and maximum surface height, respectively. In addition, the surface height distribution was analyzed by calculating the percentage of area in each third of the total height range. Peak histograms were also obtained to evaluate the distribution and concentration of surface peaks. Peak volume and valley volume parameters

were used to complement the analysis by quantifying the volumetric contribution of protruding and depressed regions on the ground surfaces. These parameters provided a more comprehensive description of the alumina surface topography than Ra alone, allowing the identification of localized peaks, deep valleys, craters, and irregularities associated with brittle material removal and debris interaction during grinding. Complementary surface analyses were performed by confocal microscopy using an Olympus LEXT OLS4000 microscope. The confocal images were used to qualitatively evaluate the surface morphology of the ground alumina specimens under each lubrication-cooling condition.

These parameters provided a comprehensive characterization of the surface topography generated under the different grinding conditions. For each workpiece, ten longitudinal and ten transverse measurements were performed. The average values obtained from these measurements were used for the statistical and comparative analyses. In addition to the characterization of the ground surfaces, the profilometer was also employed to evaluate the diametral wheel wear. After the grinding tests, the profile of the active wheel surface was imprinted onto an ABNT 1020 steel plate, producing a negative replica of the wheel geometry. This replica was subsequently measured using the profilometer, allowing the determination of wheel wear and the calculation of parameters related to grinding wheel performance and service life.

Grinding forces were measured using a Kistler 9257BA dynamometer mounted on the surface grinding machine, as shown in Fig. 1(A). The dynamometer output signals were connected to a National Instruments NI-9207 analog data acquisition module, which was integrated with a National Instruments cDAQ-9188 Ethernet chassis. Data acquisition was performed at a sampling frequency of 200 Hz, and the signals were recorded and processed using LabVIEW software. The acquired data was subsequently used for the analysis of the force components generated during the grinding process. A steel fixture was developed to ensure consistent positioning of the ceramic workpieces relative to the dynamometer throughout the experimental campaign. The workpieces were mounted onto the fixture using an adhesive composed of 50 wt.% rosin, 25 wt.% paraffin, and 25 wt.% beeswax. This fixation method provided adequate support during grinding while allowing the specimens to be removed after testing.

The specific grinding energy was determined to evaluate the efficiency of the material removal process under the investigated grinding conditions. To quantify the volume of material removed, the workpieces were weighed before and after the grinding tests using a SHIMADZU AUW220D analytical balance. Prior to each weighing procedure, the specimens

were cleaned in an ultrasonic bath containing isopropyl alcohol for 10 min to remove residual cutting fluid, adhered particles, and other surface contaminants. The density of each specimen was determined using Archimedes' principle, allowing the measured mass loss to be converted into removed material volume. Subsequently, the specific grinding energy was calculated according to Eq. (2), using the average grinding power measured during each test and the corresponding material removal rate.

$$u = \frac{P}{Qw} \qquad (2)$$

where (u) is the specific grinding energy (J/mm³), (P) is the grinding power (W), and (Qw) is the material removal rate (mm³/s).

Table 1 - Grinding parameters

Condition	Description
Grinding machine	(Vitor & Buono, model VB-1224). The machine is equipped with a horizontal spindle and a hydraulic reciprocating table measuring 600 × 300 mm.
Machining process	Tangential grinding
Grinding wheel	Diamond grinding wheel manufactured by Rediam (model 461722), featuring an outer diameter of 300 mm, a width of 10 mm, and an abrasive layer thickness of 6 mm. The abrasive grains consisted of synthetic diamond with a D91 grit size, corresponding to the MESH 170/200 range, bonded by a resin bond with grade R hardness
Wheel speed (v_s)	31,4 m/s
Table feed rate (v_f)	4 m/min
Depth of cut (a) / cycle	0.04 mm / 50 cycles, totaling a 2 mm reduction in the workpiece thickness
Grinding width (b)	4 mm
Workpiece	Al_2O_3 ceramic specimens (Alumina 1000 SG, Almatis), 6 × 6 × 40 mm, sintered at 1600 °C for 2 h.
Lubri-cooling conditions	Conventional (flood) Minimum Quantity Lubrication (MQL) Minimum Quantity Lubrication, 1:5 dilution (MQL 1:5) Minimum Quantity Lubrication, 1:5 dilution with Wheel Cleaning Jet (MQL 1:5 + WCJ)
Cutting fluid	ME-1 semisynthetic water-miscible cutting fluid (Quimatic Tapmatic, Brazil).
Cutting fluid flow/pressure	Conventional flood cooling: 7 L/min Minimum Quantity Lubrication (MQL): 170 mL/h, 8 bar Minimum Quantity Lubrication, 1:5 dilution (MQL 1:5): 170 mL/h, 8 bar Minimum Quantity Lubrication, 1:5 dilution with Wheel Cleaning Jet (MQL 1:5 + WCJ): 170 mL/h, 8 bar
Dresser	Conglomerate-type multi-granular dresser, manufactured by Master Diamond, in a parallelepiped shape, with dimensions of 15 mm x 8 mm x 10 mm
Dressing depth (a_d) / cycle	0.2 mm / 50 cycles – 0,004 mm per cycle
Dressing speed (v_d)	500 mm/min

Figure 8 presents an overview of the methodology adopted in this study, including the experimental conditions, response variables, and analyses performed.

This replica was then measured to determine the wheel wear. Based on the diametral wheel wear values, the G-ratio was calculated by relating the volume of material removed from the workpiece, Zw, to the worn volume of the grinding wheel, Zs, according to Eq. (3) (Lauer-Schmaltz; König, 1980).

$$\boldsymbol{G_{ratio} = \frac{Z_w}{Z_s}} \qquad (3)$$

The acquired force data were used to evaluate the mechanical behavior of the grinding process under each lubrication-cooling condition. The grinding power was calculated from the tangential grinding force and the grinding wheel speed, according to Eq. (4) (Shaw, 1996):

$$P = Ft * Vs \qquad (4)$$

where P is the grinding power (W), Ft is the tangential grinding force (N), and vs is the grinding wheel speed (m/s). This parameter was used to compare the energy demand of the grinding process under the different lubrication-cooling conditions. The overall cost and pollution analyses were performed to provide additional information on the economic and environmental effects of reducing cutting fluid consumption.

After defining the workpiece, grinding wheel, and grinding parameters, the cost analysis was carried out by considering the grinding wheel cost, cutting fluid cost, energy cost, and labor cost associated with the process. These calculations were performed according to Eqs. (5), (6), (7), (8), and (9), proposed by (Field; Kegg; Buescher, 1980) and (Pusavec et al., 2010), adapted by (Lopes et al., 2021). For the pollution analysis, Eqs. (10), (11), and (12) were used to determine the carbon emissions associated with grinding power, compressed air consumption, recirculating system energy, and cutting fluid use. The parameters adopted in the cost and pollution analyses are presented in Table 2.

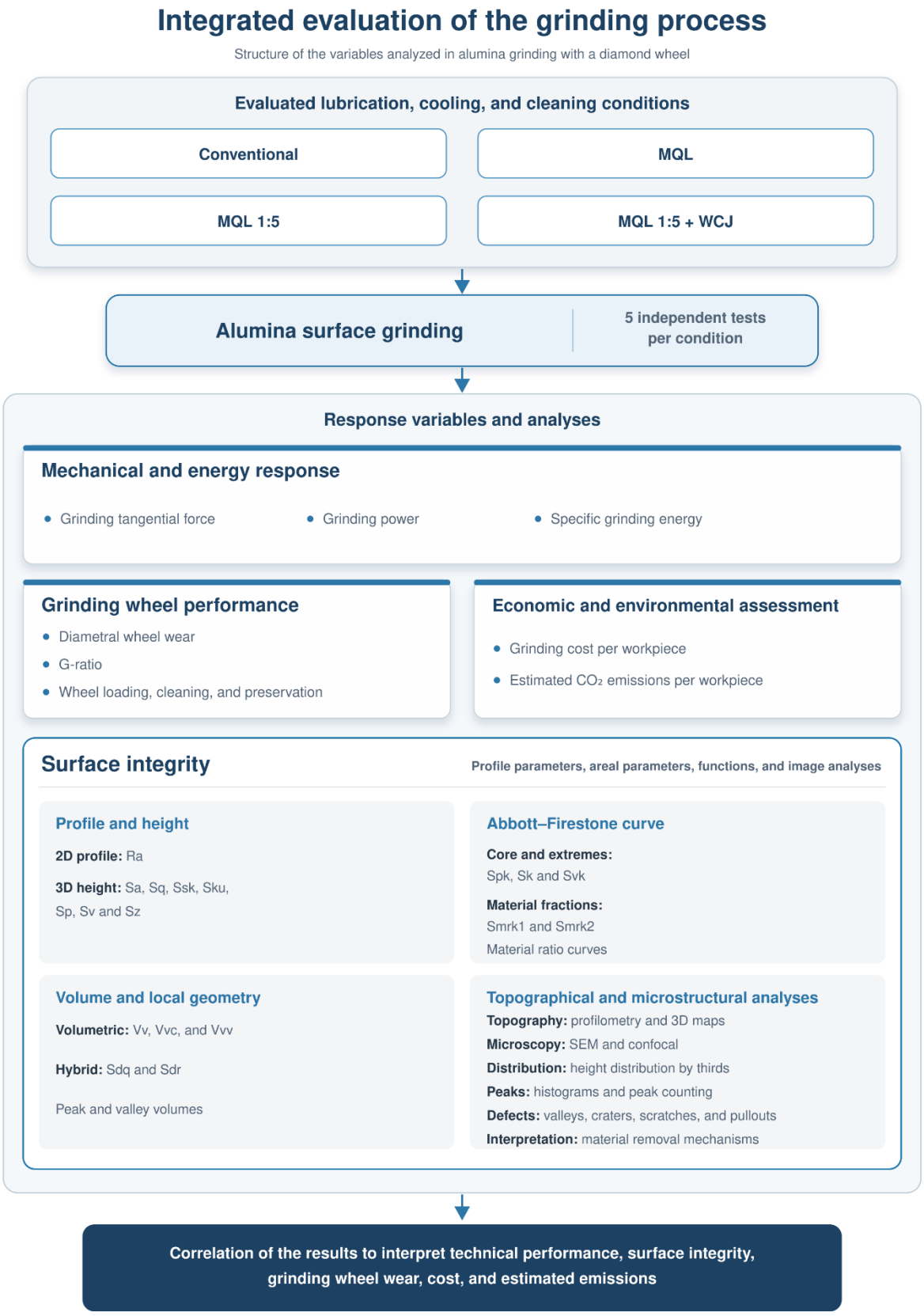


Figure 8. Overview of the experimental methodology, including the evaluated lubrication, cooling, and wheel-cleaning conditions, grinding tests, response variables, and surface integrity, economic, and environmental analyses.

Four lubrication, cooling, and cleaning conditions were investigated, with five independent tests performed for each condition. The evaluation included mechanical and energetic responses, grinding wheel performance, surface integrity, process costs, and estimated CO_2 emissions.

By correlating these complementary factors, the study provided a comprehensive assessment of the technical, economic, and environmental feasibility of each technique. This integrated approach was essential because the suitability of a grinding condition cannot be determined from a single parameter, but rather from the balance between process efficiency, wheel preservation, surface quality, cost, and environmental impact.

During the preparation of this thesis, artificial intelligence tools were used solely as auxiliary resources. ChatGPT, developed by OpenAI, was employed to review the English translation and improve linguistic clarity. All scientific content, interpretations, and analyses are the sole responsibility of the author.

$$C_{wheel} = \frac{C_s * V}{G} + \frac{\pi * b_s * C_s}{N_d} * (d_s * a_d - a_d^2) \quad (5)$$

$$C_{fluid} = \frac{v_{jet}}{N_c} * (C_f + C_w) * \left(\frac{D_{nc}}{v_w} + \frac{L_w}{v_w} * N_g + t_{so}\right) \quad (6)$$

$$C_{energy} = \frac{(P_c + P_{bo} + P_{air}) * C_e}{60000} * \left(\frac{D_{nc}}{v_w} + \frac{L_w}{v_w} * N_g + t_{so}\right) \quad (7)$$

$$C_{labor} = \frac{M}{60} * \left(\frac{D_{nc}}{v_w} + \frac{L_w}{v_w} * N_g + t_{so}\right) \quad (8)$$

$$C_{method} = C_{wheel} + C_{fluid} + C_{energy} + C_{labor} \quad (9)$$

$$CE_{energy} = \frac{(P_c + P_{bo} + P_{air}) * CE_e * 3,6}{60000} * \left(\frac{D_{nc}}{v_w} + \frac{L_w}{v_w} * N_g + t_{so}\right) \quad (10)$$

$$CE_{fluid} = \frac{V_{jet} * k_p * CE_{oil}}{N_c} * \left(\frac{D_{nc}}{v_w} + \frac{L_w}{v_w} * N_g + t_{so}\right) \quad (11)$$

$$CE_{method} = CE_{fluid} + CE_{energy} \quad (12)$$

Table 2 Parameters used for grinding cost and pollution analysis.

Symbol	Description	Units	Values			
a_d	Total radial infeed in dressing wheel	[mm]	0.20			
a_e	Depth of cut in the workpiece	[mm]	2.0			
b_s	Width of grinding wheel	[mm]	10.0			
L_w	Length of workpiece	[mm]	40			
b_w	Width of workpiece	[mm]	4.0			
N_g	Number of grinding strokes	[-]	50			
t_{so}	Spark-out time	[min]	0.5			
C_r	Grinding wheel price	[US$]	851.79			
d_s	Outer diameter of wheel	[mm]	300.0			
d_{min}	Minimum wheel diameter	[mm]	295.59			
Ω	Grinding wheel rotation	[rad/s]	183.78			
Vw	Table rate	[mm/min]	4000			
N_d	Number of workpieces between dressing	[-]	1.0			
Dnc	Non-cutting movement Distance	[mm]	860.0			
V	Volume of workpiece removed in grinding	[mm³]	320.0			
C_{air}	Compressed air cost	[US$/m³]	0.0106 (Hitchcox, 2015)			
C_e	Energy cost	[US$/kWh]	0.12 (“Electricity prices”, 2020)			
CE_e	Carbon emission by energy	[kgCO_2/MJ]	0.128 (Abellan-Nebot; Rogero, 2019)			
CE_{oil}	Carbon emission by oil	[kgCO_2/l]	3.0616 (Pusavec et al., 2010)			
C_s	Cost of usable grinding wheel	[US$/mm³]	0.041291121			
C_w	Cost of disposal the cutting fluid	[US$/l]	0.085 (Demirbas; Kobya, 2017)			
M	Labor or overhead on grinder	[US$/h]	20 (Pusavec et al., 2010)			
Cooling-lubrication methods			Flood	MQL	MQL 1:5	MQL 1:5 + WCJ
k_p	Oil dilution proportion	[-]	0.03	1	0.167	0.167
P_{air}	Air compressor power	[W]	0	5500	5500	5500
P_{bo}	Oil pump power	[W]	372.85	0	0	0
V_{jet}	Fluid flow	[l/min]	7.0	0.00283	0.00283	0.00283
N_c	Number of fluids recircle	[-]	10.0	1.0 (Wang et al., 2020)	1.0 (Wang et al., 2020)	1.0 (Wang et al., 2020)
V_{air}	Compressed air flow	[m³/min]	0	0.85	0.85	1.982
C_f	Metalworking fluid cost	[US$/l]	0.4125	13.75	2.296	2.296

4. RESULTS AND DISCUSSION

This section presents and discusses the experimental results obtained during alumina grinding under different lubrication-cooling conditions. First, the process behavior is evaluated through tangential grinding force and specific grinding energy, supported by SEM images to identify the main material removal mechanisms on the ground surfaces. Then, surface integrity is analyzed using three-dimensional roughness parameters and Abbott-

Firestone curves. Diametrical wheel wear is discussed in detail, considering the influence of debris removal, wheel loading, diamond grain exposure, and possible three-body abrasion mechanisms. Also, the process and grinding wheel performance are evaluated through grinding power, G-ratio, and confocal microscopy images, allowing the relationship between energy demand, wheel wear, and material removal behavior to be analyzed. Then, the surface topography is discussed based on Ra, Sz, Sp, Sv, height-area distribution, peak histogram, and peak and valley volume parameters. Finally, the economic and environmental performance of each condition is evaluated through cost analysis and CO_2 emissions. This structure enables the correlation between process efficiency, surface quality, grinding wheel performance, and sustainability.

4.1. Tangential force and specific grinding energy

Ceramic grinding presents difficulties primarily related to the integrity and quality of the workpiece. Along with this, the high hardness and mechanical strength make the grinding wheel, even diamond, quickly lose the cutting ability and material removal (Marinescu et al., 2016). The removal of chips in ceramic materials is directly linked to the formation of a crack, which increases local stress, and ultimately causes chip removal via brittle fracture of the work material. Thus, there is great difficulty in operating in elasto-plastic regimes during the grinding of ceramic materials, preventing the application of greater cutting depth in order to ensure the surface integrity of the ground component (Marinescu et al., 2013b).

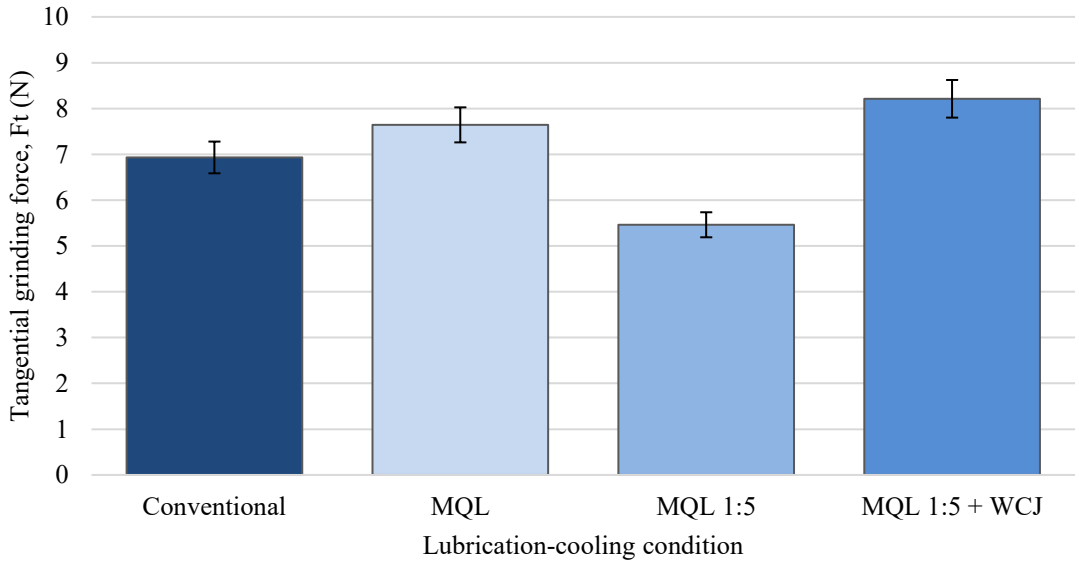


Figure 8. Tangential grinding force for various conditions.

Figure 9 shows the force data obtained in the tests. Conventional condition, taken with reference value, generated average tangential forces of 6.93 N. With reduced cutting fluid, in the MQL condition, average increases of 10.26% were observed. For the MQL 1:5 conditions, average reductions of 21.2% in tangential force were observed, while diluted MQL 1:5 + WCJ generated an increase of 18.46%. The given relationship between force and volume of material removed, represented by the specific grinding energy is shown in Figure 3. Following the same trend in tangential force values, the condition that yielded the lowest specific grinding energy was the application of MQL 1:5, representing a reduction of approximately 19% compared to the conventional condition. Pure MQL and MQL 1:5 + WCJ showed increases of 11.74% and 20.85 %, respectively, compared to the conventional condition. However, because it is alumina grinding, simply observing the tangential force and specific grinding energy may not be sufficient to determine the optimal grinding conditions.

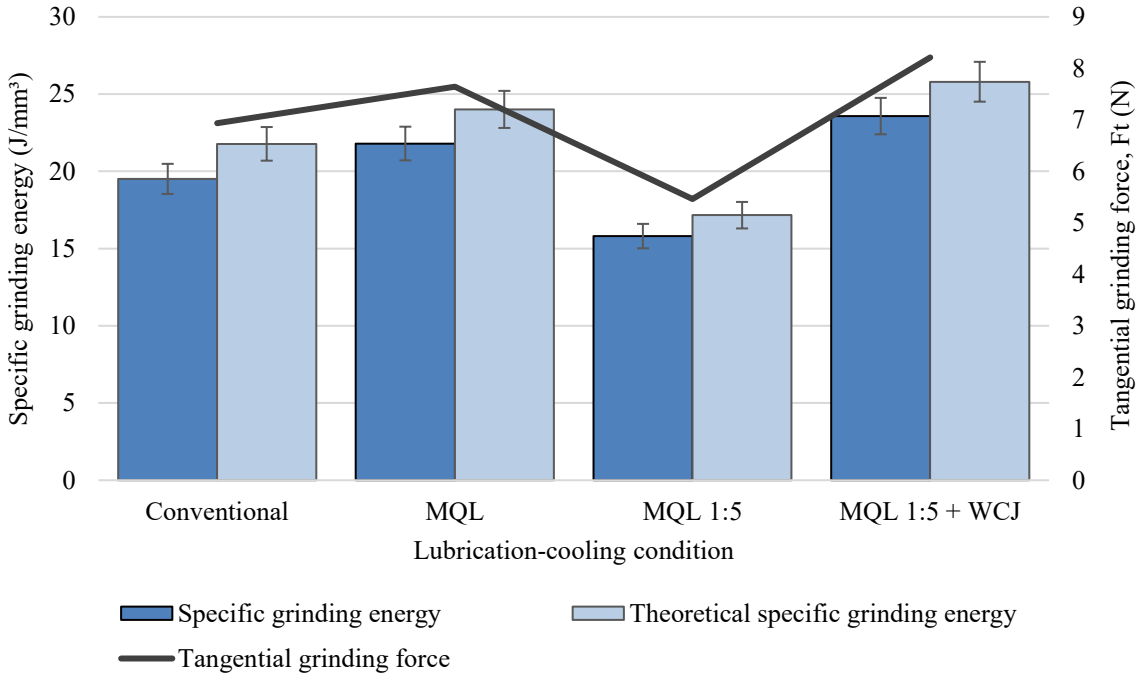


Figure 9. Specific grinding energy (real and theorical) compared with tangential grinding force for various conditions

Figure 10 compares the specific grinding energy calculated from the experimentally measured removed volume with the theoretical specific grinding energy calculated from the geometrical volume of material removal, also including the tangential grinding force for each lubrication-cooling condition. The results show that both specific energy calculations followed the same general trend as the tangential force, indicating that the mechanical effort

during grinding strongly influenced the energy required for material removal. The MQL 1:5 condition presented the lowest tangential force and, consequently, the lowest specific grinding energy values, while the MQL 1:5 + WCJ condition resulted in the highest values. This behavior indicates that the application of WCJ increased the effective interaction between the diamond grains and the alumina surface, probably due to improved debris removal and greater exposure of active abrasive grains. However, the theoretical specific grinding energy was consistently higher than the experimental value calculated from the measured removed volume. This difference can be attributed to the brittle nature of alumina. During grinding, material removal does not occur only by the ideal geometrical volume defined by the depth of cut and contact conditions. Instead, crack propagation, grain pull-out, crater formation, chipping, and localized brittle fracture may remove additional material from the workpiece. As a result, the real removed volume obtained from weighing the specimens tends to be higher than the theoretical volume, increasing the denominator in the specific energy calculation and reducing the experimental specific energy value. Therefore, the comparison between theoretical and experimental values reinforces that alumina grinding is strongly affected by brittle fracture mechanisms, and that specific grinding energy should be interpreted together with tangential force, wheel wear, and surface integrity rather than as an isolated indicator of process efficiency.

The increase in tangential force and specific energy observed with WCJ can be explained by the combined effect of wheel cleaning, fluid dilution, and contact conditions. In the present study, WCJ was applied with MQL diluted at a 1:5 ratio, resulting in lower oil concentration and, consequently, lower lubricating capacity than the 1:1 dilution used by Moraes et al. (2019). Thus, although the cleaning jet removed debris from the grinding wheel surface and exposed more active diamond grains, these grains interacted with the alumina surface under a more lubrication-limited condition, increasing the effective abrasive-workpiece interaction. In addition, differences between cylindrical grinding and surface grinding may affect fluid access, debris evacuation, contact geometry, and the balance between brittle fracture, cutting, and ploughing. Therefore, the higher tangential force and specific energy with WCJ do not necessarily indicate poorer grinding performance, but rather a more intense abrasive-workpiece interaction, involving both effective cutting and possible ploughing under limited lubrication, which is consistent with the improved wheel wear behavior observed for this condition.

Images obtained by SEM show the surface condition of the ground samples. Figure 11 represents the surface of the ground workpiece using the conventional method. According to

Figure 11b, it is possible to determine the presence of voids and cracks between the grains, since the mechanical characteristics of the alumina prevented, in this case, the ploughing–cutting transition reveals possible plastic deformation of the grains during removal. This characteristic is demonstrated during the grinding of alumina and other ceramic materials (Zhang et al., 2003). Even so, it is possible to notice the presence of traces, in smaller proportions, of plastically deformed regions. Despite this typical characteristic of chip removal, by changing the applied lubrication method, the conditions of chip formation and removal can be changed, mainly due to the temperature at the cutting interface.

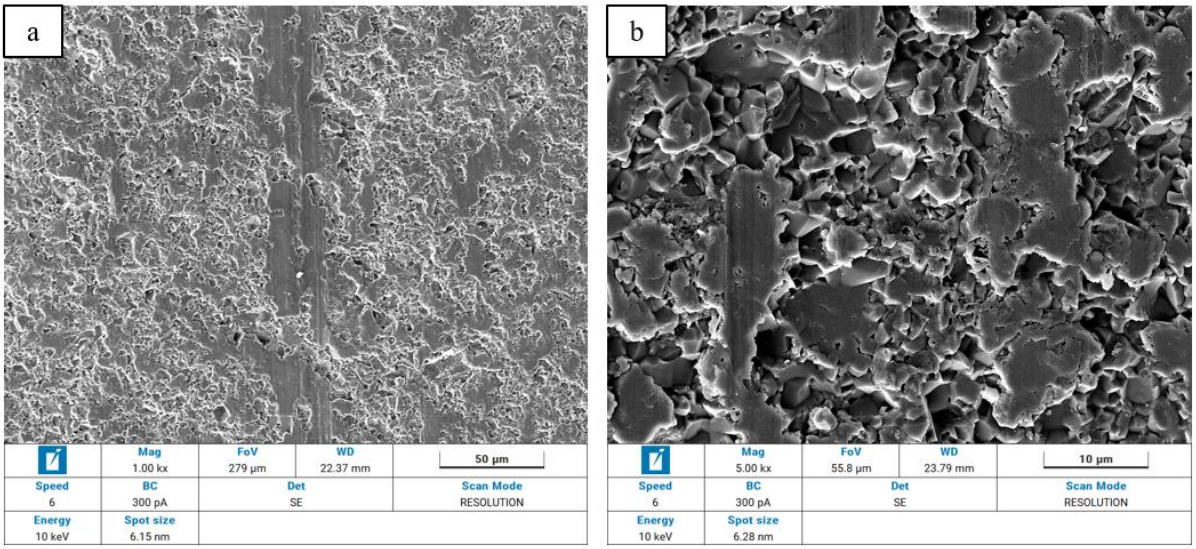


Figure 10. SEM images of the workpiece ground with conventional condition, a) 1000 x and b) 5000X

In Figure 12, the surface ground using MQL is shown. Its comparison with Figure 4 represents a plastically deformed surface, with traces of deformation aligned with the direction of the cut. In this case, the plastic deformation that occurred is dependent on factors linked to the increase in temperature, linked to the progressive loss of cutting of the grinding wheel, wheel loading and lower cooling capacity, justifying the increase in tangential force. As temperature increases, alumina becomes more susceptible to plastic deformation during cutting. In addition, Shaw (1996) points out that the increase in contact length during grinding is a crucial factor for increasing the specific grinding energy, consistent with plastically removed chips.

Even in this condition, the presence of debris in the contact area affected the surface quality. It is evident that the plastically deformed traces exhibit discontinuities, indicating that the presence of the third element at the cutting interface may have negatively affected the ground region.

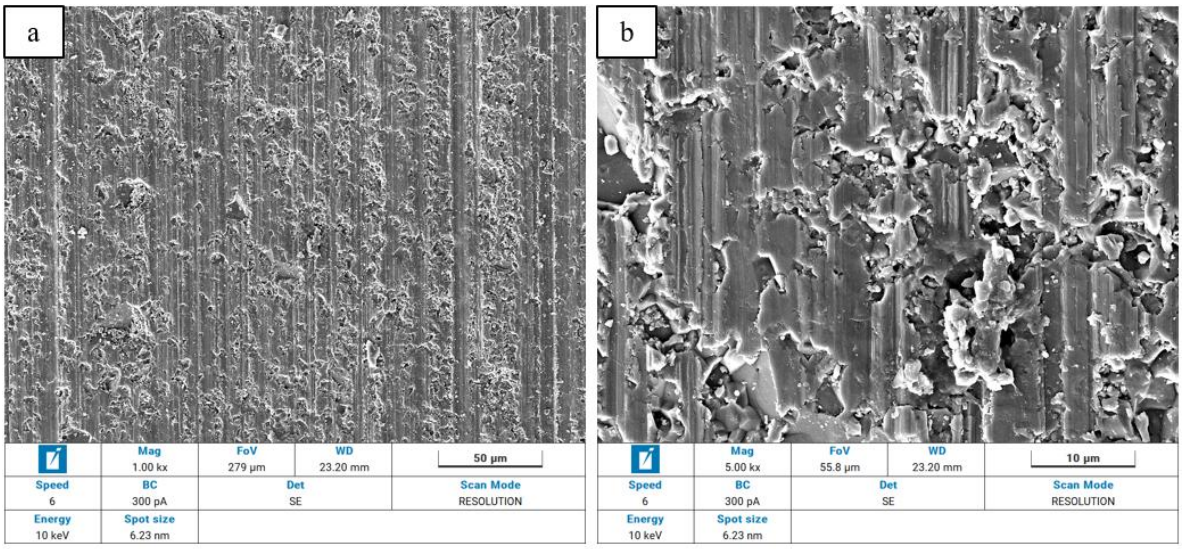


Figure 11. SEM images of the workpiece ground with MQL, a) 1000 x and b) 5000X.

With the use of diluted MQL, data were presented that demonstrate the reduction of cutting force and specific grinding energy. Analyzing Figure 13, it is remarkable that the ground surface comprises visual aspects indicating the presence of brittle removal, characterized by empty spaces and cracks, but also presents regions with aspects of plastic deformation, indicating an intermediate condition between the conventional method and the pure MQL.

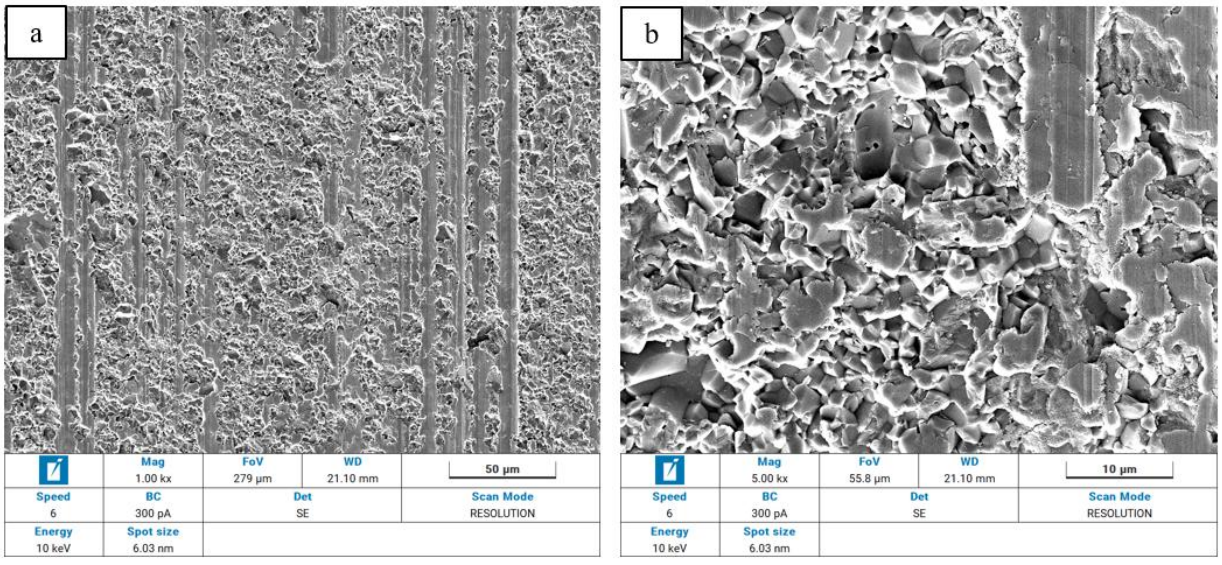


Figure 12. SEM images of the workpiece ground with MQL 1:5, a) 1000 x and b) 5000X.

Marinescu et al. (2016) points out that the grinding of ceramic material in mixed conditions, ductile and brittle, can be energetically more favorable than a purely brittle removal, in particular conditions. In this case, the shear conditions, especially the temperature,

resulted in favorable conditions for the reduction of the tangential force and specific grinding energy, compared to the other conditions. However, as it is an experimental condition, additional evaluations are necessary in view of the process.

The WCJ application with the MQL is positively demonstrated in grinding works, considering that one of the problems linked to the MQL, the presence of wheel loading, is improved. The surface of the workpiece using MQL 1:5 + WCJ is shown in Figure 14. Compared to the previous images, the plastically deformed regions present features with greater definition. Such a perspective demonstrates that, even in the situation of reduced volume of cutting fluid, the greater removal of debris from the contact interface allowed greater cutting capacity of the grinding wheel. In this way, an active cutting surface of the grinding wheel together with the higher cutting temperature, allowed the alumina to present more evident ductile-like deformation and ploughing marks during grinding. Such ductile-like removal mechanisms and higher cutting capacity increased the specific energy given off to the plowing formation and increased the contact length between chip and abrasive grain exit surface, increasing the values presented in Figures 9 and 10. The presence of the WCJ allowed the grinding wheel to be successively cleaned and allowed each cutting cycle to continue the reported phenomenon. Although grinding under these conditions presents higher forces and specific energy, such removal conditions can effectively generate better dimensional quality and surface integrity of the workpiece (Marinescu et al., 2016).

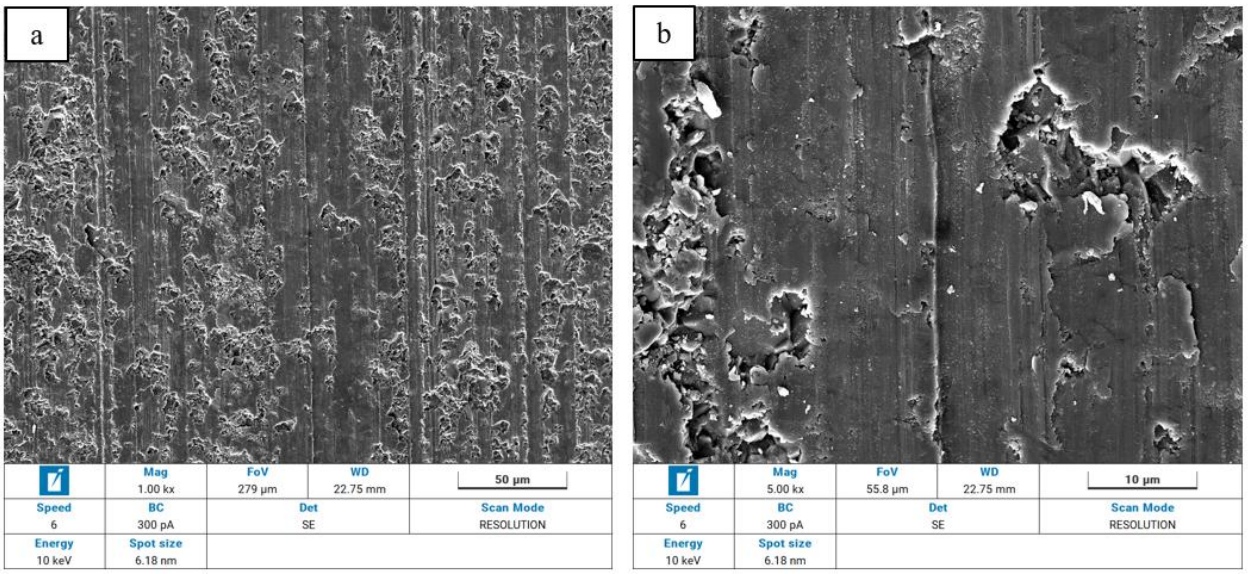


Figure 13. SEM images of the workpiece ground with MQL 1:5 + WCJ, a) 1000x and b) 5000X.

4.2. Surface Roughness and Topograph

Surface texture was analyzed using areal roughness parameters, considering not only the average surface amplitude, but also the height distribution, the functional contribution of peaks and valleys, the volumetric parameters associated with surface voids, and the hybrid parameters related to local gradients and developed area. This approach is particularly relevant in the grinding of advanced ceramics, since surfaces with similar average roughness may exhibit significant differences in terms of grooves, deep valleys, localized material pull-out, and features associated with brittle material removal. The parameters obtained for the ground surfaces under the different cooling-lubrication conditions are presented in Table 3.

4.2.1. Sa parameter and 3D profilometer images

The Sa values obtained under the different cooling-lubrication conditions are presented in Figure 16. The analysis of the average surface texture amplitude (Sa) in Figure 16 indicates that MQL did not reduce surface roughness compared with the conventional condition. Sa increased from 0.64 μm to 0.75 μm under MQL and to 0.80 μm under MQL 1:5, corresponding to increases of 17% and 26%, respectively. Therefore, the application of MQL, especially in the diluted condition, did not improve the surface finish of the ground surface. In contrast, MQL 1:5 + WCJ resulted in the lowest Sa value, equal to 0.53 μm, representing reductions of approximately 17%, 30%, and 34% compared with the conventional, MQL, and MQL 1:5 conditions, respectively. This behavior suggests that the wheel-cleaning jet contributed to reducing surface roughness, which is also consistent with the 3D topography of this condition, visually less irregular than those obtained under MQL without wheel cleaning (Figure 15). The Sq parameter, also presented in Table 3, followed a trend similar to that of Sa, and the Sq/Sa ratio showed a maximum variation of only 3% among the evaluated conditions. Thus, Sq did not provide additional relevant information for the analysis of surface amplitude, justifying the use of Sa as the main parameter in this discussion.

To complement the quantitative evaluation presented in Table 3, the ground surfaces were examined using 3D surface topography to assess the spatial distribution of surface irregularities and the main morphological features produced under each cooling-lubrication condition. The 3D surface topographies of the ground surfaces are shown in Figure 15.

Table 3 Surface roughness parameters

Parameter	Unit	Condition			
		Conventional	MQL	MQL 1:5	MQL 1:5 + WCJ
Sa	µm	0.64	0.75	0.80	0.53
Sq	µm	0.82	0.93	1.02	0.68
Ssk	-	-0.24	-0.37	-0.70	-0.65
Sku	-	3.44	3.08	3.38	4.55
Spk	µm	0.75	0.58	0.54	0.46
Sk	µm	1.92	2.47	2.32	1.68
Svk	µm	0.97	0.99	1.47	0.94
Smrk1	%	11.71	7.33	6.79	7.75
Smrk2	%	88.26	89.00	83.44	89.05
Vv	µm³/µm²	1.08	1.18	1.21	0.84
Vvc	µm³/µm²	0.97	1.07	1.05	0.75
Vvv	µm³/µm²	0.11	0.12	0.16	0.09
Sdq	-	0.45	0.43	0.41	0.39
Sdr	%	9.68	8.69	7.78	7.15

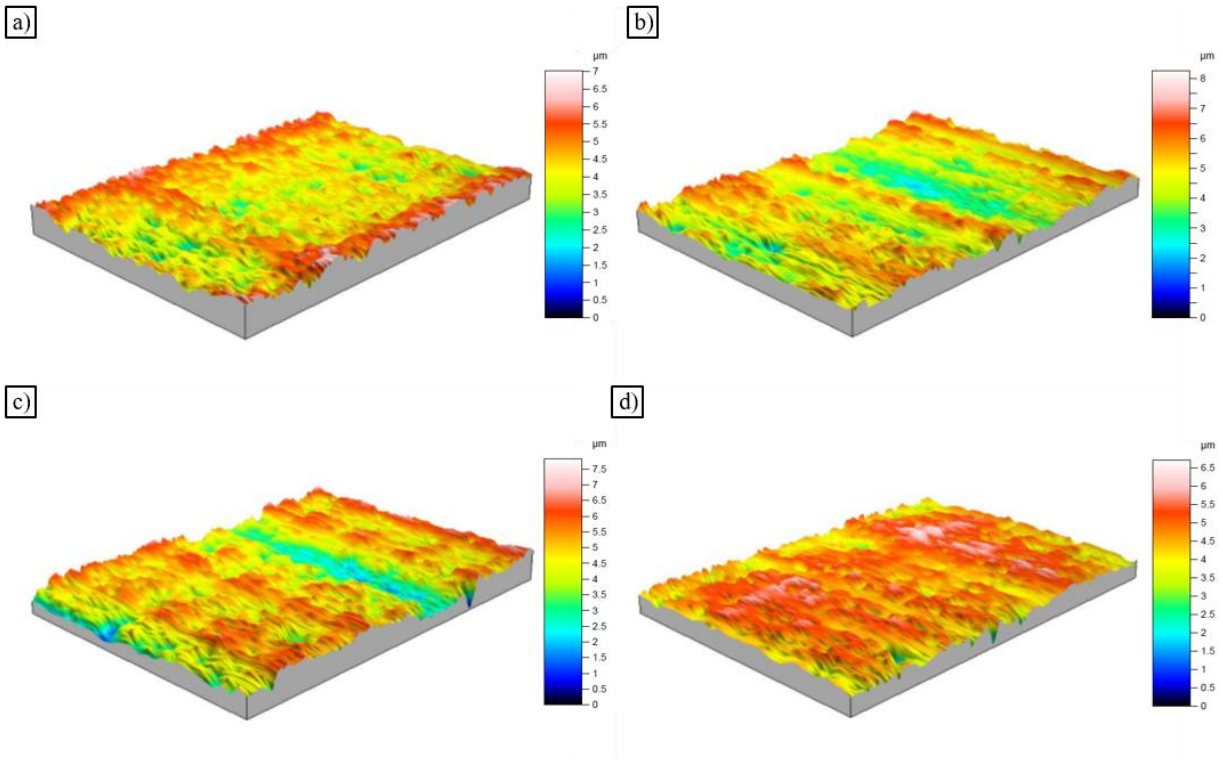


Figure 14. 3D profilometer images of the ground surfaces: a) Conventional, b) MQL, c) MQL 1:5, d) MQL 1:5 + WCJ

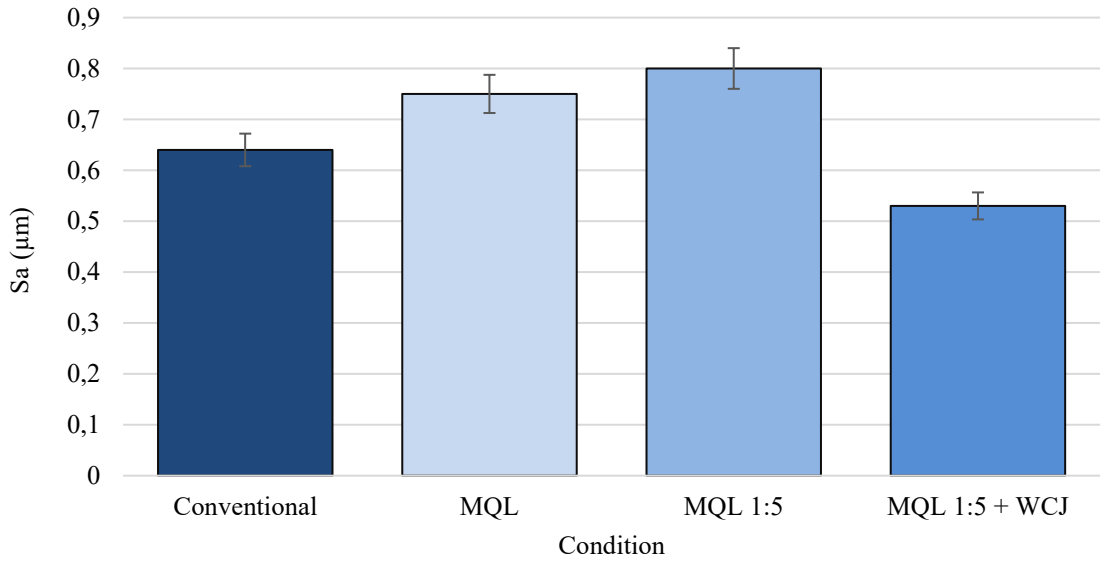


Figure 15. Sa parameter

The reduction observed under the MQL 1:5 + WCJ condition may be associated with the action of the wheel-cleaning jet in removing debris and material adhered to the grinding wheel surface, thereby reducing wheel loading and three-body abrasion. Thus, the lubricating effect of MQL appears to have been more effective when combined with wheel cleaning, favoring a more stable interaction between the diamond grains and the alumina surface.

4.2.2. Abbott-Firestone curves

Figure 10 presents the skewness (Ssk) and kurtosis (Sku) values of the ground surfaces in the present study, mapped onto the typical morphological space of machining processes.

As observed in Figure 17, the Ssk and Sku values remained within the typical morphological field of ground surfaces for all tested conditions, characterized by negative skewness and kurtosis higher than 3.

Negative skewness indicates a relative predominance of valleys in the height distribution, whereas kurtosis higher than 3 indicates the presence of more pronounced peaks and/or valleys. Compared with the conventional condition, which presented an Ssk value of −0.24, the MQL conditions showed more negative values, reaching −0.37 for MQL, −0.70 for MQL 1:5, and −0.65 for MQL 1:5 + WCJ, indicating a greater contribution of valleys to the surface topography.

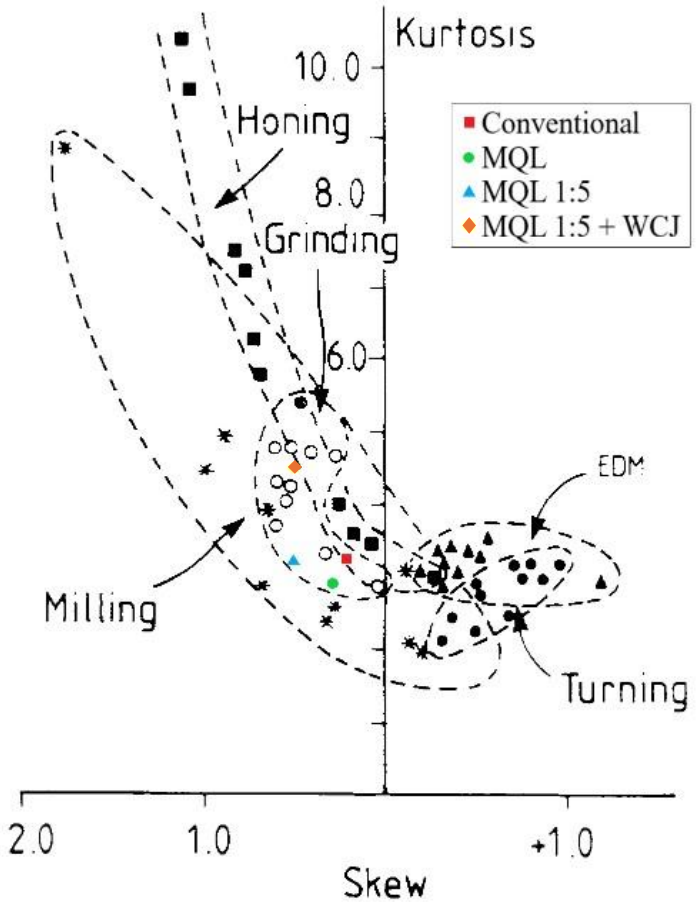


Figure 16. Morphological space of skewness and kurtosis for different machining processes, including the results obtained in the present study. Adapted from ((Whitehouse, 1994)).

Regarding kurtosis, the main highlight was the increase in Sku to 4.55 with the application of the wheel-cleaning jet, the highest value among the evaluated conditions. This behavior indicates the presence of more pronounced localized topographical features in the height distribution, possibly associated with greater exposure of the diamond grains after wheel cleaning.

Figure 18 presents the Abbott-Firestone curves obtained for the ground surfaces under the different cooling-lubrication conditions.

The Abbott-Firestone curve is widely used for the functional characterization of surfaces. The parameters obtained from this curve, Spk, Sk, Svk, Smrk1, and Smrk2, are presented in Table 3. Spk is related to the peak region, which tends to be removed during the initial contact. Sk represents the core roughness, associated with load-bearing capacity and wear resistance, whereas Svk describes the valley region, related to fluid and debris retention. Smrk1 and Smrk2 define the transition limits between the peak, core, and valley regions; therefore, Smrk1 was used as the material ratio of the peak region, while 100% − Smrk2 was used to estimate the material ratio associated with the valley region.

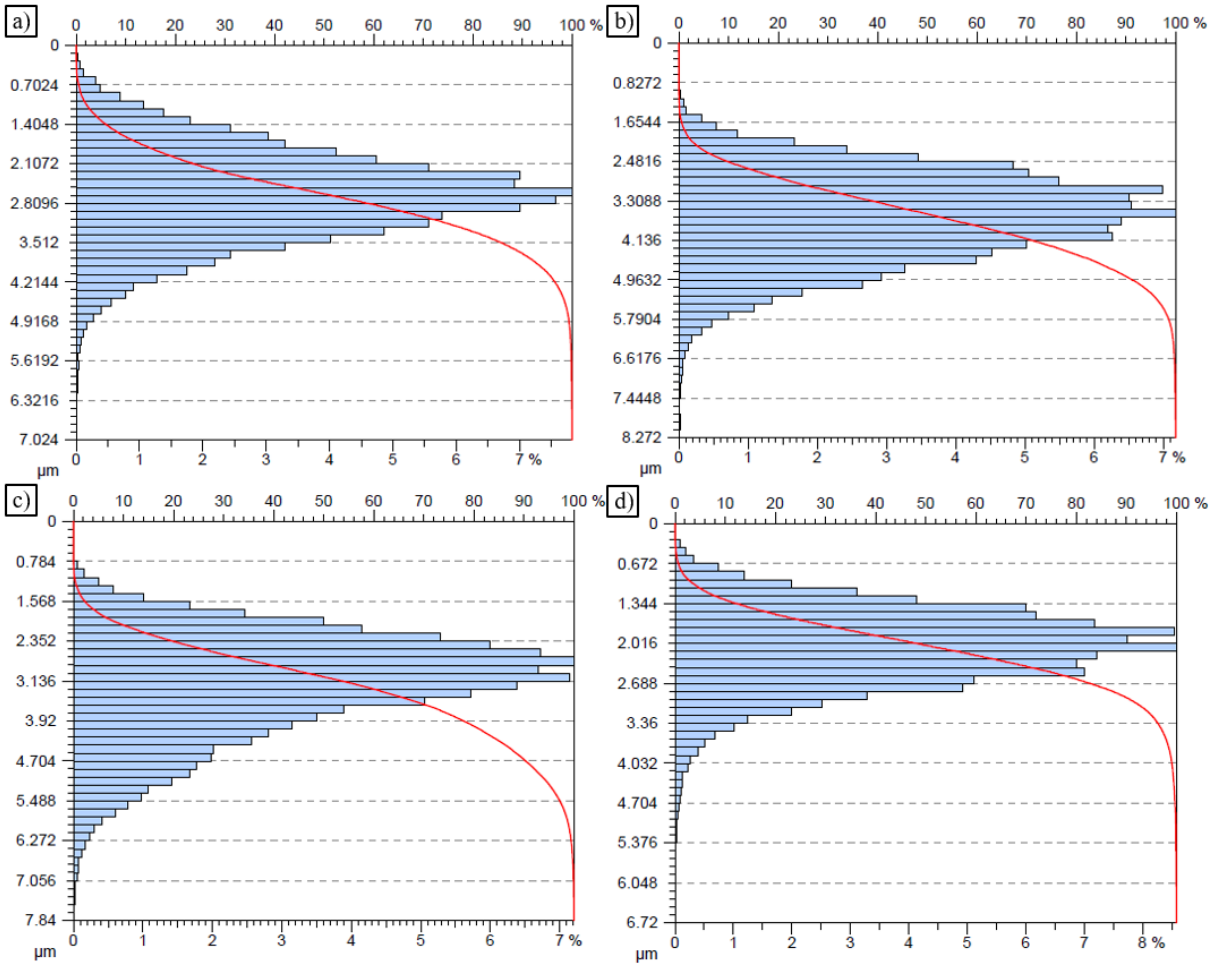


Figure 17. Abbott-Firestone curves of the ground surfaces: a) Conventional, b) MQL, c) MQL 1:5, d) MQL 1:5 + WCJ

As shown in Figure 18, the conventional condition exhibited the most pronounced peak region, with the highest Spk value (0.75 µm) and Smrk1 (11.71%). In comparison, Spk decreased under MQL and MQL 1:5 to 0.58 µm and 0.54 µm, respectively, reaching its lowest value under MQL 1:5 + WCJ (0.46 µm). A different behavior was observed for Sk, for which MQL and MQL 1:5 showed the largest values, 2.47 µm and 2.32 µm, respectively, compared with 1.92 µm for the conventional condition and 1.68 µm for MQL 1:5 + WCJ. The valley-related parameters were more critical under MQL 1:5, which presented the highest Svk (1.47 µm) and the largest 100% − Smrk2 value of 16.56%. In the remaining conditions, Svk remained within a narrower range, from 0.94 µm to 0.99 µm, while 100% − Smrk2 varied between 10.95% and 11.74%.

Overall, the MQL 1:5 + WCJ condition provided the most favorable functional response among the evaluated conditions, as it combined the lowest Spk, Sk, and Svk values. This indicates a simultaneous attenuation of the peak region, core roughness, and valley depth, resulting in a more controlled surface texture from a functional perspective. This

behavior may be attributed to the action of the wheel-cleaning jet in removing debris and material adhered to the active surface of the grinding wheel, thereby reducing wheel loading and three-body abrasion. As a result, the interaction between the diamond grains and the alumina surface tends to become more stable and uniform, leading to less pronounced peak, core, and valley regions in the Abbott-Firestone curve.

4.2.3. Vvv, Sdq and Sdr Parameters

Figure 19 presents the dale void volume parameter, Vvv, used to complement the Abbott-Firestone analysis.

The Vvv parameter, referred to as dale void volume, quantifies the volume associated with the valley region of the surface texture. As shown in Figure 19, Vvv reached its highest value under the MQL 1:5 condition, equal to 0.16 µm³/µm², whereas MQL 1:5 + WCJ presented the lowest value, 0.09 µm³/µm². The conventional and MQL conditions showed intermediate values of 0.11 µm³/µm² and 0.12 µm³/µm², respectively.

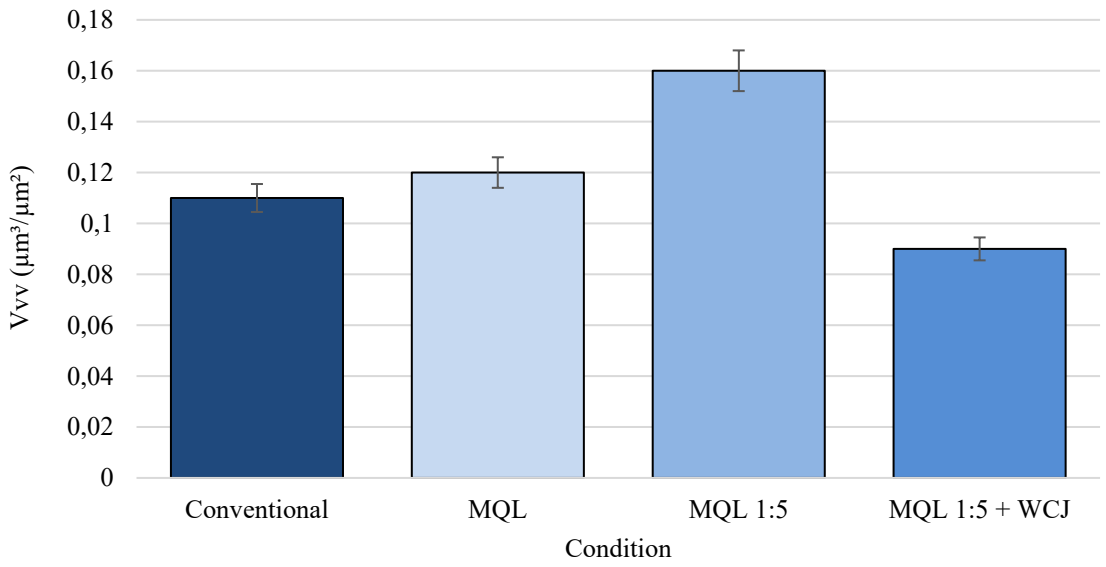


Figure 18. Vvv parameter

The higher Vvv value obtained under MQL 1:5 indicates a more developed valley region, which may favor fluid and debris retention in tribological applications. However, in the context of this study, this result also confirms the more pronounced presence of surface depressions, in agreement with the higher Svk value and the more negative Ssk observed for this condition. Conversely, the lower Vvv obtained under MQL 1:5 + WCJ indicates a

reduced contribution of deep valleys, suggesting that wheel cleaning helped limit the formation of pronounced depressions and produced a more topographically regular texture. In addition, MQL 1:5 + WCJ also showed the lowest Vv and Vvc values, equal to 0.84 $\mu m^3/\mu m^2$ and 0.75 $\mu m^3/\mu m^2$, respectively, indicating reductions in both the total void volume and the core void volume of the surface texture. Figure 20 presents the hybrid parameters Sdq and Sdr obtained under the different cooling-lubrication conditions. The Sdq parameter, referred to as the root mean square gradient, represents the local slope of the surface. Higher Sdq values indicate steeper local gradients and more abrupt topographical transitions. The Sdr parameter, referred to as the developed interfacial area ratio, represents the percentage increase in the developed surface area relative to the projected area. Therefore, higher Sdr values indicate a larger effective surface area, associated with a texture of greater topographical complexity.

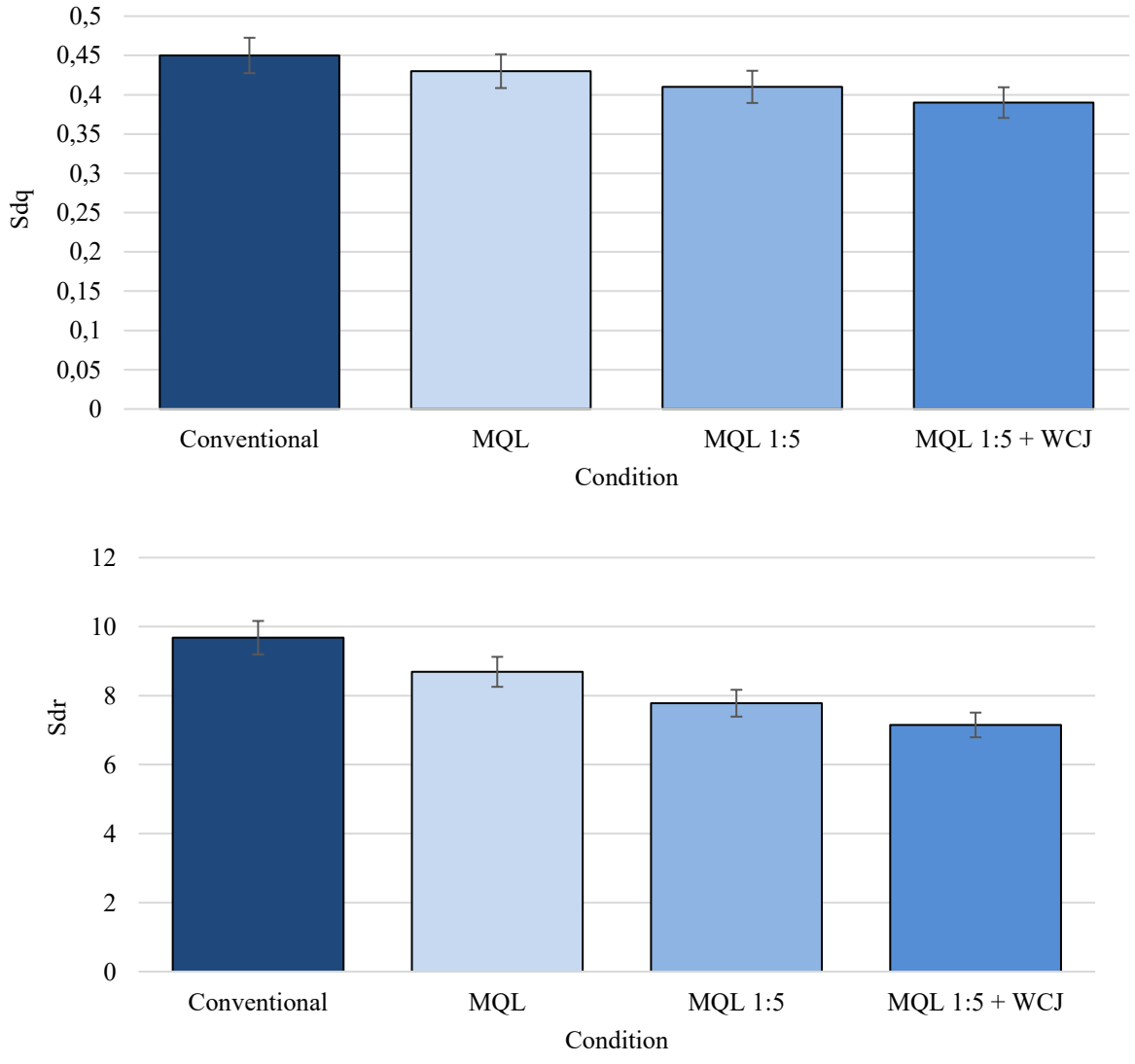


Figure 19. Sdq and Sdr parameters

As shown in Figure 20, Sdq and Sdr progressively decreased with the application of MQL, particularly when MQL 1:5 was combined with WCJ. Sdq decreased from 0.45 in the conventional condition to 0.43 under MQL, 0.41 under MQL 1:5, and 0.39 under MQL 1:5 + WCJ. A similar trend was observed for Sdr, which decreased from 9.68% to 8.69%, 7.78%, and 7.15%, respectively. Since Sdq is related to local surface gradients and Sdr to the increase in developed area relative to the projected area, these results indicate that wheel cleaning produced a texture with lower topographical gradients and reduced surface complexity.

This behavior is relevant because, in ceramic materials, higher local slopes and larger developed areas may be associated with abrupt grooves, microfractures, material pull-out, and regions associated with brittle removal. Thus, the simultaneous reduction in Sdq and Sdr under MQL 1:5 + WCJ suggests a surface with lower local gradients and fewer abrupt topographical irregularities. This interpretation is consistent with the SEM micrographs (Figures 11, 12, 13 and 14) and the 3D surface topographies (Figure 15), in which the wheel-cleaning condition exhibited a more regular surface, indicating a lower contribution of localized brittle-removal events.

The combined analysis of amplitude, functional, volumetric, and hybrid parameters indicates that the MQL 1:5 + WCJ condition produced the most regular topography among the evaluated conditions. This condition combined a lower average texture amplitude, reduced Spk, Sk, and Svk values, lower Vvv, and decreased Sdq and Sdr values. Therefore, the application of the wheel-cleaning jet limited the formation of deep valleys, decreased the functional core roughness, and reduced the local surface gradients. These results suggest that wheel cleaning promoted a more stable abrasive interaction, probably by removing debris and material adhered to the active surface of the grinding wheel. As a result, the diamond grains tended to remain more exposed and active for a longer period, favoring the cutting action and reducing the occurrence of three-body abrasion and localized brittle-removal events. Thus, the combination of MQL 1:5 and WCJ was the most effective condition for controlling the surface topography of ground alumina.

4.2.4. Ra parameter

Figure 21 shows the Ra values obtained under the different lubrication-cooling conditions.

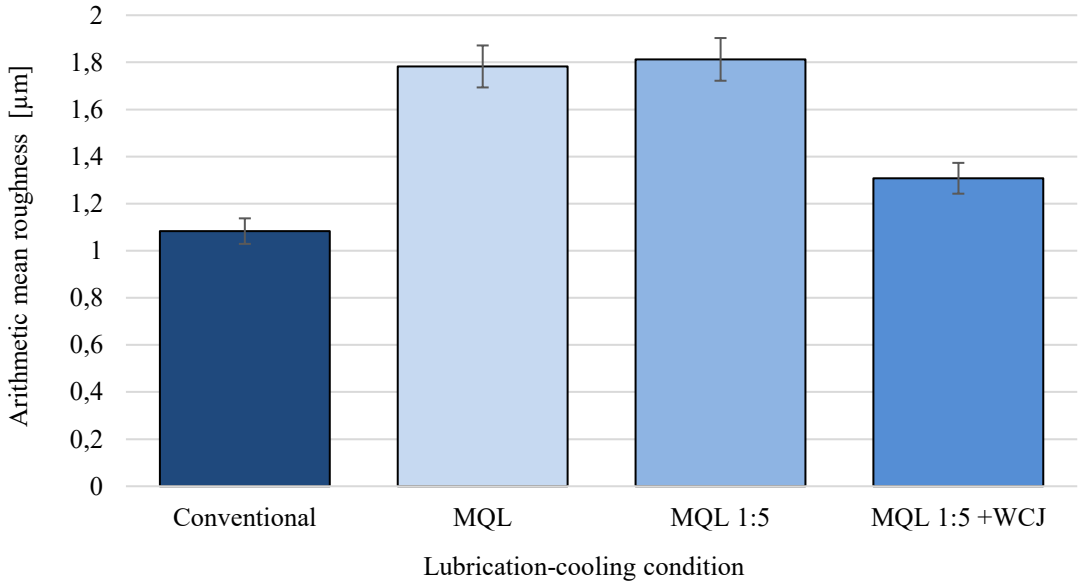


Figure 20. Ra values for each lubrication-cooling condition.

The conventional flood condition presented the lowest Ra value, approximately 1.09 µm, and was used as the technical reference for surface finish. This result is consistent with the higher cooling and flushing capacity of the flood method, which favors debris removal from the wheel-workpiece interface and contributes to a more stable cutting action. The MQL and MQL 1:5 conditions resulted in higher Ra values, approximately 1.78 µm and 1.81 µm, respectively. These values represent increases of about 63% and 66% compared with the conventional condition. This behavior indicates that the reduction in cutting fluid volume impaired the ability to remove debris from the grinding zone, favoring wheel loading and the presence of loose alumina particles between the wheel and the workpiece. In the case of MQL 1:5, the higher Ra value is also consistent with the low G-ratio as discussed in Section 4.4, indicating that dilution alone was not sufficient to preserve the cutting ability of the diamond grinding wheel.

The application of WCJ to the diluted MQL condition reduced Ra to approximately 1.31 µm. Although this value was still higher than that obtained under conventional flood grinding, it was considerably lower than those observed for pure MQL and MQL 1:5 without wheel cleaning. Compared with MQL 1:5, the use of WCJ reduced Ra by approximately 28%. This improvement can be attributed to the ability of the cleaning jet to remove debris adhered to the grinding wheel surface, reduce wheel loading, and maintain greater exposure of active

diamond grains. As a result, the wheel-workpiece interaction became more stable, reducing the formation of severe surface irregularities. Therefore, the Ra results show that MQL 1:5 + WCJ provided the best surface finish among the MQL-based conditions. This confirms that the reduction in fluid consumption must be accompanied by an effective wheel-cleaning strategy to avoid excessive deterioration of the ground alumina surface. However, because Ra represents only an average roughness value, additional topographical analyses are necessary to understand the distribution of peaks, valleys, and localized defects generated under each lubrication-cooling condition.

4.2.5. Analyses based on height distribution

Figure 22 presents the percentage area distribution of the ground alumina surfaces according to three height ranges.

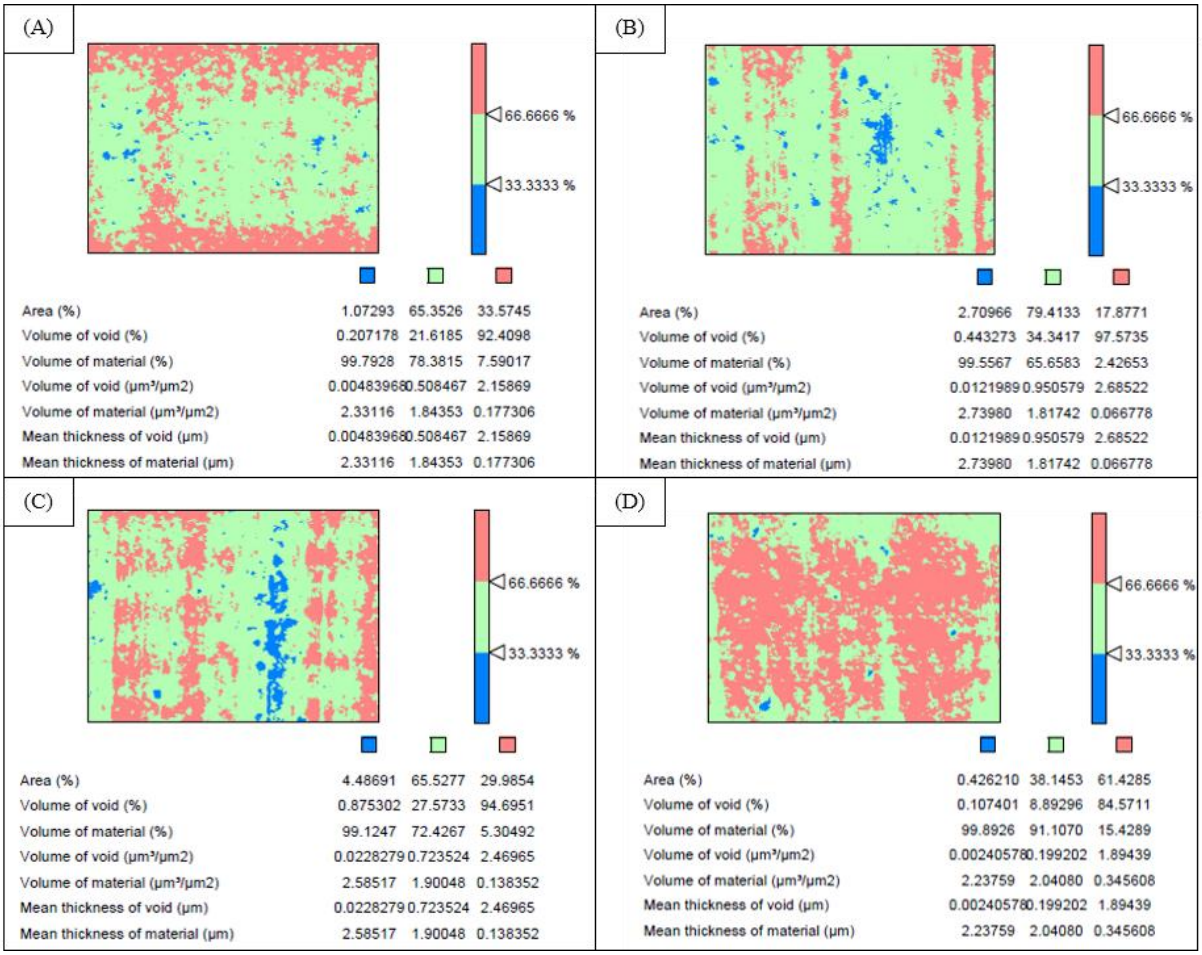


Figure 21. Percentage area distribution of the ground surfaces according to height thirds: a) conventional, b) MQL, c) MQL 1:5 and d) MQL 1:5 + WCJ

The lower third represents the most depressed regions of the surface, which may be associated with valleys, grooves, craters, and material pull-out. The middle third corresponds to the main functional region of the surface, where most of the material support is generally concentrated. The upper third represents the highest regions, related to peaks, asperities, and protruding surface features. However, this analysis must be interpreted as complementary, since the percentage of area in each height range depends on the leveling procedure and on the height reference adopted by the software.

The conventional condition showed a predominance of area in the middle third, corresponding to approximately 65.35% of the analyzed surface. The upper third represented 33.57%, while the lower third accounted for only 1.07%. This distribution suggests that, although the surface generated under flood grinding contained elevated regions, the participation of highly depressed areas was limited. This behavior is consistent with the lower Ra value obtained for the conventional condition and with the good G-ratio as discussed in Section 4.4, indicating a more stable grinding condition with effective debris removal.

For the MQL condition, the highest area concentration was also observed in the middle third, reaching approximately 79.41%. The upper third represented 17.88%, while the lower third increased slightly to 2.71%. At first, the large concentration in the middle height range could suggest a more homogeneous surface. However, this result should not be interpreted alone, since MQL also presented higher Ra and lower G-ratio compared with the conventional condition. Therefore, although most of the surface area remained concentrated in the intermediate range, the reduced cleaning capacity of MQL probably favored debris retention and a less efficient abrasive interaction, which affected both surface roughness and grinding wheel performance.

The MQL 1:5 condition presented the highest percentage of area in the lower third, approximately 4.49%, among all tested conditions. This result indicates a greater relative contribution of depressed regions on the surface. In the context of alumina grinding, these regions may be associated with deeper grooves, craters, brittle fracture marks, or localized material pull-out. This interpretation agrees with the Ra results, in which MQL 1:5 showed the highest roughness value, and with the G-ratio results, which indicated the poorest grinding wheel performance. Therefore, the height-area distribution reinforces that dilution alone was not sufficient to ensure stable material removal or to preserve the cutting ability of the diamond grinding wheel.

In contrast, the MQL 1:5 + WCJ condition showed the lowest area fraction in the lower third, only 0.43%, suggesting a reduced occurrence of highly depressed regions. This is

an important result because valleys, craters, and pull-out regions are particularly critical in brittle ceramics, as they may act as stress concentrators and compromise surface integrity. Although this condition presented a high area fraction in the upper third, approximately 61.43%, this does not necessarily indicate a worse surface condition. Instead, when analyzed together with the Ra and G-ratio results, it suggests that the wheel cleaning jet reduced the formation of severe valleys while maintaining a more active abrasive surface.

Overall, the percentage area distribution supports the hypothesis that WCJ improved the grinding behavior of diluted MQL. While MQL 1:5 without cleaning showed the greatest contribution of depressed regions, MQL 1:5 + WCJ minimized the lower-height area fraction, indicating fewer severe valleys and craters. This behavior can be attributed to the ability of the cleaning jet to remove alumina debris from the wheel surface, reduce wheel loading, and maintain greater exposure of active diamond grains during grinding. Therefore, this analysis complements the Ra results and reinforces that the use of WCJ is important to make diluted MQL more effective in alumina grinding.

4.2.6. Histogram of peaks

Figure 23 presents the peak count histograms obtained for the ground alumina surfaces. This analysis complements Ra by showing the distribution and uniformity of surface peaks. More concentrated histograms indicate a more homogeneous topography, while broader distributions suggest greater surface irregularity and less stable material removal. The conventional condition, Figure 23(a), showed a relatively concentrated distribution, consistent with its lower Ra and stable grinding behavior. The MQL condition, Figure 23(b), presented a broader distribution shifted toward higher peak heights, indicating greater topographical dispersion, probably due to the lower cleaning capacity of the reduced fluid flow.

The MQL 1:5 condition, Figure 23(c), exhibited the least uniform distribution, with a broader peak population and greater dispersion. This result is consistent with its higher Ra, greater contribution of depressed regions, and lower G-ratio, indicating unstable material removal and poorer wheel performance. In contrast, MQL 1:5 + WCJ, Figure 23(d), showed a more concentrated and regular histogram compared with the other MQL-based conditions. This suggests that the wheel cleaning jet reduced wheel loading and promoted a more uniform interaction between the diamond grains and the alumina surface. Therefore, the peak histogram reinforces that WCJ improved the topographical regularity of the ground surface.

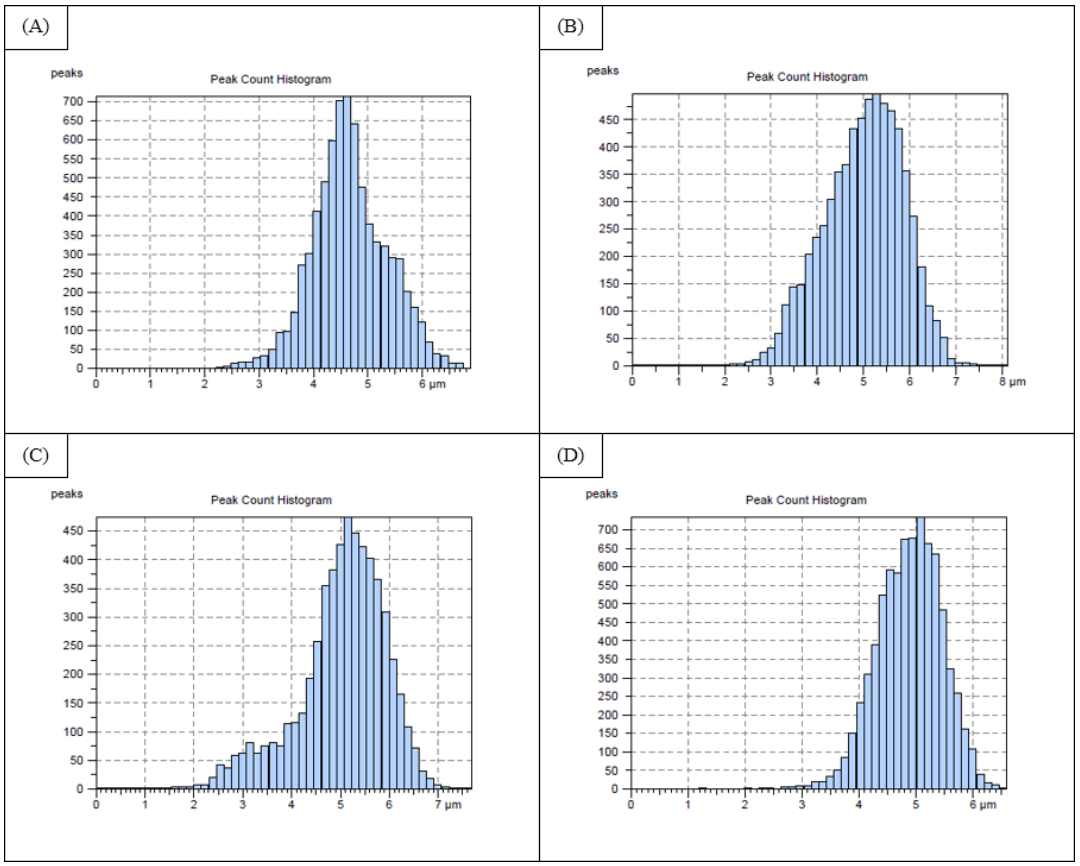


Figure 22. Histogram of peaks: a) conventional, b) MQL, c) MQL 1:5 d) MQL 1:5 + WCJ

4.2.7. Peak and valley volumes

Figure 24 presents the peak and valley volume analysis of the ground alumina surfaces. In this analysis, the hole parameters represent depressed regions of the surface, such as valleys, craters, grooves, and pull-out zones, whereas the peak parameters represent protruding regions associated with asperities and elevated irregularities. For brittle materials such as alumina, the valley-related parameters are particularly important, since severe depressed regions may indicate unstable material removal and greater surface damage. The conventional condition, Figure 24(a), presented intermediate values for both hole and peak volumes, and can be considered a technical reference. The MQL condition, Figure 24(b), showed an increase in both peak and valley severity compared with the conventional condition, indicating a more irregular topography. This result is consistent with the higher Ra value and suggests that the lower cleaning capacity of MQL favored the formation of more pronounced surface features. The most critical condition was MQL 1:5, Figure 24(c), which presented the highest valley volume and the greatest mean valley depth among the tested conditions. In addition, it also showed high peak volume. This combination indicates a surface with greater amplitude between depressed and elevated regions, suggesting a more

severe topography with deeper grooves, craters, and local pull-out. This interpretation is coherent with the higher Ra and the lowest G-ratio obtained for this condition, reinforcing that lower grinding power did not correspond to better grinding performance.

In contrast, MQL 1:5 + WCJ, Figure 24(d), showed a much lower valley volume than the other conditions. This is one of the most important results of the topography analysis, since it indicates that the wheel cleaning jet reduced the formation of severe valleys and depressed defects on the alumina surface. Although this condition still presented peak regions, the lower valley severity suggests a less critical surface from the viewpoint of surface integrity. Overall, the peak and valley volume analysis reinforces that MQL 1:5 + WCJ provided the best balance among the MQL-based conditions. While MQL 1:5 reduced environmental impact and power demand, it generated the most severe topography. By contrast, the addition of WCJ not only improved grinding wheel performance, but also helped control relevant topographical defects, especially valleys and crater-like regions, making diluted MQL more technically viable for alumina grinding.

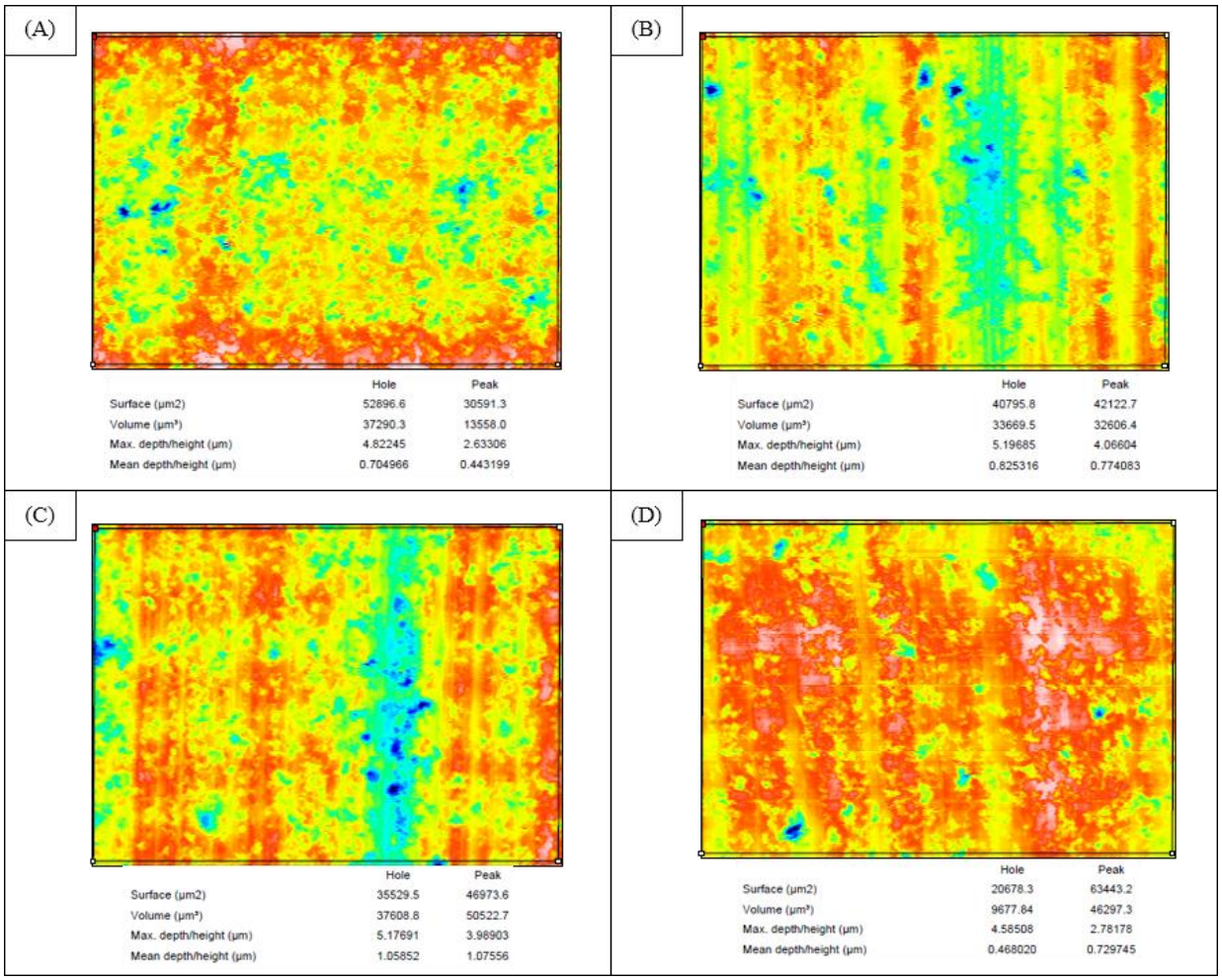


Figure 23. Peak and valley volume: a) conventional, b) MQL, c) MQL 1:5 and d) MQL 1:5 + WCJ

4.3. Diametral Wheel Wear

The diametral wheel wear results revealed a strong influence of the lubrication-cooling strategy on the performance of the diamond grinding wheel during alumina grinding. The measured wear values are presented in Figure 25.

These results indicate that wheel wear was not governed only by tangential grinding force or specific grinding energy, but also by the ability of each lubrication-cooling condition to remove debris, reduce wheel loading, and maintain active diamond grain exposure. The conventional condition resulted in low diametral wheel wear, reaching 3.61 µm, which can be attributed to the high cooling and flushing capacity of the abundant fluid. Similar behavior was reported by Lopes et al. (2023b) and Tavares et al. (2024) who observed that conventional lubrication generally leads to lower wheel wear due to its superior cooling and cleaning efficiency.

Although brittle removal mechanisms were observed on the alumina surface, the conventional fluid likely removed detached ceramic particles from the contact zone, reducing wheel loading, limiting three-body abrasion, and preserving the abrasive layer.

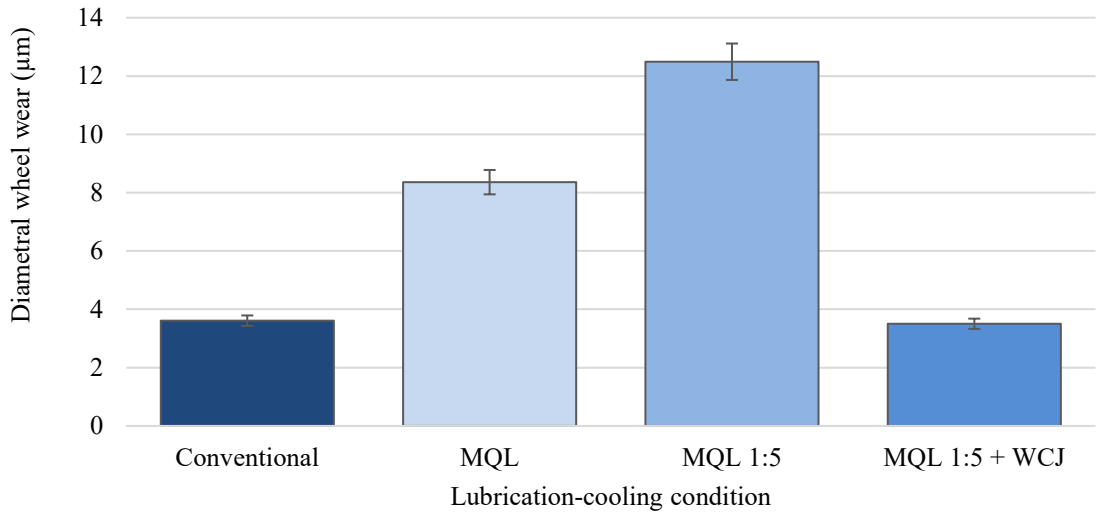


Figure 24. Diametral wheel wear of the diamond grinding wheel for each lubrication-cooling condition.

In contrast, the MQL condition increased the diametral wheel wear to 8.36 µm, approximately 131.6% higher than the conventional condition. Although MQL provides lubrication directly to the contact region, its low fluid volume limits cooling and debris removal, favoring alumina particle retention at the wheel-workpiece interface. This can

increase local friction, bond abrasion, wheel loading, and abrasive grain loss. Similar behavior was reported by Talon et al. (2022) who observed higher wheel wear under MQL than flood during alumina grinding, mainly due to the lower cooling and cleaning capacity of MQL. Lopes et al. (2023a) also found that pure MQL generated the worst wear condition, associating this result with higher thermal and mechanical loads, wheel loading, and abrasive grain macrofracture. Therefore, these studies support the interpretation that the higher wear observed under MQL is related to insufficient cooling and flushing, despite its environmental advantages.

The most critical condition was MQL 1:5, which produced the highest diametral wheel wear, 12.49 μm, approximately 246.0% higher than the conventional condition and 49.4% higher than MQL. This result is particularly relevant because MQL 1:5 also presented the lowest tangential force and specific grinding energy, showing that lower mechanical effort did not indicate a less aggressive condition for the grinding wheel. Instead, the high wear suggests that dilution reduced the lubrication efficiency without providing sufficient cleaning action.

This behavior may be explained by the lower oil concentration at the wheel-workpiece interface, which reduced the formation of an effective lubricating film. At the same time, the limited fluid flow was insufficient to remove fractured alumina particles from the grinding zone. These hard and angular ceramic fragments may have remained trapped between the wheel and the workpiece, increasing the contribution of three-body abrasion. As a result, loose alumina debris could abrade the wheel bond, damage diamond cutting edges, promote grain microfracture, and contribute to grain pull-out.

This interpretation is consistent with the surface integrity results, since MQL 1:5 presented the highest Sa and Svk, indicating a rougher surface with deeper valleys, craters, and material pull-out. Therefore, the same brittle and unstable removal mechanism that damaged the alumina surface likely contributed to the increased wheel wear.

In contrast, adding WCJ to the diluted MQL condition drastically reduced wheel wear from 12.49 μm to 3.504 μm, corresponding to a reduction of approximately 71.9%. This was the lowest wear value among all tested conditions and was very close to the conventional condition, with a difference of only about 2.9%. The beneficial effect of WCJ can be attributed to its ability to remove adhered material and loose ceramic particles from the wheel surface, reducing wheel loading and helping maintain diamond grain exposure. Consequently, the contact became less dominated by free abrasive particles and more controlled by the fixed diamond grains, reducing three-body abrasion, bond wear, and abrasive layer degradation.

The importance of the grinding wheel surface condition is supported by previous studies. Zhang et al. (2024) showed that abrasive water jet dressing can modify the topography of diamond grinding wheels by removing bond material and increasing abrasive grain protrusion, improving the cutting ability of the tool. However, they also highlighted that excessive jet action may promote grain spalling, indicating that the jet effect must be properly controlled. In the same direction, De Moraes et al. (2024) reported that WCJ improved MQL-based grinding of alumina by reducing wheel loading, removing agglomerates from the abrasive surface, decreasing friction, and helping maintain abrasive grain aggressiveness. These findings support the present results, in which WCJ reduced wheel loading, limited the permanence of alumina debris in the contact zone, and drastically decreased diametral wheel wear.

An interesting aspect of the MQL 1:5 + WCJ condition is that it presented the highest tangential force and the highest specific grinding energy, but the lowest wheel wear. This reinforces that higher force does not necessarily mean higher wheel wear in ceramic grinding. In this case, the higher force may be related to a larger number of active diamond grains effectively engaging with the workpiece surface. Since the wheel was cleaner, more abrasive grains were exposed and participated in controlled cutting. Therefore, the increase in force reflected a more effective cutting interaction rather than a more damaging tribological condition.

Figure 26 qualitatively demonstrates the effectiveness of WCJ in removing alumina debris from the grinding wheel surface. After dry grinding, Figure 26 (A) shows a large amount of white material adhered to the abrasive track, indicating severe wheel loading. After applying WCJ for 10 seconds, Figure 26 (B) shows a visibly cleaner surface, confirming the ability of the jet to remove adhered alumina particles. Although this test was performed under dry grinding only to demonstrate the cleaning mechanism, the images support that WCJ can reduce wheel loading, limit the permanence of loose ceramic debris in the contact zone, and improve process stability.

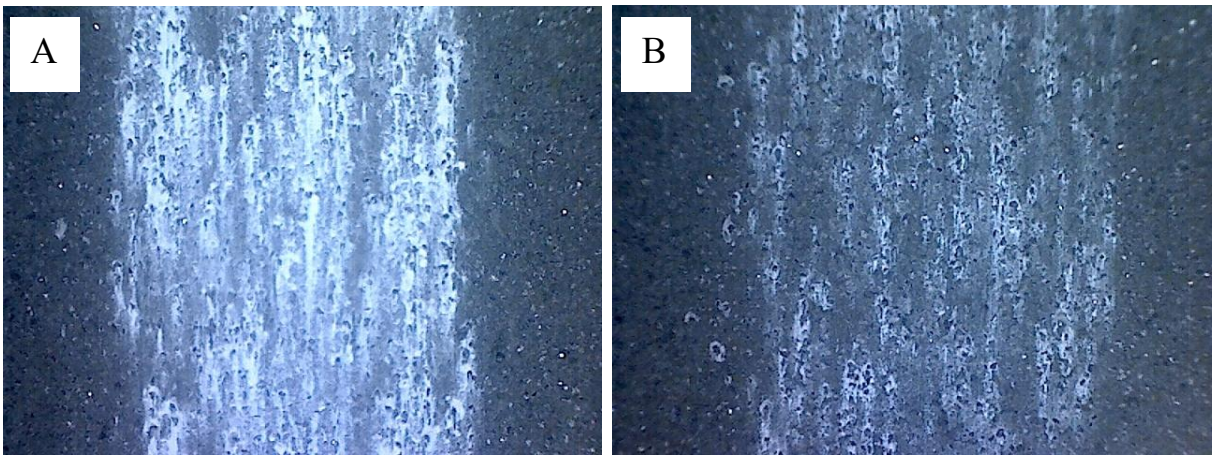


Figure 25. (A) Grinding wheel surface after one machining operation. (B) Grinding wheel surface after application of the wheel cleaning jet for 10 seconds.

Overall, the wear results show that wheel cleaning was decisive for the performance of MQL-based conditions. Without WCJ, diluted MQL intensified wheel wear due to insufficient lubrication, limited debris removal, wheel loading, and probable three-body abrasion. With WCJ, debris removal improved significantly, reducing wheel wear to a level comparable to conventional grinding. Therefore, MQL 1:5 + WCJ is a promising strategy for reducing fluid consumption while preserving the grinding wheel.

4.4. Grinding Power and G-Ratio

In grinding processes, given the high heat formation during material removal, variations in the volume of cutting fluid applied, as well as the implementation of dilutions and WCJ significantly alter factors such as grinding power and G-ratio. It is important to note that the increase in grinding power is generally associated with greater energy demand during material removal, while the increase in G-ratio is directly related to greater process efficiency (Shaw, 1996).

The average grinding power obtained during the tests is shown in Figure 27. The grinding power obtained with the conventional application of cutting fluid is assumed as a reference value, reaching values of 217.8 W. In sequence, it is possible to observe that MQL and MQL 1:5 + WCJ generate increases of 10.26 and 18.47%, respectively, while the MQL 1:5 without WCJ generated reductions of 21.2 % in this parameter.

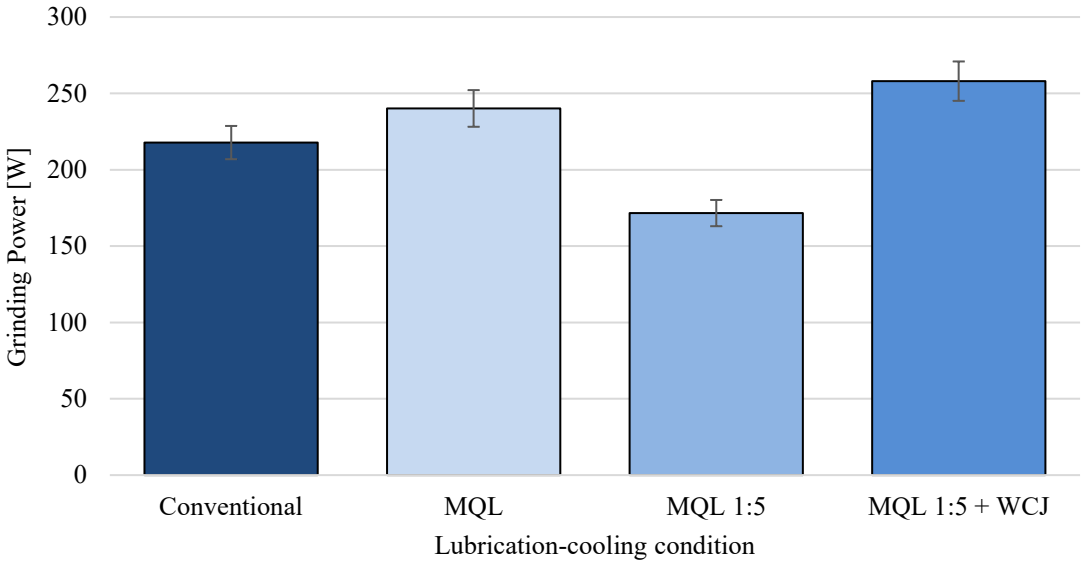


Figure 26. Grinding Power for various conditions.

In isolation, the increase in the dilution of the cutting fluid together with the reduction in the overall volume of fluid, presented in the MQL 1:5, could indicate better grinding conditions. However, the G-ratio values presented in Figure 28 do not corroborate this statement. In this situation, the G-ratio obtained for the MQL 1:5 was 17.8, followed by the pure MQL with 26.8. In comparison, conventional flood grinding obtained a G-ratio of 62.97, slightly surpassed by MQL 1:5 + WCJ, with a G-ratio of 63.84. Thus, although MQL 1:5 presented lower grinding power values, the high values of diametrical wear through the loss of abrasive grains did not allow the proportional removal of work material.

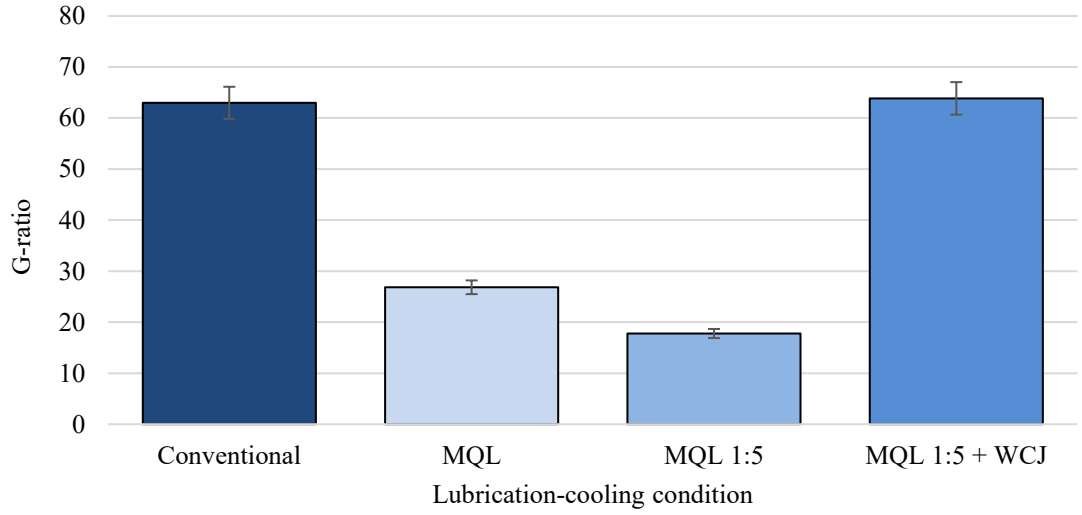


Figure 27. Average G-ratio for various conditions.

This characteristic of loss of abrasive material is directly linked to the grinding wheel wear mechanisms (Malkin; Guo, 2008a). When the abrasive grain loses its cutting ability, the abrasive grain fractures and generates a new cutting edge capable of removing the work material again. If the temperature and friction conditions are not favorable, there is degradation and fracture of the binder, generating the complete removal of the abrasive grain. That said, the lower lubricity caused by the higher water content in the MQL 1:5 condition, together with the presence of machining debris, promoted successive abrasive grain loss and accelerated wheel wear. In analogy, pure MQL allowed less loss of abrasive material, mainly due to the greater lubrication capacity compared to MQL 1:5.

Figure 29 shows the topography of the workpieces obtained with confocal microscopy. From these images, it is possible to identify typical characteristics of brittle removal, characterized by removed grains and craters on the surface, as well as it is possible to identify plastically deformed regions, as in the condition with conventional flood shown in Figure 29.a. As they point out Malkin et al. (1996), although the largest volume of material removal occurs in the brittle condition, most of the cutting energy is dissipated in ductile material removal.

Using pure MQL, a surface with greater traces of plastic deformation is observed (Figure 29.b. Together with the grinding power data, it is possible to corroborate that the greater presence of plowing would be directly linked to the increase in this parameter, as identified by other authors during alumina grinding (Chen et al., 2010).

In relation to Figure 29.c, it is possible to see a reduction in plowing when compared with Figure 29.b, however, the loss of grinding wheel material already discussed may have culminated in a ground component with greater geometric and superficial errors. In addition, aggressive conditions for grinding wheel degradation can negatively affect the surface integrity of the workpiece, generating cracks originating from surface defects (Su et al., 2025). The surface obtained under MQL 1:5 + WCJ is shown in Figure 29.d. Although it has presented higher grinding power compared to the conventional condition, this condition has surface characteristics similar to the conventional condition. The presence of WCJ can remove debris at the cutting interface, preventing loss of wheel cut or debris entrapment at the contact interface. Thus, good material removal conditions were obtained, along with the best G-ratio condition with the use of MQL.

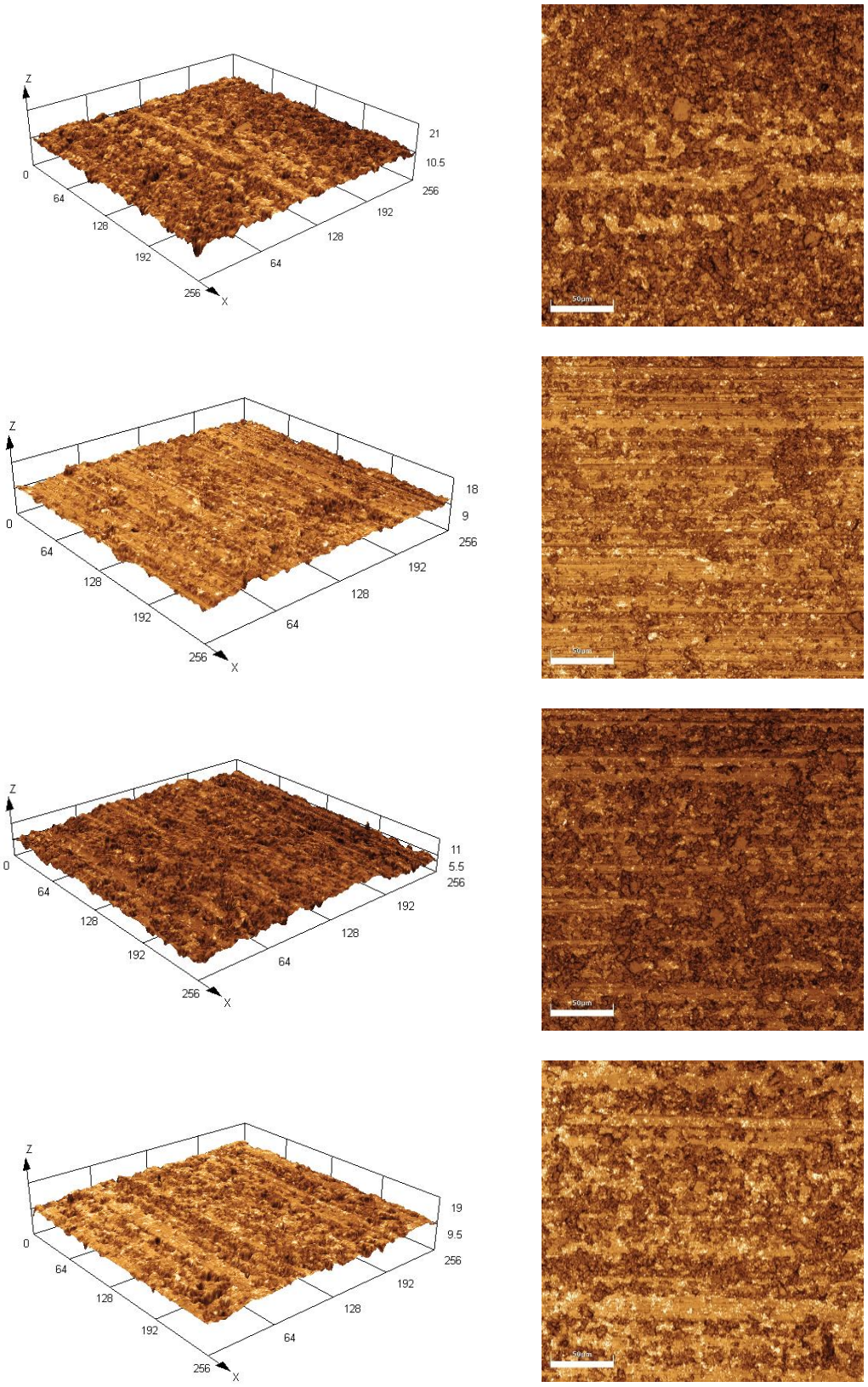


Figure 28. Confocal images of workpieces: a) conventional, b) MQL, c) MQL 1:5 and d) MQL 1:5 + WCJ

4.5. Cost Analysis

Figure 30 presents the grinding cost obtained for each lubrication-cooling condition. The conventional flood condition resulted in the highest cost, approximately 34 US$/piece. This behavior is mainly associated with the large amount of cutting fluid used in the flood system, as well as the additional costs related to fluid recirculation, disposal, and energy consumption of the pumping system. Although the conventional condition presented good technical performance in terms of G-ratio, its dependence on abundant cutting fluid increased the total cost of the process.

The MQL-based conditions reduced the grinding cost compared with the conventional method. Pure MQL reduced the cost to approximately 31 US$/piece, representing a reduction of about 9% compared with flood grinding. This reduction is directly related to the drastic decrease in cutting fluid consumption, since MQL uses only a small amount of oil carried by compressed air. However, the cost reduction was not even greater because pure MQL presented lower G-ratio than the conventional condition, indicating higher grinding wheel wear and lower wheel life. The MQL 1:5 condition showed a cost very close to pure MQL, slightly lower, reaching approximately 30.7 US$/piece. The dilution of the cutting fluid reduced the amount of oil effectively consumed during the process, which contributed to decreasing the fluid-related cost. However, this condition also presented the lowest G-ratio among all tested conditions, indicating severe grinding wheel wear. Therefore, although MQL 1:5 reduced fluid consumption and grinding power, its poor wheel performance limited the economic advantage that could be obtained from fluid dilution alone.

The lowest cost was obtained with the MQL 1:5 + WCJ condition, approximately 30 US$/piece, corresponding to a reduction of about 11% compared with the conventional flood condition. This result indicates that the additional use of compressed air for the wheel cleaning jet did not increase the total process cost significantly. On the contrary, the WCJ improved the cleaning of the grinding wheel surface, reduced wheel loading, and contributed to maintaining active diamond grains during grinding. As a consequence, this condition achieved the highest G-ratio and reduced the cost associated with grinding wheel wear.

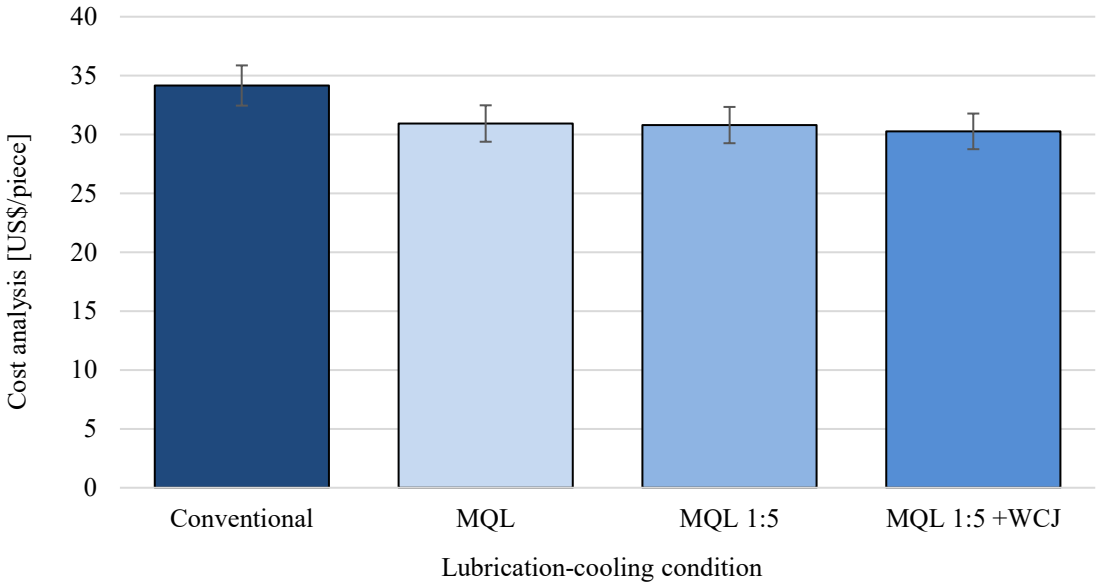


Figure 29. Grinding cost analysis for each lubrication-cooling condition.

Therefore, the cost analysis shows that the economic performance of the process cannot be evaluated only by the volume of cutting fluid used. Although MQL 1:5 reduced fluid consumption, its low G-ratio increased the relevance of wheel wear in the total cost. In contrast, MQL 1:5 + WCJ combined reduced fluid consumption with high grinding wheel efficiency, resulting in the best economic performance among the tested conditions. Thus, from a cost perspective, diluted MQL assisted by WCJ represents the most advantageous alternative, since it reduces the dependence on conventional flood lubrication while preserving the diamond grinding wheel and improving process efficiency.

4.6. CO_2 Emission

Figure 31 presents the carbon emission values obtained for each lubrication-cooling condition. The conventional flood condition generated the highest carbon emission, approximately 0.81 $kgCO_2$/piece. This result is mainly associated with the large volume of cutting fluid used in the process, as well as the energy required for fluid pumping and recirculation. Although the conventional method provides efficient cooling, lubrication, and debris removal, its dependence on abundant cutting fluid increases the environmental impact of the grinding process.

The MQL condition reduced carbon emissions to approximately 0.62 $kgCO_2$/piece, representing a reduction of about 23% compared with conventional flood grinding. This reduction is directly related to the drastic decrease in cutting fluid consumption, since MQL uses only a small amount of oil transported by compressed air. However, despite this

environmental advantage, pure MQL presented lower process efficiency in terms of G-ratio, indicating that the reduction in fluid consumption alone was not sufficient to ensure the best overall grinding performance.

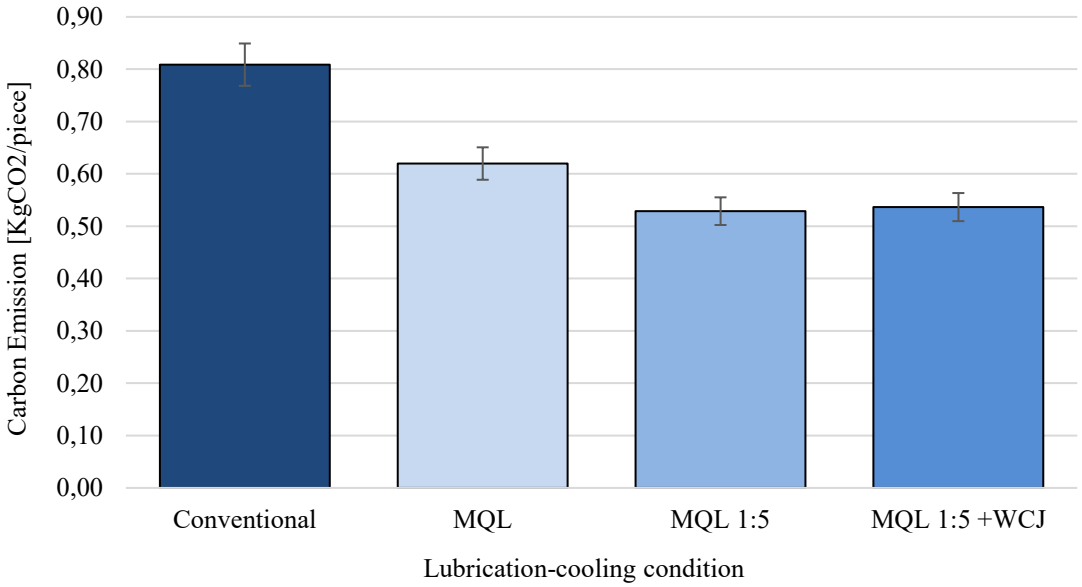


Figure 30. Carbon Emission for each lubrication-cooling condition.

The lowest carbon emission was obtained with the MQL 1:5 condition, reaching approximately 0.53 kgCO_2/piece, corresponding to a reduction of about 35% compared with the conventional condition. This behavior can be attributed to the lower oil concentration in the diluted fluid and the reduced volume of cutting fluid applied during grinding. However, this condition also presented the lowest G-ratio and the highest grinding wheel wear. Therefore, although MQL 1:5 was the best condition from a strictly environmental point of view, its poor technical performance limits its practical application in industrial alumina grinding.

The MQL 1:5 + WCJ condition showed a carbon emission value very close to that of MQL 1:5, approximately 0.54 kgCO_2/piece. This indicates that the additional compressed air used for the wheel cleaning jet did not significantly increase the environmental impact of the process. More importantly, this condition combined low carbon emission with the best G-ratio and improved grinding wheel performance. The WCJ contributed to removing debris from the wheel surface, reducing wheel loading, and maintaining active diamond grains, which improved process efficiency without substantially increasing CO_2 emissions.

Overall, the carbon emission analysis shows that all MQL-based conditions reduced environmental impact compared with conventional flood grinding. However, the best environmental result should not be evaluated only by the lowest CO_2 value. While MQL 1:5 produced the lowest emission, its low G-ratio indicates severe wheel wear and poor process efficiency. In contrast, MQL 1:5 + WCJ provided the best balance between reduced carbon emission and technical performance, making it the most promising alternative for sustainable alumina grinding with diamond wheels.

5. CONCLUSIONS

This study investigated the effects of conventional flood cooling, pure MQL, diluted MQL at a 1:5 ratio, and MQL 1:5 combined with a wheel cleaning jet (WCJ) on the grinding of alumina with a diamond grinding wheel. Tangential grinding force, specific grinding energy, surface integrity, diametrical wheel wear, G-ratio, operating cost, and estimated CO_2 emissions were evaluated. Under the investigated experimental conditions, the following conclusions can be drawn:

- The lubrication-cooling strategy directly affected the mechanical response of the process. MQL 1:5 produced the lowest tangential grinding force and specific grinding energy, whereas MQL 1:5 + WCJ produced the highest values. However, the results demonstrated that lower grinding force and energy did not necessarily correspond to better overall grinding performance.
- The surface analyses showed distinct responses depending on the parameter considered. Conventional flood cooling resulted in the lowest Ra, whereas MQL 1:5 + WCJ produced the lowest Sa, Sk, Svk, Vvv, Sdq, and Sdr values. Therefore, the combined strategy provided the most favorable overall areal topography and the best surface response among the MQL-based conditions, with fewer severe valleys and localized irregularities.
- Conventional flood cooling resulted in low diametrical wheel wear of 3.61 μm and a G-ratio of 62.98. Pure MQL increased wheel wear to 8.36 μm and reduced the G-ratio to 26.84, indicating that its limited cooling and debris-removal capacity impaired wheel performance.
- MQL 1:5 produced the highest diametrical wheel wear, 12.49 μm, and the lowest G-ratio, 17.77, despite producing the lowest grinding force and specific energy. This result indicates that the reduction in mechanical effort was

accompanied by an unfavorable tribological condition at the wheel–workpiece interface.

- The poor performance of MQL 1:5 was likely related to its reduced lubrication efficiency and insufficient debris removal. The retention of hard alumina particles may have intensified wheel loading, bond abrasion, abrasive-grain loss, and three-body abrasion. These mechanisms are considered probable interpretations and should be confirmed by direct wheel-loading and debris analyses.
- The application of WCJ substantially improved the performance of diluted MQL. Diametrical wheel wear decreased from 12.49 to 3.504 μm, representing a reduction of approximately 71.9%. The G-ratio increased from 17.77 to 63.84, becoming numerically comparable to the value obtained with conventional flood cooling.
- The higher tangential grinding force and specific grinding energy obtained with MQL 1:5 + WCJ did not result in greater wheel wear. This behavior may be associated with more effective debris removal and the preservation of active diamond grains. However, the relative contributions of cutting, ploughing, and brittle fracture require further investigation.
- Conventional flood cooling provided good technical performance but resulted in the highest operating cost because of the large volume of cutting fluid required. The MQL-based strategies considerably reduced fluid consumption and the associated operating costs.
- MQL 1:5 produced the lowest estimated CO_2 emissions but also exhibited the lowest G-ratio and the highest wheel wear. Therefore, its lower estimated emissions did not compensate for its limited technical performance.
- The estimated CO_2 emissions of MQL 1:5 + WCJ were approximately 33.3% lower than those of conventional flood cooling, decreasing from 0.81 to 0.54 kg CO_2 per workpiece. Although its emissions were slightly higher than those of MQL 1:5 alone, the combined strategy provided substantially better technical performance. Therefore, MQL 1:5 + WCJ achieved a more favorable balance between reduced cutting-fluid consumption, lower estimated CO_2 emissions, wheel preservation, and surface quality, considering the system boundary and assumptions adopted in the environmental model.

Overall, MQL 1:5 + WCJ provided the most favorable qualitative balance between wheel preservation, areal surface topography, operating cost, and cutting-fluid consumption. Under the tested conditions, the combined strategy proved to be a promising alternative to conventional flood cooling for alumina grinding, as it reduced fluid consumption while maintaining a G-ratio comparable to the conventional condition and limiting the detrimental effects associated with wheel loading and three-body abrasion. Nevertheless, this conclusion is restricted to the experimental conditions and the economic and environmental assumptions adopted in this study.

SCIENTIFIC PRODUCTION

The research activities conducted throughout this doctoral project resulted in four scientific publications, comprising two journal articles and two full papers presented at international conferences. These publications disseminate complementary findings on the grinding of alumina ceramics under minimum quantity lubrication (MQL), addressing process performance, surface integrity, grinding wheel wear, surface topography, energy demand, economic performance, and CO_2 emissions.

The following journal articles resulted from this thesis:

- "Surface integrity and wear mechanisms in MQL grinding of alumina ceramics assisted by wheel cleaning," published in The International Journal of Advanced Manufacturing Technology. DOI: https://doi.org/10.1007/s00170-026-18903-y. This article investigates the effects of MQL and the wheel-cleaning jet on the surface integrity of alumina ceramics and on grinding wheel wear mechanisms. The analysis includes three-dimensional surface roughness parameters, Abbott–Firestone functional parameters, grinding forces, specific grinding energy, wheel wear, and scanning electron microscopy.
- "Process performance, wheel wear, surface topography, cost, and CO_2 emissions in MQL-based alumina grinding assisted by wheel cleaning jet," published in The International Journal of Advanced Manufacturing Technology. DOI: https://doi.org/10.1007/s00170-026-19153-8. This article provides an integrated assessment of the grinding process by correlating process performance, grinding wheel wear, surface topography, operational costs, and CO_2 emissions.

The following full papers were presented at international conferences:

- “Sustainable Grinding of Advanced Ceramics through the Evaluation of MQL as an Eco-Friendly Alternative,” presented at the 14th International Workshop on Advances in Cleaner Production (IWACP), held in Jouy-en-Josas, France, from October 13 to 16, 2025. This study evaluated MQL as a more environmentally sustainable alternative to conventional flood lubrication in the grinding of alumina ceramics, focusing primarily on surface roughness and CO_2 emissions.
- “Sustainable ceramic grinding with MQL focusing on power consumption and CO_2 emissions,” presented at the 20th CIRP Conference on Intelligent Computation in Manufacturing Engineering (CIRP ICME ’26), held in the Gulf of Naples, Italy, from July 8 to 10, 2026. This paper examines the sustainability of MQL-assisted ceramic grinding by analyzing power consumption, surface roughness, and CO_2 emissions under different lubrication conditions.

Collectively, these publications demonstrate the scientific contribution and dissemination of the research developed in this thesis at both journal and international conference levels. While the conference papers provided focused assessments of the environmental performance of MQL-assisted grinding, the journal articles consolidated a more comprehensive analysis of the process, including its technological, economic, and environmental implications.

SUGGESTIONS FOR FUTURE WORK

Although this thesis contributed to understanding the grinding of alumina using MQL-based lubrication-cooling strategies assisted by a wheel cleaning jet (WCJ), several aspects require further investigation. Future studies should particularly focus on the phenomenology of three-body abrasion and the mechanisms responsible for material removal, since these phenomena were used to interpret the experimental results but were not directly quantified in the present study.

A central research priority should be to determine how detached alumina particles interact with the grinding wheel, workpiece, and bond material. The results obtained with MQL 1:5 were consistent with the occurrence of debris accumulation and three-body

abrasion; however, direct experimental evidence is still required. Interrupted grinding tests should therefore be conducted at different stages of wheel wear to quantify wheel loading and monitor its evolution. The grinding wheel surface could be characterized using scanning electron microscopy, energy-dispersive X-ray spectroscopy, confocal microscopy, and three-dimensional image analysis. These techniques would help identify adhered alumina, bond abrasion, grain fracture, grain pull-out, and changes in abrasive-grain protrusion.

The debris generated under each lubrication-cooling condition should also be systematically collected and characterized. Particle size distribution, morphology, chemical composition, and fracture features could be evaluated using laser diffraction, SEM, and EDS. These analyses would help determine whether the particles remain trapped in the contact zone, become embedded in the wheel bond, or act as loose abrasives between the wheel and workpiece. Tribological tests under controlled conditions could complement the grinding experiments and help distinguish two-body abrasion from three-body abrasion.

Further research is also needed to clarify the mechanisms of material removal during alumina grinding. The relative contributions of brittle fracture, ductile-regime cutting, ploughing, intergranular fracture, transgranular fracture, grain pull-out, and crushing should be investigated. Cross-sectional microscopy, SEM, Raman spectroscopy, X-ray diffraction, microhardness measurements, residual stress analysis, and subsurface crack characterization could be used to relate the active removal mechanisms to force, specific energy, surface topography, wheel wear, and grinding conditions. This investigation would also help explain why MQL 1:5 + WCJ produced higher tangential grinding force and specific grinding energy while simultaneously reducing wheel wear.

The WCJ operating parameters should also be optimized, including jet pressure, airflow rate, nozzle angle, nozzle distance, application time, and position relative to the grinding zone. These variables may affect debris removal, grain exposure, wheel loading, and the balance between cutting, ploughing, and brittle fracture. Factorial designs or response surface methodologies could be employed to identify suitable operating windows and interactions between WCJ parameters and MQL dilution.

Different diamond grinding wheel specifications should be evaluated, including abrasive grain size, concentration, bond type, porosity, wheel structure, and abrasive-layer thickness. These characteristics directly influence debris accommodation, cutting-edge density, grain retention, bond erosion, material removal mechanisms, wheel wear, and G-ratio. Such investigations would clarify whether the effectiveness of WCJ depends on the wheel specification and its ability to transport debris away from the contact zone.

Future studies should include direct temperature measurements in the grinding zone. Temperature data would help distinguish the effects of lubrication, cooling, and wheel cleaning and verify whether thermal conditions contribute to the observed changes in material removal, surface integrity, and wheel wear. These measurements could be correlated with force, power, acoustic emission, vibration, wheel loading, and surface damage.

The surface and subsurface integrity analyses should be expanded to include residual stresses, microhardness, fracture toughness, subsurface crack depth, phase transformations, and thermal damage. This is particularly important for advanced ceramics because defects that are not visible on the ground surface may reduce the mechanical strength and reliability of the final component.

Other advanced ceramics, including zirconia, silicon carbide, silicon nitride, and ceramic composites, should also be investigated. These materials exhibit different fracture behavior, toughness, thermal properties, and debris characteristics. Their evaluation would help determine whether the benefits observed for MQL 1:5 + WCJ are specific to alumina or can be extended to other advanced ceramics.

Long-duration and industrial-scale grinding tests should be conducted to evaluate wheel loading, wheel wear progression, process stability, dressing frequency, and surface quality over a larger volume of removed material. These experiments would provide a more representative assessment of the industrial applicability and long-term performance of the combined lubrication-cooling strategy.

The economic and environmental analyses should be expanded through a life cycle assessment that includes cutting-fluid production, transportation and disposal, compressed-air generation, grinding-wheel manufacturing and consumption, dressing operations, equipment maintenance, and end-of-life impacts. Including wheel consumption is particularly important because the lubrication-cooling conditions produced substantial differences in diametrical wear and G-ratio.

Finally, process monitoring and artificial intelligence techniques could be used to identify changes in the grinding regime and predict wheel loading, wheel wear, surface roughness, and surface damage. Signals such as force, power, acoustic emission, vibration, and temperature could be combined with wheel-surface and debris analyses to develop models capable of distinguishing changes in material removal mechanisms and detecting the onset of three-body abrasion.

Overall, future research should move beyond performance comparisons and seek direct experimental evidence of the physical and tribological phenomena occurring in the

grinding zone. A deeper understanding of three-body abrasion, debris behavior, wheel loading, and material removal mechanisms is essential for explaining the effects observed in this study and for optimizing the interaction between MQL dilution, WCJ parameters, grinding-wheel specification, and process conditions.

REFERENCES

ABELLAN-NEBOT, Jose v; ROGERO, Miguel Ortells. Sustainable machining of molds for tile industry by minimum quantity lubrication. **Journal of Cleaner Production**, v. 240, p. 118082, 2019.

AGARWAL, Sanjay. On the mechanism and mechanics of wheel loading in grinding. **Journal of Manufacturing Processes**, v. 41, n. March, p. 36–47, 2019.

ALBERDI, R. *et al.* Strategies for optimal use of fluids in grinding. **International Journal of Machine Tools and Manufacture**, v. 51, n. 6, p. 491–499, 2011.

ANDERSON, D.; WARKENTIN, A.; BAUER, R. Experimental validation of numerical thermal models for dry grinding. **Journal of Materials Processing Technology**, v. 204, n. 1–3, p. 269–278, 11 ago. 2008.

AURICH, J. C. *et al.* High-performance dry grinding using a grinding wheel with a defined grain pattern. **CIRP Annals**, v. 57, n. 1, p. 357–362, 2008.

ÁVILA, Benício Nacif *et al.* Grinding effect of thermoplastic mold steel using green manufacturing concepts combined with various conventional wheels. **International Journal of Advanced Manufacturing Technology**, v. 129, n. 5, p. 2443–2456, 1 nov. 2023.

BARCZAK, L. M.; BATAKO, A. D. L.; MORGAN, M. N. A study of plane surface grinding under minimum quantity lubrication (MQL) conditions. **International Journal of Machine Tools and Manufacture**, v. 50, n. 11, p. 977–985, 2010.

BENEDICTO, E.; CAROU, D.; RUBIO, E. M. Technical, Economic and Environmental Review of the Lubrication/Cooling Systems Used in Machining Processes. **Procedia Engineering**, v. 184, p. 99–116, 2017.

BHARATHI, V. *et al.* A review on the challenges in machining of ceramics. **Materials Today: Proceedings**, v. 46, p. 1451–1458, 1 jan. 2021.

BIANCHI, E. C. *et al.* Estudo comparativo entre a agressividade superficial obtida na retificação com rebolos de óxido de alumínio e CBN, fabricados com ligantes resinóide e vitrificado. **Cerâmica**, v. 57, n. 344, p. 431–437, dez. 2011.

BIANCHI, E. C. *et al.* Limpeza da superfície de corte de rebolos por um sistema de ar comprimido na retificação cilíndrica externa de mergulho de materiais cerâmicos refrigerados com a técnica da mínima quantidade de lubrificante (MQL). **Cerâmica**, 2012.

BIANCHI, E. C. *et al.* Plunge cylindrical grinding with the minimum quantity lubrication coolant technique assisted with wheel cleaning system. **International Journal of Advanced Manufacturing Technology**, v. 95, n. 5–8, p. 2907–2916, 2018.

BIANCHI, Eduardo Carlos *et al.* **Análise do Comportamento da Microestrutura de Materiais Endurecidos Retificados com Rebolos de CBN**. *[S.l.: S.n.]*.

BLACKLEY, W. S.; SCATTERGOOD, R. O. Chip topography for ductile-regime machining of germanium. **Journal of Engineering for Industry,** v. 116, p. 263–266, 1994.

BRUNI, C. *et al.* Effect of the lubrication-cooling technique, insert technology and machine bed material on the workpart surface finish and tool wear in finish turning of AISI 420B. **International Journal of Machine Tools and Manufacture**, v. 46, n. 12–13, p. 1547–1554, 2006.

CARTER, C. Barry; NORTON, M. Grant. **Ceramic Materials**. *[S.l.]*: Springer, 2007.

CHEN, Jianyi *et al.* Grinding characteristics in high speed grinding of engineering ceramics with brazed diamond wheels. **Journal of Materials Processing Technology**, v. 210, n. 6–7, p. 899–906, 1 abr. 2010.

CHOI, Hon Zong; LEE, Suk Woo; JEONG, Hae Do. The cooling effects of compressed cold air in cylindrical grinding with alumina and CBN wheels. *In*: 2002.

CHOUDHARY, Amit; NASKAR, Anirban; PAUL, S. Effect of minimum quantity lubrication on surface integrity in high-speed grinding of sintered alumina using single layer diamond grinding wheel. **Ceramics International**, v. 44, n. 14, p. 17013–17021, 1 out. 2018.

CHOUDHARY, Amit; PAUL, S. The wear mechanisms of diamond grits in grinding of alumina and yttria-stabilized zirconia under different cooling-lubrication schemes. **Wear**, v. 454–455, p. 203315, 15 ago. 2020.

DA SILVA, Leonardo Roberto *et al.* Analysis of surface integrity for minimum quantity lubricant-MQL in grinding. **International Journal of Machine Tools and Manufacture**, v. 47, n. 2, p. 412–418, 2007.

DE MORAES, Douglas Lyra *et al.* Performance of SAE 52100 steel grinding using MQL technique with pure and diluted oil. **The International Journal of Advanced Manufacturing Technology**, v. 105, n. 10, p. 4211–4223, 13 dez. 2019.

DE MORAES, Douglas Lyra *et al.* Advances in precision manufacturing towards eco-friendly grinding process by applying MQL with cold air compared with cooled wheel cleaning jet. **The International Journal of Advanced Manufacturing Technology**, v. 113, n. 11–12, p. 3329–3342, 2 abr. 2021.

DE MORAES, Douglas Lyra *et al.* Eco-friendly machining of advanced ceramics: wheel cleaning jet for greenhouse gas reduction. **The International Journal of Advanced Manufacturing Technology 2024 132:1**, v. 132, n. 1, p. 745–757, 15 mar. 2024.

DEBNATH, Sujan; REDDY, Moola Mohan; YI, Qua Sok. Environmental friendly cutting fluids and cooling techniques in machining: a review. **Journal of Cleaner Production**, v. 83, p. 33–47, nov. 2014.

DEMIRBAS, E.; KOBYA, M. Operating cost and treatment of metalworking fluid wastewater by chemical coagulation and electrocoagulation processes. **Process Safety and Environmental Protection**, v. 105, p. 79–90, 1 jan. 2017.

DHAR, N. R.; KAMRUZZAMAN, M.; AHMED, Mahiuddin. Effect of minimum quantity lubrication (MQL) on tool wear and surface roughness in turning AISI-4340 steel. **Journal of Materials Processing Technology**, v. 172, n. 2, p. 299–304, fev. 2006.

DO NASCIMENTO, Wesley R. *et al.* A study on the viability of minimum quantity lubrication with water in grinding of ceramics using a hybrid-bonded diamond wheel. **Proceedings of the Institution of Mechanical Engineers, Part B: Journal of Engineering Manufacture**, v. 230, n. 9, p. 1630–1638, 2016.

Electricity prices. Disponível em: <https://www.globalpetrolprices.com/electricity_prices/>. Acesso em: 16 nov. 2020.

EMAMI, M.; SADEGHI, M. H.; SARHAN, Ahmed A. D. Investigating the effects of liquid atomization and delivery parameters of minimum quantity lubrication on the grinding process of Al2O 3 engineering ceramics. **Journal of Manufacturing Processes**, 2013a.

EMAMI, M.; SADEGHI, M. H.; SARHAN, Ahmed A. D. Investigating the effects of liquid atomization and delivery parameters of minimum quantity lubrication on the grinding process of Al2O 3 engineering ceramics. **Journal of Manufacturing Processes**, v. 15, n. 3, p. 374–388, ago. 2013b.

FARFAN-CABRERA, Leonardo I. *et al.* Microalgae Oil-Based Metal Working Fluids for Sustainable Minimum Quantity Lubrication (MQL) Operations—A Perspective. **Lubricants**, v. 11, n. 5, 1 maio 2023.

FATHALIAN, Mostafa *et al.* A Comprehensive Study of Al2O3 Mechanical Behavior Using Density Functional Theory and Molecular Dynamics. **Molecules**, v. 29, n. 5, 1 mar. 2024.

FAWCETT, S. C.; DOW, T. A. Development of a model for precision contour grinding of brittle materials. **Precision Engineering**, v. 13, p. 270–276, 1991.

FERNANDES, Lucas de Martini *et al.* Advanced ceramic grinding process combined to hazard mitigation to the employees' health by using an alternative lubri-refrigeration technique. **The International Journal of Advanced Manufacturing Technology**, v. 127, n. 5, p. 2921–2934, 2023.

FIELD, M.; KEGG, R.; BUESCHER, S. Computerized Cost Analysis of Grinding Operations. **CIRP Annals**, v. 29, n. 1, p. 233–237, 1 jan. 1980.

GERLING, Heinrich. **À volta da máquina-ferramenta**. Tradução: Fernando Figueiredo Conceição. *[S.l.]*: Editorial Reverté, 1967.

GROOVER, Mikell P. **Fundamentals of modern manufacturing: materials, processes, and systems**. Seventh ed. *[S.l.]*: John Wiley & Sons, 2010. v. 2

GUEROULT, B.; CHERIF, K. State of the art review on friction and wear mechanisms of ceramics. **Journal of the Ceramic Society**, v. 63, n. 2, p. 132–142, 1994.

HADAD, Mohammadjafar. An experimental investigation of the effects of machining parameters on environmentally friendly grinding process. **Journal of Cleaner Production**, v. 108, p. 217–231, 2015.

HASSUI, A.; DINIZ, A. E. Correlating surface roughness and vibration on plunge cylindrical grinding of steel. **International Journal of Machine Tools and Manufacture**, v. 43, n. 8, p. 855–862, 2003.

HITCHCOX, Alan. **Determine the Cost of Compressed Air for Your Plant**. Disponível em: <https://www.hydraulicspneumatics.com/technologies/air-compressors/article/21884932/determine-the-cost-of-compressed-air-for-your-plant>.

HOWES, T. D. *et al.* **Environmental Aspects of Grinding Fluids**. *[S.l.: S.n.]*.

HU, K. X.; CHANDRA, A. A fracture mechanics approach to modeling strength degradation in ceramic grinding processes. **Journal of Engineering for Industry**, v. 115, p. 73–84, fev. 1993.

IRANI, R. A.; BAUER, R. J.; WARKENTIN, A. A review of cutting fluid application in the grinding process. **International Journal of Machine Tools and Manufacture**, v. 45, n. 15, p. 1696–1705, 2005.

JACKSON, M. J. *et al.* High-speed grinding with CBN grinding wheels - applications and future technology. **Journal of Materials Processing Technology**, v. 110, n. 1, p. 78–88, mar. 2001.

JACKSON, M. J. *et al.* Laser cleaning and dressing of vitrified grinding wheels. **Journal of Materials Processing Technology**, v. 185, n. 1–3, p. 17–23, 30 abr. 2007.

JAVARONI, R. L. *et al.* Minimum quantity of lubrication (MQL) as an eco-friendly alternative to the cutting fluids in advanced ceramics grinding. **The International Journal of Advanced Manufacturing Technology**, v. 103, n. 5–8, p. 2809–2819, 28 ago. 2019.

JAVARONI, Rafael Liberatti *et al.* Grinding hardened steel using MQL associated with cleaning system and cBN wheel. **The International Journal of Advanced Manufacturing Technology**, v. 107, n. 5–6, p. 2065–2080, 13 mar. 2020.

JIANG, Guo *et al.* **A critical review on the chemical wear and wear suppression of diamond tools in diamond cutting of ferrous metals**. **International Journal of Extreme Manufacturing**IOP Publishing Ltd, , 1 mar. 2020.

KENDALL, K. Complexities of compression. **Proceedings of the Royal Society of London. Series A, Mathematical and Physical Sciences**, v. 361, p. 245–263, 1978.

KINGERY, W. D.; BOWEN, K.; UHMANN, D. R. **Introduction to ceramics**. Second Edition ed. New York: John Wiley & Sons, Inc., 1976.

KITAJIMA, K. *et al.* Study on mechanism of ceramics grinding. *In*: jan. 1992.

KLOCKE, Fritz. **Manufacturing processes 2: grinding, honing, lapping**. 1. ed. *[S.l.]*: Springer-Verlag Berlin Heidelberg, 2009.

KRISHNAN, Saravanan Vanal *et al.* **Technical review: Improvement of mechanical properties and suitability towards armor applications – Alumina composites**. **Ceramics International**Elsevier Ltd, , 1 set. 2021.

LAUER-SCHMALTZ, H.; KÖNIG, W. Prof Dr Ing. Phenomenon of Wheel Loading Mechanisms in Grinding. **CIRP Annals - Manufacturing Technology**, v. 29, n. 1, p. 201–206, 1980.

LI, Kun *et al.* Health risks from exposure to metal-working fluids in machining and grinding operations. **International Journal of Occupational Safety and Ergonomics**, v. 9, n. 1, p. 75–95, 2003.

LI, X. S.; LOW, I. M. Grinding of engineering ceramics with diamond wheels. **Key Engineering Materials**, v. 53–55, p. 307–312, 1991.

LOPES, J. C. *et al.* Application of minimum quantity lubrication with addition of water in the grinding of alumina. **International Journal of Advanced Manufacturing Technology**, v. 97, n. 5–8, p. 1951–1959, 2018a.

LOPES, José C. *et al.* Application of minimum quantity lubrication with addition of water in the grinding of alumina. **International Journal of Advanced Manufacturing Technology**, v. 97, n. 5–8, p. 1951–1959, 1 jul. 2018b.

LOPES, José Claudio *et al.* Behavior of hardened steel grinding using MQL under cold air and MQL CBN wheel cleaning. **The International Journal of Advanced Manufacturing Technology**, v. 105, n. 10, p. 4373–4387, 14 dez. 2019.

LOPES, José Claudio *et al.* Performance of austempered ductile iron (ADI) grinding using diluted oil in MQL combined with wheel cleaning jet and different CBN grains friability. **International Journal of Advanced Manufacturing Technology**, v. 107, n. 3–4, p. 1805 – 1818, 2020.

LOPES, José Claudio *et al.* Grinding comparative analysis between different proportions of water-oil applied to MQL technique and industrial production cost towards a green manufacturing. **The International Journal of Advanced Manufacturing Technology**, 2021.

LOPES, José Claudio *et al.* An experimental evaluation between pure and diluted MQL versus flood lubri-cooling focused on cost and environmental impact. **International Journal of Advanced Manufacturing Technology**, v. 129, n. 5, p. 2691–2705, 1 nov. 2023a.

LOPES, José Claudio *et al.* Reducing carbon footprint in grinding: exploring green manufacturing to mitigate CO2 emission from cutting fluids. **International Journal of Advanced Manufacturing Technology**, v. 129, n. 11, p. 5691–5708, 1 dez. 2023b.

MALI, T. D.; SHINDE, J. H.; KHANKAL, D. V. **Minimum quantity lubrication in machining: a review**. *[S.l.: S.n.]*.

MALKIN, S.; BITTER, J. E. Grinding mechanisms and strength degradation for ceramics. **Journal of Manufacturing Science and Engineering, Transactions of the ASME**, v. 111, n. 2, p. 167–174, 1989.

MALKIN, S.; GUO, C. Thermal Analysis of Grinding. **CIRP Annals - Manufacturing Technology**, v. 56, n. 2, p. 760–782, 2007.

MALKIN, S.; HWANG, T. W. Grinding Mechanisms for Ceramics. **CIRP Annals**, v. 45, n. 2, p. 569–580, 1 jan. 1996.

MALKIN, S.; RITTER, J. E. Grinding mechanisms and strength degradation for ceramics. **Journal of Engineering for Industry**, v. 111, p. 167–174, 1989.

MALKIN, Stephen; GUO, Changsheng. **Grinding Technology: Theory and Applications of Machining with Abrasives**. 2ªed ed. New York: Industrial Press Inc, 2008a.

MALKIN, Stephen; GUO, Changsheng. **Grinding Technology: Theory and Applications of Machining with Abrasives**. 2ª ed ed. New York: Industrial Press Inc, 2008b.

MARINESCU, I. D.; ZENG, R. Acoustic emission investigation of ceramic lapping process. *In*: Storrs: 1996.

MARINESCU, Ioan D. **Handbook of Advanced Ceramics Machining**. Boca Raton, Florida: CRC Press, 2007.

MARINESCU, Ioan D. *et al.* **Handbook of Machining with Grinding Wheels**. 1. ed. New York: CRC Press, 2007.

MARINESCU, Ioan D. *et al.* **Tribology of Abrasive Machining Processes**. *[S.l.]*: Elsevier, 2013a.

MARINESCU, Ioan D. *et al.* **Tribology of Abrasive Machining Processes**. 2 ed. ed. *[S.l.]*: Elsevier, 2013b.

MARINESCU, Ioan D. *et al.* **Handbook of Machining with Grinding Wheels**. *[S.l.]*: CRC Press, 2016.

MORETTI, Guilherme Bressan *et al.* Wheel cleaning jet (WCJ) strategy for green grinding: mitigating greenhouse impact in VP50IM steel machining with green silicon carbide wheel. **International Journal of Advanced Manufacturing Technology**, v. 129, n. 5, p. 2125–2137, 1 nov. 2023.

NAKAJIMA, T.; UNO, Y.; FUJIWARA, T. Cutting mechanism of fine ceramics with a single point diamond. **Precision Engineering**, v. 11, p. 19–25, jan. 1989.

OLIVEIRA, Danilo de Jesus *et al.* Improving minimum quantity lubrication in CBN grinding using compressed air wheel cleaning. **Journal of Materials Processing Technology**, v. 212, n. 12, p. 2559–2568, 2012a.

OLIVEIRA, Danilo de Jesus *et al.* Improving minimum quantity lubrication in CBN grinding using compressed air wheel cleaning. **Journal of Materials Processing Technology**, v. 212, n. 12, p. 2559–2568, 2012b.

OLIVEIRA, Danilo De Jesus *et al.* Improving minimum quantity lubrication in CBN grinding using compressed air wheel cleaning. **Journal of Materials Processing Technology**, v. 212, n. 12, p. 2559–2568, 2012c.

OLIVEIRA, J. F. G. *et al.* Industrial challenges in grinding. **CIRP Annals - Manufacturing Technology**, v. 58, n. 2, p. 663–680, 2009.

PATRA, Saroj Kumar; SWAIN, Suchismita. Effects of minimum quantity lubrication (MQL) in grinding: Principle, applications and recent advancements. **Materials Today: Proceedings**, v. 69, p. 96–106, 2022.

PUSAVEC, Franci *et al.* Transitioning to sustainable production – part II: evaluation of sustainable machining technologies. **Journal of Cleaner Production**, v. 18, n. 12, p. 1211–1221, 1 ago. 2010.

QU, Shuoshuo *et al.* Investigating Minimum Quantity Lubrication in Unidirectional Cf/SiC composite grinding. **Ceramics International**, v. 46, n. 3, p. 3582–3591, 15 fev. 2020.

RABIEI, F. *et al.* Performance improvement of minimum quantity lubrication (MQL) technique in surface grinding by modeling and optimization. **Journal of Cleaner Production**, v. 86, p. 447–460, 2015.

RASIM, Matthias; MATTFELD, Patrick; KLOCKE, Fritz. Analysis of the grain shape influence on the chip formation in grinding. **Journal of Materials Processing Technology**, v. 226, p. 60–68, 2015.

RIBEIRO, Fernando Sabino Fonteque *et al.* Grinding performance by applying MQL technique: an approach of the wheel cleaning jet compared with wheel cleaning Teflon and Alumina block. **The International Journal of Advanced Manufacturing Technology**, v. 107, n. 11–12, p. 4415–4426, 27 abr. 2020a.

RIBEIRO, Fernando Sabino Fonteque *et al.* New knowledge about grinding using MQL simultaneous to cooled air and MQL combined to wheel cleaning jet technique. **The International Journal of Advanced Manufacturing Technology**, v. 109, n. 3–4, p. 905–917, 9 jul. 2020b.

RODRIGUES, Matheus de Souza *et al.* Evaluating the impact of corrosion inhibitors on grinding process efficiency. **Wear**, v. 558–559, 15 dez. 2024.

RODRÍGUEZ, Cristina *et al.* Strength of advanced ceramics by the Small Punch Test. Proposal of a simple empirical equation for the Weibull effective volume. **Journal of the European Ceramic Society**, v. 42, n. 16, p. 7620–7630, 1 dez. 2022.

ROWE, W. Brian. **Principles of modern grinding technology**. Second edition ed. Norwich, NY: William Andrew, 2013. v. 1

ROWE, W. Brian. **Principles of modern grinding technology**. 2. ed. United States: William Andrew, 2014.

ROWE, W. Brian. **Principles of Modern Grinding Technology**. *[S.l.]*: Elsevier, 2014.

RUZZI, Rodrigo de Souza *et al.* MQL with water in cylindrical plunge grinding of hardened steels using CBN wheels, with and without wheel cleaning by compressed air. **The International Journal of Advanced Manufacturing Technology**, v. 90, n. 1–4, p. 329–338, abr. 2017.

RUZZI, Rodrigo de Souza *et al.* Topographical analysis of machined surfaces after grinding with different cooling-lubrication techniques. **Tribology International**, v. 141, p. 105962, jan. 2020.

SAID, Zafar *et al.* A comprehensive review on minimum quantity lubrication (MQL) in machining processes using nano-cutting fluids. **International Journal of Advanced Manufacturing Technology**, v. 105, n. 5–6, p. 2057–2086, 2019.

SALES, Wisley Falco; DINIZ, Anselmo Eduardo; MACHADO, Álisson Rocha. Application of cutting fluids in machining processes. **Journal of the Brazilian Society of Mechanical Sciences**, v. 23, n. 2, p. 227–240, 2001.

SANCHEZ, J. A. *et al.* Machining evaluation of a hybrid MQL-CO2 grinding technology. **Journal of Cleaner Production**, v. 18, n. 18, p. 1840–1849, 2010.

SANCHEZ, Luiz Eduardo de Angelo. **Estudo do comportamento da emissão acústica (EA) em ensaio de riscamento de materiais cerâmicos**. Tese (Doutorado em Engenharia Mecânica)—São Carlos: Escola de Engenharia de São Carlos, Universidade de São Paulo, 1997.

SATO, B. K. *et al.* Toward sustainable grinding using minimum quantity lubrication technique with diluted oil and simultaneous wheel cleaning. **Tribology International**, v. 147, p. 106276, 1 jul. 2020.

SHAREEF, Iqbal *et al.* Effect of rotary ultrasonic machining parameters on surface integrity of advanced ceramics. **Manufacturing Letters**, v. 33, p. 214–225, 1 set. 2022.

SHARMA, Anuj. **Diamond as a Precision Cutting Tool**. *[S.l.: S.n.]*. Disponível em: <www.intechopen.com>.

SHARMA, Anuj Kumar; TIWARI, Arun Kumar; DIXIT, Amit Rai. Effects of Minimum Quantity Lubrication (MQL) in machining processes using conventional and nanofluid based cutting fluids: A comprehensive review. **Journal of Cleaner Production**, v. 127, p. 1–18, jul. 2016.

SHAW, M. C. **Principles of Abrasive Processing**. *[S.l.]*: Clarendon Press, 1996.

SHOKRANI, A.; DHOKIA, V.; NEWMAN, S. T. Environmentally conscious machining of difficult-to-machine materials with regard to cutting fluids. **International Journal of Machine Tools and Manufacture**, v. 57, p. 83–101, 2012.

SILVA, L. R. *et al.* Study on the behavior of the minimum quantity lubricant - MQL technique under different lubricating and cooling conditions when grinding ABNT 4340 steel. **Journal of the Brazilian Society of Mechanical Sciences and Engineering**, v. 27, n. 2, p. 192–199, 2005.

SILVA, Leonardo R. *et al.* Environmentally friendly manufacturing: Behavior analysis of minimum quantity of lubricant - MQL in grinding process. **Journal of Cleaner Production**, v. 256, p. 103287, maio 2020.

SINHA, Manoj Kumar *et al.* An investigation on surface burn during grinding of Inconel 718. **Journal of Manufacturing Processes**, v. 21, p. 124–133, 2016.

SOKOVIĆ, M.; MIJANOVIĆ, K. Ecological aspects of the cutting fluids and its influence on quantifiable parameters of the cutting processes. **Journal of Materials Processing Technology**, v. 109, n. 1–2, p. 181–189, 1 fev. 2001.

SREEJITH, P.; NGOI, B. Dry machining: Machining of the future. **Journal of Materials Processing Technology**, v. 101, n. 1, p. 287–291, 2000.

SRIVASTAVA, A. K.; SRI RAM, K.; LAL, G. K. A simple analysis for evaluating grinding wheel loading. **International Journal of Machine Tools and Manufacture**, v. 28, n. 2, p. 181–190, 1988.

STACHURSKI, Wojciech *et al.* The Influence of the Depth of Grinding on the Condition of the Surface Layer of 20MnCr5 Steel Ground with the Minimum Quantity Lubrication (MQL) Method. **Materials 2022, Vol. 15, Page 1336**, v. 15, n. 4, p. 1336, 11 fev. 2022.

SU, Chong *et al.* Surface formation and crack damage in grinding of alumina ceramic insulation coating. **Ceramics International**, v. 51, n. 7, p. 8544–8557, 1 mar. 2025.

SUBRAMANIAN, K.; RAMANATH, S.; MATSUDA, Y. Precision production grinding of fine ceramics. **Industrial Diamond Review**, v. 5, p. 254–257, 1990.

SWAIN, M. V. Microfracture about scratches in brittle solids. *In*: 1979.

TALON, Anthony Gaspar *et al.* Green manufacturing concept applied to the grinding process of advanced ceramics using an alternative lubri-refrigeration technique. **The International Journal of Advanced Manufacturing Technology**, v. 123, n. 7, p. 2771–2782, 2022.

TAVARES, André Bueno *et al.* Evaluating the effect of WCJ with MQL in grinding VP50IM steel with black silicon carbide wheel. **The International Journal of Advanced Manufacturing Technology 2024 135:7**, v. 135, n. 7, p. 3717–3736, 30 out. 2024.

TAWAKOLI, T. *et al.* An experimental investigation of the effects of workpiece and grinding parameters on minimum quantity lubrication-MQL grinding. **International Journal of Machine Tools and Manufacture**, v. 49, n. 12–13, p. 924–932, out. 2009.

TONSHOFF, H. K.; WOBKER, H. G.; LIERSE, T. **Mechanisms of material removal in the machining of brittle materials.** *[S.l.: S.n.]*.

TSUKUDA, A. *et al.* Relationship between grinding mechanism and residual cracks in single point grinding test of alumina ceramics with different grain sizes. **Journal of the Ceramic Society of Japan**, v. 103, p. 271–276, 1995.

UMEDA, Yasushi *et al.* Toward integrated product and process life cycle planning—An environmental perspective. **CIRP Annals**, v. 61, n. 2, p. 681–702, 1 jan. 2012.

WALKER, Tim. **MQL Handbook**. *[S.l.]*: Unist company, 2013. v. 1

WANG, Y.; HSU, S. M. Wear and wear transition mechanisms of ceramics. **Wear**, v. 195, p. 112–122, 1996.

WANG, Zixuan *et al.* Assessment and optimization of grinding process on AISI 1045 steel in terms of green manufacturing using orthogonal experimental design and grey relational analysis. **Journal of Cleaner Production**, v. 253, p. 119896, 20 abr. 2020.

WARNECKE, G.; ROSENBERGER, U. Basics of process parameter selection in grinding of advanced ceramics. *In*: 1995.

WEBSTER, J.; TRICARD, M. Innovations in Abrasive Products for Precision Grinding. **CIRP Annals**, v. 53, n. 2, p. 597–617, 1 jan. 2004.

WEI, Changxu *et al.* **Material removal mechanism and corresponding models in the grinding process: A critical review**. **Journal of Manufacturing Processes**Elsevier Ltd, , 6 out. 2023.

WINTER, Marius *et al.* Life cycle assessment of cubic boron nitride grinding wheels. **Journal of Cleaner Production**, v. 107, p. 707–721, nov. 2015.

WINTER, Marius; HERRMANN, Christoph. Eco-efficiency of Alternative and Conventional Cutting Fluids in External Cylindrical Grinding. **Procedia CIRP**, v. 15, p. 68–73, jan. 2014.

XU, H. H. K.; JAHANMIR, S.; IVES, L. K. Material removal and damage formation mechanisms in grinding silicon nitride. **Journal of Materials Research**, v. 11, p. 1717–1724, 1996.

ZHANG, B. Effect of scratching fluids on surface integrity of ceramics. *In*: 1990.

ZHANG, Bi *et al.* Grinding induced damage in ceramics. **Journal of Materials Processing Technology**, v. 132, n. 1–3, p. 353–364, 10 jan. 2003.

ZHANG, Zhenzhong *et al.* Enhancing the grinding performance of RB-SiC ceramic using abrasive water jet dressed diamond grinding wheels. **Tribology International**, v. 194, p. 109477, 1 jun. 2024.

ŽMAK, Irena *et al.* **Alumina-Based Cutting Tools—A Review of Recent Progress**. **Materials**Multidisciplinary Digital Publishing Institute (MDPI), , 1 jun. 2025.